

Distribution of trace gases with adverse effects on fuel cells

D. Klemp, R. Wegener, R. Dubus, L. Karadurmus, N. Kille, Z. Tan

Energie & Umwelt / Energy & Environment Band / Volume 539 ISBN 978-3-95806-551-2



Forschungszentrum Jülich GmbH Institut für Energie- und Klimaforschung Troposphäre (IEK-8)

Distribution of trace gases with adverse effects on fuel cells

D. Klemp, R. Wegener, R. Dubus, L. Karadurmus, N. Kille, Z. Tan

Bibliografische Information der Deutschen Nationalbibliothek. Die Deutsche Nationalbibliothek verzeichnet diese Publikation in der Deutschen Nationalbibliografie; detaillierte Bibliografische Daten sind im Internet über http://dnb.d-nb.de abrufbar.

This book is based on our work for the BMWi joint project ALASKA, Subproject: "Evaluation of air pollutant scenarios for the design of pollutant gas filters and cathode regeneration cycles for automotive fuel cells", Funding reference: 03ET6036D. The authors would like to thank Dr. Christian Ehlers for his work during the measurement phase of the project. The authors also thank Prof. A. Wahner and Dr. Franz Rohrer for discussions and critical reviewing of the manuscript.

Herausgeber Forschungszentrum Jülich GmbH

und Vertrieb: Zentralbibliothek, Verlag

52425 Jülich

Tel.: +49 2461 61-5368 Fax: +49 2461 61-6103 zb-publikation@fz-juelich.de

www.fz-juelich.de/zb

Umschlaggestaltung: Grafische Medien, Forschungszentrum Jülich GmbH

Titelbild: Sascha Kreklau (MobiLab II-Zeichnung, Bild links unten),

Dr. Christian Ehlers (MobiLab I-Zeichnung, Bild links oben)

Druck: Grafische Medien, Forschungszentrum Jülich GmbH

Copyright: Forschungszentrum Jülich 2021

Schriften des Forschungszentrums Jülich Reihe Energie & Umwelt/Energy & Environment, Band/Volume 539

ISSN 1866-1793 ISBN 978-3-95806-551-2

Vollständig frei verfügbar über das Publikationsportal des Forschungszentrums Jülich (JuSER) unter www.fz-juelich.de/zb/openaccess.



Contents

1	Ir	ntroduction	.4
2	0	Overall objective of the project	. 5
	2.1	The joint project ALASKA	. 5
	2.2	Contributions of Forschungszentrum Jülich	. 5
	2.3	Conditions under which the project was carried out	. 7
	2.4	Institution	. 8
3	Ir	nteraction of Meteorology and Atmospheric Chemistry	.9
4	Т	he mobile laboratory MobiLab	13
	4.1	MobiLab-I	13
	4.2	MobiLab-II	18
	4.3	Special suitability of the measuring system	22
5	R	Representative measurement runs under typical traffic conditions	_
	R	esults	23
	5.1	Urban agglomerations, motorways and metropolitan regions	23
	5.2	Tunnel studies	37
	5.3	"AMS-test track" in the Stuttgart area	46
	5.4	Conclusions and Summary	57
6	Е	extension of the MobiLab-II analytics by integration of VC	С
	in	nvestigations	59
	6.1	The gaschromatographic system	60
	6.2	Measurements of low volatile hydrocarbons	66
	6.3	The reactivity concept	69
	6.4	Results of VOC concentration measurements	73

Introduction 1

The introduction of fuel cell technology into the field of motor vehicle propulsion enables both a reduction in primary energy consumption and a reduction in dependence on the primary energy source mineral oil. A major advantage of this propulsion technology is reduction of greenhouse gas emissions when renewable energy is used for fuels as hydrogen [Robinius, 2019]. Moreover, fluctuations in electricity energy supply from renewable sources can be dampened when electricity is efficiently converted and stored as hydrogen.

For the competitive application of this technology of fuel cell technology in the field of vehicle propulsion, however, considerable research is still required in some areas. In addition to the necessary cost and weight reduction, this also applies to the long-term stability and robustness of fuel cell stack itself.

It is known that fuel cell stacks react to the admixture of harmful gases into the intake cathode air with performance losses, which primarily result from the poisoning of the catalysts. The effect does not only depend on the total burden of pollutants but on their peak concentrations. With this regard there is a need for research into both the effects of pollutants on fuel stacks and their distribution in the atmosphere.

The work presented here was funded by BMWi in the period from December 2014 to November 2017 and describes the results of the subproject 03ET6036D, which was carried out by Forschungszentrum Jülich.

Overall objective of the project

The overall objective of the project was to quantify the effects of harmful gases in the cathode air of fuel cell stacks under real operating conditions in road traffic. The aim is to develop suitable filter technologies to protect the fuel cell stack from harmful gases as well as regeneration strategies which are able to discharge the unfiltered harmful gases from the stack and thus increase the robustness and service life of the stacks for automotive fuel cell applications. These questions were addressed within the Project ALASKA: "Auswertung von Luftschadstoffszenarien zur Auslegung von Schadgasfiltern und Kathodenregenerationszyklen für Automotiv-Brennstoffzellen".

The joint project ALASKA

Four project partners contributed to the joint project.

The IEK-8 of Forschungszentrum Jülich used a mobile measurement laboratory to investigate the concentrations of harmful trace gases in real traffic conditions.

The ZBT GmbH [ZBT, 2017] (speaker of the ALASKA consortium) and the Daimler AG [Daimler AG, 2017] dealt with the quantification of the effects of harmful gases and with the development of regeneration strategies.

MANN+HUMMEL Innenraumfilter GmbH & Co. KG [Mann und Hummel, 2017] developed suitable filter technologies for the protection of fuel cell stacks. A first summary of important results of the ALASKA project is published [Talke et al., 2018].

2.2 Contributions of Forschungszentrum Jülich

As part of this joint project, the IEK-8 at Forschungszentrum Jülich investigated the concentrations of noxious trace gases (harmful gas components) under real traffic conditions. For this purpose, representative measurements were carried out for various road types and climatic conditions. The applied high-resolution trace gas analysis by means of a mobile measuring laboratory allowed not only the determination of the averaged concentration values but also the detection of peak concentrations. In this

way, it was possible to record the actual concentrations of pollutants occurring in real road traffic, which affect the performance of the fuel cell in the short term and its lifetime in the long term. The data are a prerequisite for manufacturers of mobile fuel cells to design systems that are optimized in terms of costs and service life.

The mobile laboratory "MobiLab" of the IEK-8 was used to monitor pollutant gas concentrations within this project. MobiLab was equipped with a comprehensive set of instruments to characterize the concentration of pollutants with high temporal resolution. In addition to the rapid analysis of nitrogen oxides (NO, NO₂), SO₂, CO₂, CO, CH₄, NH₃ and O₃ were also determined with one-second temporal resolution.

Since the increase of CO₂ in proximity to roads are caused almost exclusively by trafficinduced (engine) combustion processes, the measured trace gas concentrations can be normalized to the instantaneous fuel consumption of the measured vehicle fleet. This procedure offers the possibility to derive the emission of trace gases with respect to the amount of fuel consumed, so that the measured concentrations can be related to the traffic density. On the other hand, this procedure offers the possibility to derive a measure for trace gas concentration levels of NO, NO₂, SO₂, NH₃ and volatile organic compounds (VOC) of a traffic-polluted environment from the measurement of the CO2 concentration hub alone¹. In this way, under Central European conditions, a relatively simple CO2 measurement can be used to directly deduce a rough estimation of the trace gas load, e.g. while driving through a road tunnel².

In section 4 the procedure we have chosen for specifying the actual concentrations of harmful gases is explained in detail.

¹ This is possible because both the trace gases released and the CO₂ formed during the combustion of the fuel originate from the same source (exhaust emissions from the measured vehicle fleet). The validity of this estimation has its limits, of course, as the emission factors of the measured vehicle fleet change

over time. This approach of course requires a regular update of the respective trace gas to CO2 ratios of the actual car fleet. [Ehlers et al., 2016] have for example shown that NO_x emissions from traffic have decreased by an average of 4 %/year over a period of 20 years.

² It should be pointed out that this approach is not only useful for the system design of fuel cell systems, but can also be used, for example, to assess the potential health hazards of traffic-related emissions.

2.3 Conditions under which the project was carried out

The investigation of the effects of trace gases introduced by the air into Polymer Electrolyte Membrane (PEM) fuel cells revealed clear damage potentials on both the anode and cathode sides, which have a negative effect on the power output and service life of the PEM fuel stack. While the gas used on the anode side can be effectively cleaned from harmful gases, the cathode side is in contact with outside air which can be contaminated with high trace gas contents.

The effect of the trace gases on the fuel cell can be differentiated between reversible and irreversible damages. Typical trace gases causing irreversible damage to the fuel cell stack are SO₂, H₂S and NH₃³. Sulfur containing compounds deactivate the catalyst material by establishing strong bonds between active catalytical centres and the sulfur atoms [Mothadi et al., 2004].

A largely reversible damage effect is reported for the two nitrogen oxide components NO and NO₂ [Yang et al., 2006, ZBT, IUTA, 2009, ZBT, IUTA, 2012]. There is evidence that NO and NO2 cause damage of different severity by adsorption at the catalyst [cf. Chen et al., 2011]. At the same concentration, the NO causes a faster degradation of a fuel cell stack compared to NO2. [Private Communication, U. Misz, ZBT, 2015]. Overall, it is clear that many questions regarding the damage potential of NO and NO₂ have not yet been answered [e.g. Zamel and Li, 2011].

As far for organic gases adsorption on the catalyst can lead both to reversible (e.g. toluene [St. Pierre et al., 2014]) and irreversible (benzene) [Moore et al., 2000]) effects [El-Deab et al., 2013, Antolini, 2004].

³ In the case of NH₃ there are contradictory statements in the literature on the reversibility of NH₃ harmful gas effects. While [Imamurea et al., 2009] report reversible impairments by NH₃ contents in the cathode air, [Halseid et al., 2009] come to the conclusion that the NH3 influence on the fuel cell stack is irreversible. An essential factor in the mode of action of NH3 is the negative influence of the membrane as NH₄+ [Lopes et al., 2014].

2.4 Institution

The Forschungszentrum Jülich GmbH (FZJ) carries out interdisciplinary research in the fields of health, energy, environment and information based on its key competences: Physics and Supercomputing. The Institute for Energy and Climate Research (IEK) investigates modern energy conversion techniques within the framework of energy and environmental protection, taking into account the "Energiewende" that has been decided upon, and therefore takes a comprehensive look at the consequences of energy use and the associated emissions.

The IEK-8: Troposphere subinstitute investigates the physical and chemical processes of the troposphere that have a significant influence on the chemical composition of the atmosphere. These include (1) the release (emission) of trace substances from soil sources, transport and industry, (2) the chemical transformation of trace substances in the atmosphere and (3) the distribution of pollutants by transport. The IEK-8 has been active in the field of air chemistry for more than 3 decades and quantifies the composition of the atmosphere as well as the reaction processes taking place in it under different atmospheric conditions. By means of observations on the ground, in the air and in space, the chemistry and dynamics of man-made (anthropogenic) and natural (biogenic) trace substances in the atmosphere are monitored.

For more than 20 years, the working group "Energy-Related Emissions" has been working on the quantification of anthropogenic trace substance emission and immission strengths and has recently published the results of its own long-term studies on the development of VOC and nitrogen oxide emissions in traffic-polluted areas in Germany [Ehlers et al., 2016]. Further fields of work are the verification of existing emission inventories [Mannschreck et al., 2002, Klemp et al., 2002] and detailed emission measurements of vehicles in real road traffic [Mittermaier and Klemp, 2004, Klemp et al., 2012].

Interaction of Meteorology and Atmospheric Chemistry

The ratio of NO and NO₂ which determines the potential damage of nitrogen oxides to fuel cells is controlled by meteorology. As an example, the seasonal dependencies of the nitrogen oxide concentrations in polluted areas and their influence on mean daily variations and speciation of the nitrogen oxides (NO, NO₂) is presented here.

Fig. 1 shows average daily variations of inner city nitrogen oxide levels under summer and winter conditions. The measurements took place in the inner city area of Bad Homburg and give a good overview of the daytime and seasonal dependence of the occurring nitrogen oxide concentrations [Ehlers et al., 2017]. In addition, the 1-sigma fluctuation ranges of the corresponding monthly averages are marked in grey.

The following trends for the "urban background" can be seen in Fig. 1:

- The mean nitric oxide values in winter are about a factor two higher than those during summer. Various reasons are responsible: First, emissions from road traffic are strongly linked to the outside temperature (see Fig. 21). The lower temperatures in winter lead to longer heating phases of the SCR catalytic converters of diesel vehicles than in summer. Moreover, meteorological and air-chemical reasons additionally reinforce this seasonal trend. The more frequent inversion weather conditions in winter combined with low wind speeds favor the accumulation of concentrations near the ground. In addition, the slowing down of photochemical degradation processes in winter leads to a considerable enrichment of regional background concentrations in continental background regions of urban agglomerations.
- In principle, the diurnal behaviour of nitrogen oxides for traffic-related areas is similar over the course of the day, with the first approximation being determined by traffic intensity. On closer examination, the influence of other factors becomes clear: During the day, ozone is produced by photolysis of NO₂. At night, the ground cools faster than the air above. At stagnant conditions a shallow inversion layer is formed where the emitted nitrogen oxides are concentrated. Since NO2 is not photolyzed, ozone is completely consumed by reaction with NO. Traffic emissions during the morning rush hours cause the nitrogen oxide mixing ratios to increase. Right after sunrise, NO₂ is photolyzed which results in an increase of the NO/NO₂-

ratio compared to nocturnal conditions. As the sun warms the ground, the inversion disappears and air from upper layers enriched with ozone and depleted with nitrogen oxides is mixed in, which reduces both the total amount of NOx and the ratio of NO to NO2. During the evening rush hours, the NOx concentrations are usually lower, as the inversion layer hasn't built up yet.

- In winter, the sunset is prior to the evening rush hour. The NO₂ concentration is higher, because it is not photolyzed. Accordingly, the NO peak is lower compared to the NO peak during summer.
- Another reason for the differences between morning and evening NO peak level is probably due to the special properties of the oxidation catalysts of diesel vehicles. Diesel vehicles without SCR catalysts are mainly responsible for traffic-related NO_x emissions [Wichmann-Fiebig, 2017]. In the morning, shortly after the cold-start of the engines, the oxidation catalytic converters of diesel vehicles are not yet ready for operation. The combustion-initiated nitrogen oxide emissions (almost only in the form of NO) therefore pass the cold oxidation catalyst unchanged and are not, as under warm operating conditions, converted to a considerable extent to NO2 in the oxidation catalyst. Especially during the evening rush hour in winter, in addition to the lack of NO₂ photolysis, this contributes to a decreased NO/NO₂ ratio (see Fig. 1).

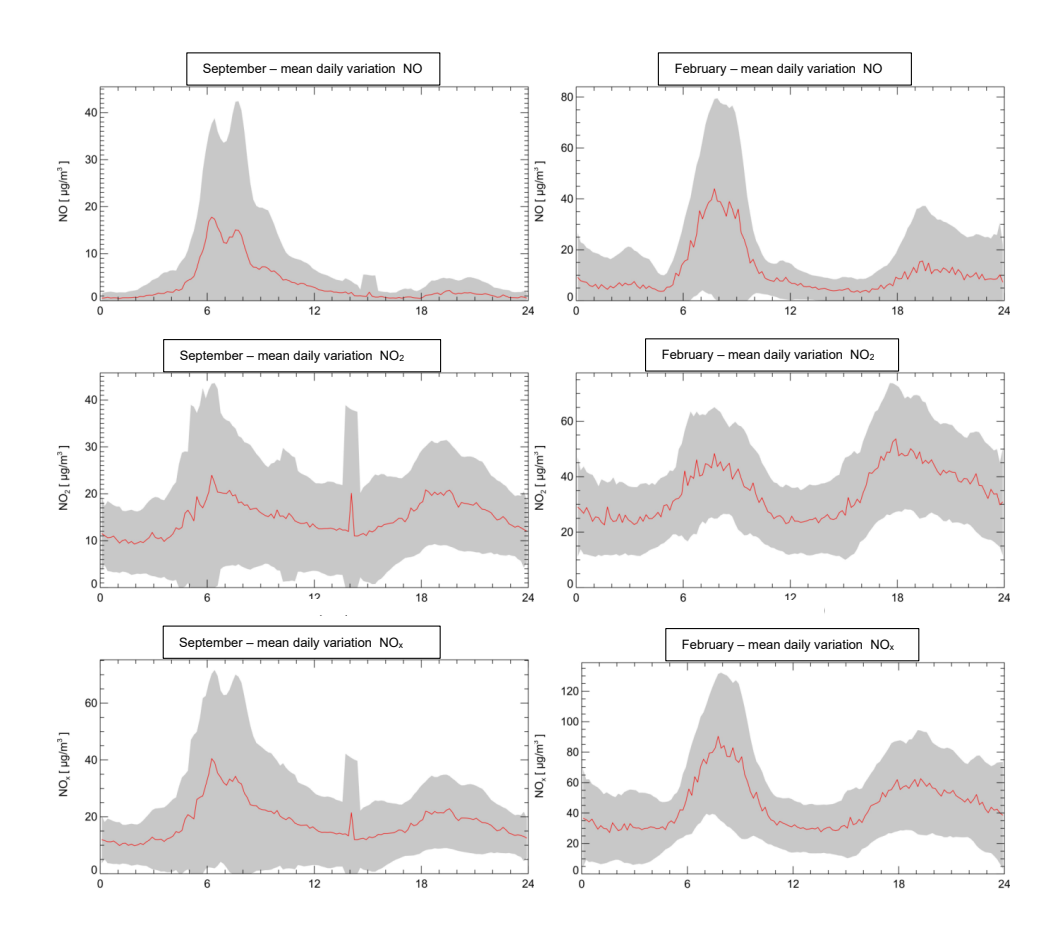


Fig. 1: Mean daily cycles of the monthly average for nitrogen oxides in an inner-city environment (city park, distance approx. 100 m from the next road, so-called "urban background") for the months of February and September. In addition, the 1-sigma fluctuation ranges of the concentrations of NO, NO₂ and NO_x (colored grey) are given. To record the nitrogen oxide data, high-resolution chemiluminescence analysis (Eco-Physics) with an upstream photolysis converter for the conversion of NO₂ to NO was used. The time of day is given in UTC, i.e. time offset to CET (winter, here: February): 1 hour or to CEST (summer, here: September): 2 hours. From: [Ehlers et al., 2017].

The inner-city emission ratio of NO/NO₂ is essentially determined by the distance to the sources, radiation intensity and the prevailing ozone concentration. Fig. 2 shows the NO/NO₂ ratio averaged over one month for inner-city conditions measured in a park at a distance of approx. 100 m from a through road.

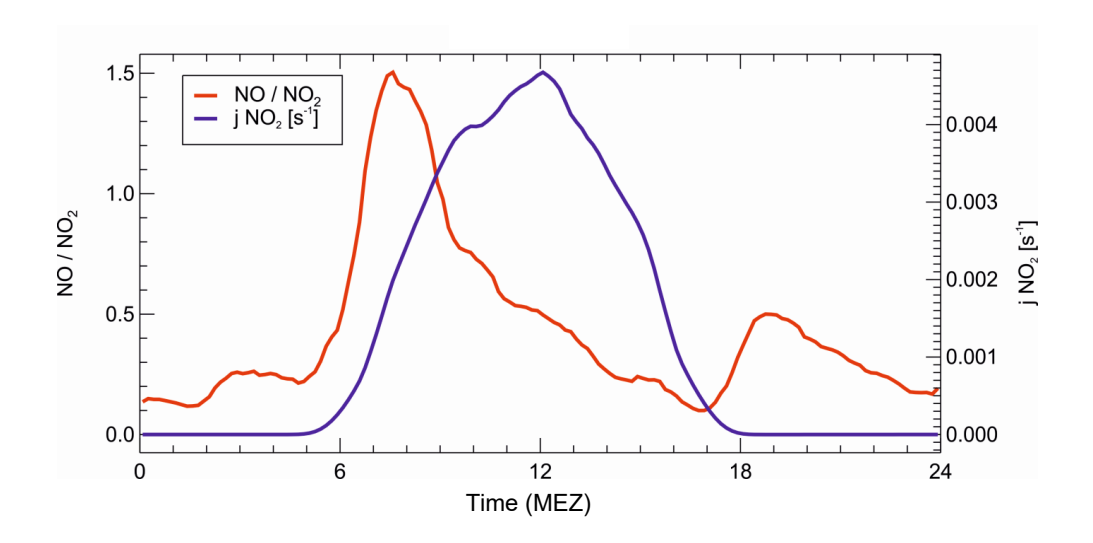


Fig. 2: Averaged NO/NO₂ ratios [ppb/ppb] for March 2014 as a function of time of day (MEZ), measured in Bad Homburg city center (red). The measurements were performed at a distance of approx. 100 m from a through road in a park. On the right axis the intensity of the averaged photolysis frequency jNO₂ (blue) is also plotted as a function of the time of day. It can be seen that the available solar radiation significantly influences the NO/NO₂ ratio (from: [Ehlers et al., 2017]), which decreases from morning conditions of almost 1.5 over the day reacheing a minimum NO/NO₂ ratio of 0.25, only to rise again after sunset (for details on the responsible air-chemical processes, see e.g. Klemp et al., 2012]).

A significant difference between the nitrogen oxide ratios NO/NO_2 in the "urban background" and the NO/NO_2 ratios observable at street level must be pointed out: While the seasonal trends of NO_x observed measuring at an urban background station correspond to the NO_x trend measured at a traffic station, this does not apply to the ratio of NO/NO_2 . In the vicinity of a highly-trafficked road the NO/NO_2 ratio is determined by the source ratio and only to a lesser extent by the subsequent chemical processes compared to the NO/NO_2 ratio of the urban background.

Basically, the higher the traffic intensity and the smaller the influence of the chemical processes, the closer the observable NO/NO₂ ratios are to the ratios in the exhaust.

The mobile laboratory MobiLab 4

The Forschungszentrum Jülich carried out extensive measurement runs with the mobile laboratory (MobiLab) under traffic-typical conditions and recorded a climatology of the seasonal course of the measured trace gas concentrations.

The work was carried out by the Institute for Energy and Climate Research (IEK) of Forschungszentrum Jülich GmbH, Subinstitute IEK-8: Troposphere.

4.1 MobiLab-I

In recent years, a number of studies [Bukowiecki et al., 2002; Pirjola et al., 2004; Kittelson et al., 2004; Weijers, 2004; Westerdahl et al., 2004; Urban, 2010; Ehlers, 2013] have demonstrated that mobile measurement systems are particularly suitable for recording and investigating concentration fields in anthropogenically contaminated environments.

In the past few years, IEK-8 of Forschungszentrum Jülich has carried out extensive investigations in this field of research in the context of three dissertations [Urban, 2010; Ehlers, 2013; Wenk, 2016] and acquired special expertise in the field of high-resolution measurements of pollutants.

In the first phase of the ALASKA project, measurement runs were carried out with MobiLab-I, the predecessor of our current mobile measurement laboratory MobiLab. The development of MobiLab-I on the basis of a Mercedes VITO4 is the result of a dissertation which was successfully completed in 2010 [Urban, 2010]. The main starting points of this dissertation were the recording of immission concentrations of relevant trace substances in urban agglomerations and in rural backgrounds. The aim of the investigations was the characterization of these scenarios and the model-based description of the photooxidant formation by means of a zero-dimensional box model.

⁴ When using a Mercedes VITO with a common passenger cell for operators and technical equipment, it is prohibited to carry open supply gas cylinders for safety reasons. MOBILAB-I could only be operated during the measurement run if the required supply gas cylinders were carried in a metal cage on the roof of the Mercedes VITO.

Subsequently, the mobile measurement laboratory was further optimized and upgraded within the scope of another doctoral thesis [Ehlers, 2013], so that mobile measurements with durations of up to 6 hours were now possible. Results of these investigations were presented in conferences and published [Ehlers et al., 2014], [Ehlers et al., 2016].

In parallel, MobiLab was additionally equipped with a fast GC-MS system with a time resolution of 3 minutes. The focus of these investigations was the in-situcharacterization of different VOC-mixes from biogenic and anthropogenic environments [Wenk, 2016].

Fig. 3 shows the MobiLab-I in its last stage of expansion, as it was realized by C. Ehlers [Ehlers, 2013] (see also Table 3). With this expansion stage, any leeway with regard to electrical power supply, available installation space and maximum vehicle weight was exhausted. The purchase of a larger carrier vehicle became unavoidable for any further expansion of the metrological equipment. In particular, the integration of the fast IR laser detection system for NH₃ (manufacturer LosGatos Inc., USA) with a powerful scroll pump (Edwards, XDS30), procured from ALASKA project funds, was impracticable in the MobiLab-I measuring laboratory for space and weight reasons.

Table 1 lists the gas phase analysis integrated in MobiLab-I and describes the respective detection limits at second resolution.

Table 1: Gas phase analysis of MobiLab-I at the beginning of the ALASKA project. In a later phase of the project the existing NH₃ analysis (IR-Cavity ringdown, Picarro) was supplemented by a fast tunable diode laser system with long path absorption cell (Manufacturer: LosGatos). A fast SO2 measuring system (TI 43i, manufacturer Thermo Fisher, detection limit 1 - 2 ppb, 1-second resolution) was procured from the own funds of Forschungszentrum Jülich and integrated into the MobiLab-I successor system.

Substance	Detection principle	Detection limit / Time resolution
NO, NO ₂ , O ₃	Chemiluminescence	30/50/20 ppt / 2 s
со	UV-Resonance fluorescence	2 ppb / 2 s
Total-Hydrocarbons	FID	70 ppbC / 2 s
CO ₂ and CH ₄	IR-Cavity-ringdown	CO ₂ : 2 ppm / 0.1 s CH ₄ : 5 ppb / 0.1 s
NH ₃	IR-Cavity-ringdown	2 ppb / 3 - 5 s
VOC-Canister samples	GC-MS	2 - 6 ppt for C ₂ – C ₁₂ -VOC / 10 min
In-situ VOC measurements	GC-MS	3 - 10 ppt for C ₃ – C ₉ -VOC / 3 min



Gas phase

- NO / NO₂ / O₃
- CO₂ / CH₄
- NΗ₃
- CO
- Spec. VOC

(Canister samples)

Total VOC

Particle phase

- **ELPI**
- CPC

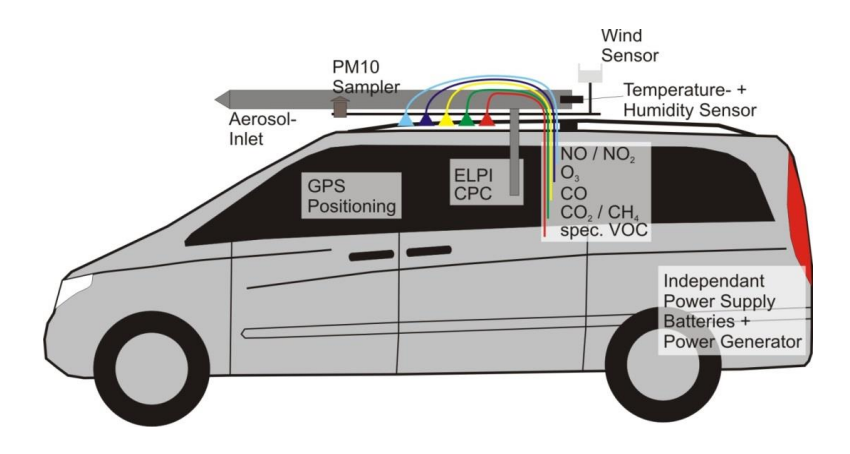


Fig. 3: Mobile measurement laboratory (MobiLab-I) at Forschungszentrum Jülich. Expansion stage: Summer 2013 [Ehlers, 2013], measurement platform: Mercedes VITO, energy supply: Generator + battery buffering, position GPS, meteorology: wind direction, wind speed, humidity, temperature.

It was found that the "sticky" NH₃ had significantly higher response times than the other trace gases. In fact, the response time in case of NH₃ could be minimized substantially by using a LosGatos NH₃ measuring system with a particularly high flow rate (cf. MobiLab-II configuration), with which a second-resolved measurement of NH₃ can be achieved. A time resolution as high as possible for all trace gases of interest here is necessary, since not only the integral loads of the fuel cell stack are important, but also the peak loads occurring in traffic.

As an exemplary illustration of the variability of the concentration during a course in a city, the time series of NO_x concentration is presented in Fig. 4. The dynamic range of the measured NO_x concentrations covered more than a factor of 1000. The urban background values, determined from a low-pass filtering of the data, were a few ppb (see Fig. 5: Local background + regional background). The corresponding NO_x-hourly averages (see: Fig. 5: Average) are about 100 ppb. If only the NO_x peak concentrations were considered, short-term maxima of up to almost one ppm were found. An important aspect of the investigations within the ALASKA project was the characterization of the peak concentrations and the subsequent investigation of the damaging effect of such "concentration" peaks on the fuel cell stacks.

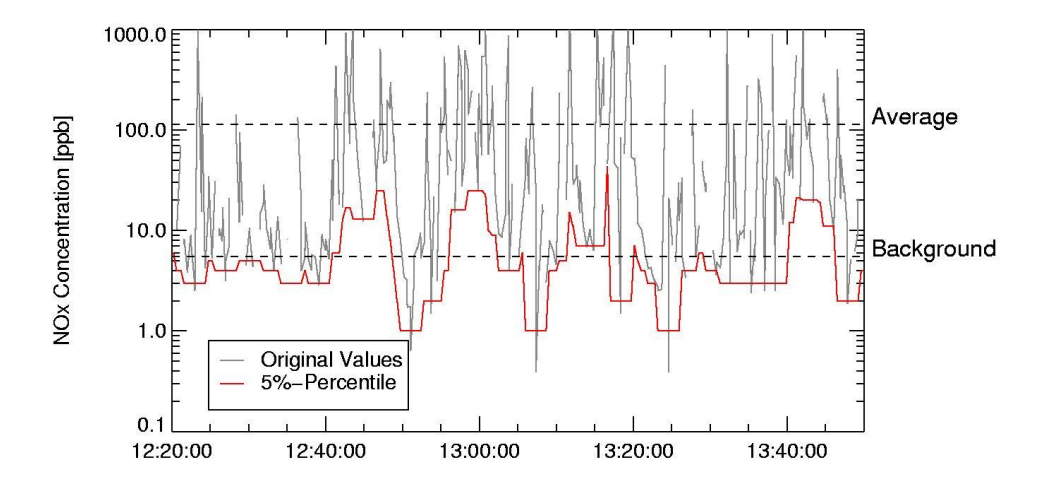


Fig. 4: Investigation of NO_x concentrations in the inner city of a metropolis (Berlin, summer 2016, urban area Neukölln) using MobiLab-I. Determination of the local background for NO_x (background) by applying a 2-minute 5% filter and calculating the associated 5th percentiles from the recorded NO_x measurement data set (measurement period, August 2016): The associated one-hour NO_x average, on the other hand, provides a value of about 120 ppb⁵.

⁵ This concentration range would be provided by a typical continuously running measuring station in the city center if, as is common practice, only 1h averages were recorded. However, no conclusions about the local background or peak values could be drawn from this.

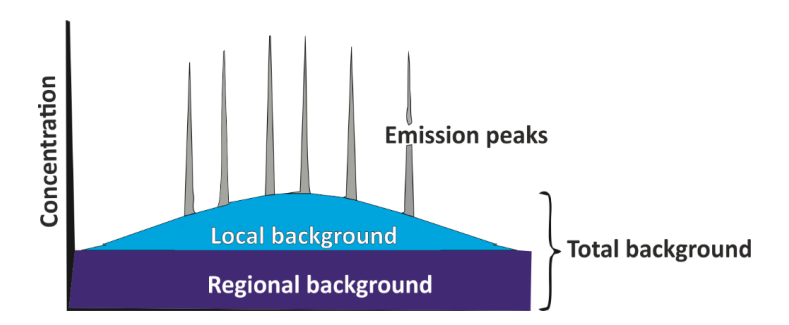


Fig. 5: Schematic representation of the formation of a trace substance in the inner city: "Regional Background" entered from the outside (the x-axis represents a cross-section through a city in space). In the urban area, the "local background" and the emission "peaks" of the nearby sources (e.g. exhaust emissions from vehicles) are added to the regional background. After a short time, mixing and dilution ensure that the emission "peaks" will be dissolved down to the local background value. (According to: Lenschow et al., 2001).

4.2 MobiLab-II

An extension of such investigations to the harmful gases NH_3 and SO_2 could not be realized with MobiLab-I without complex conversion measures. For the reasons already explained (space and weight restrictions), the necessary high-resolution measurement systems for NH_3 and SO_2 could only be integrated in a larger vehicle. A further essential goal of the on-road investigations carried out by us was not only to measure the concentration curves of individual trace gas components in a representative manner, but also to carry out these investigations simultaneously for the entire ensemble of trace gases.

Fig. 6 shows the structure of MobiLab-II with a schematic representation of the trace analytics used (cf. Table 2). MobiLab-II is based on a Mercedes Sprinter with a thermally insulating and air-conditioned box structure (cf. Fig. 7).

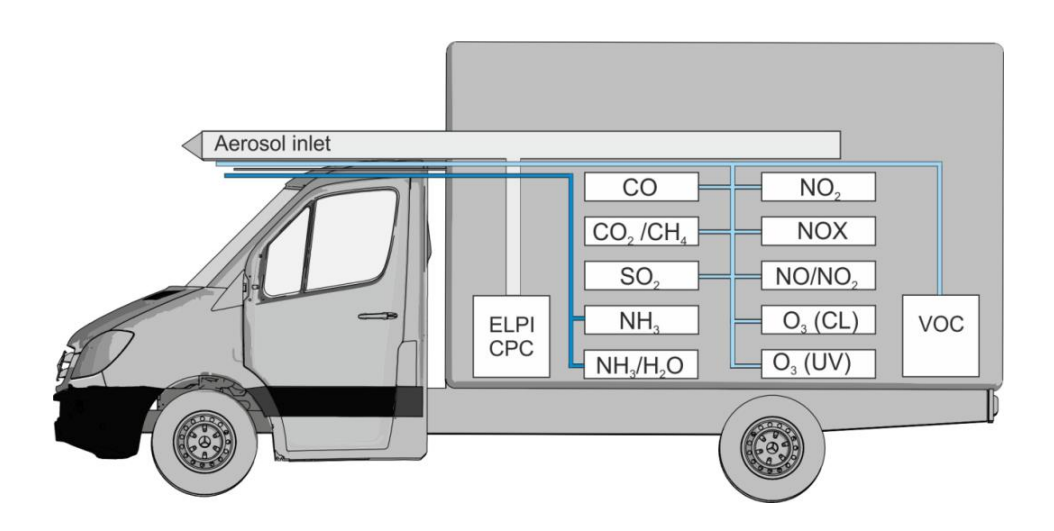


Fig. 6: MobiLab-II with schematic representation of the built-in trace analytics: Aerosol inlet: isokinetic suction of the particle phase to avoid errors in the measured aerosol distributions due to high speed differences between the own movement of the MobiLab and the speed at the entry point into the "aerosol inlet". Gas phase analysis: CO, CO₂, CH₄, SO₂, NH₃, H₂O, NO_x, NO, NO₂, O₃ (UV absorption), O₃ (rapid O₃-detection by chemiluminescence), VOC canister samples, aerosol analysis: ELPI, CPC, filter samples: gravimetric analysis, EC/OC distribution [Ehlers et al., 2017].

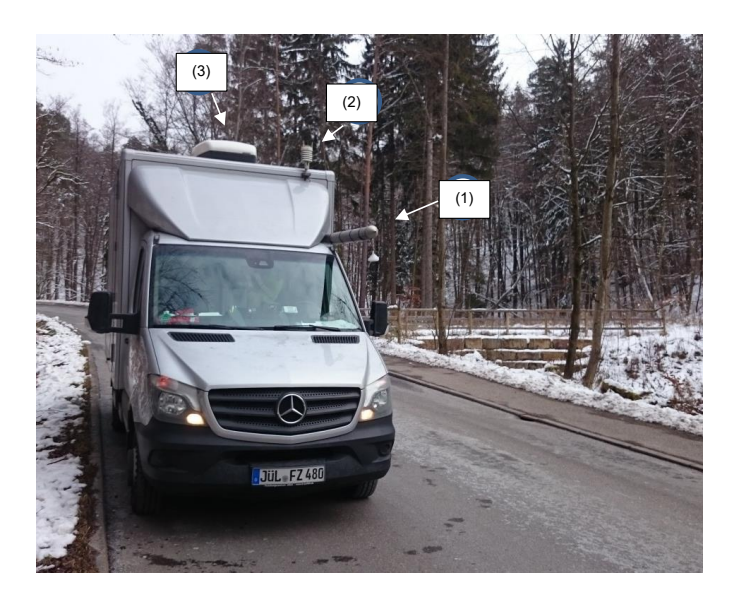


Fig. 7: MobiLab-II in winter measurements to record a climatology of relevant trace gases in Stuttgart. The suction point for the aerosol and gas phase is located on the driver's side at a height of approx. 2 m above the road (1). The gas phase inlet is additionally protected against the additional suction of water by a conically expanding funnel. The meteorological measuring apparatus (WXT 520, Vaisala) is attached to the upper edge of the wind deflector (2). The heat exchanger of the air conditioning system can be seen on the roof of the box body (3).

The analytics and the required supply gases are accommodated in a separate box structure and are thus completely separated from the driver's cab, so that the analytics can also be operated with the supply gases while the vehicle is in operation.

Table 2: Measurement equipment of MobiLab-II, available from 2016, power requirement of analytics: approx. 7 kW, supply by a 380 V three-phase generator driven by the vehicle engine (6 kW power); (MobiE) and an underfloor generator (3 kW power); (Dometic TEC40 D).

Substance	Time Resolution	Detection principle
Gas phase		
CO ₂ , CH ₄ , H ₂ O, NH ₃	0.1 s/1 s 5 s	Cavity Ringdown-Spectroscopy (<i>Picarro Inc.</i>)
NH₃	1 s	Off-axis integrated cavity output spectrometer (LosGatos Research)
СО	1 s	VUV-Resonance Fluorescence (AeroLaser GmbH)
O ₃	10 s	UV-Absorption (Environnement S. A)
NO ₂	1 s	Cavity Attenuated Phase Shift (CAPS) (Aerodyne Research)
SO ₂	1 s	Pulsed Fluorescence Analyzer (Thermo-Fisher Scientific)
NO _x , NO, O ₃	2 s	Chemiluminescence (EcoPhysics GmbH)
Total-VOC	2 s	FID-Detection (ABB Ltd)
VOC-Canister samples	10 min-Aver.	Canister samples/Offline GC/MS Agilent 6890 + MS5975 C
Particle phase		
Particle distribution (30nm-10µm), 12-stages	1 s	ELPI (Electrical Low Pressure Impactor) (Dekati Ltd)
Particle number (2nm - 3µm)	1 s	CPC-3788 (TSI GmbH)
<u>Meteorology</u>		
Temperature, Pressure, Wind speed, Wind direction	1 s	WXT 520 (Vaisala GmbH)
Meta data GPS, Camera		

4.3 Special suitability of the measuring system

- The mobile measuring laboratory is able to record the relevant pollutant concentrations during operation, so that reliable statements for the expected pollutant levels under traffic-typical conditions can be made.
- All MobiLab measuring systems have the required time resolution in the low second range so that the concentration peaks of the trace gases under consideration can be detected adequately.
- The experience gained from several measurement campaigns and the resulting high development status of MobiLab ensure that the mobile measurement laboratory at Forschungszentrum Jülich is also successfully set up for the technically complex recording of a climatology of relevant pollutant gases.
- The aim was to make meaningful statements regarding the expected pollutant levels and peak concentrations by means of suitable selection of the scenarios to be investigated and statistical validation of the results for Central European conditions.
- An important objective of the investigation was the characterization of the climatology of the pollution levels. To this end, measurement campaigns were carried out in various conurbations in Germany (Berlin, Rhine-Ruhr area in North Rhine-Westphalia, Stuttgart) during different seasons. Different climatological conditions are associated with seasonal inversion layer changes and wind speed differences, which have a significant influence on the concentration levels of the relevant pollutants.
- In addition, meteorological conditions are closely linked to photolytically initiated air-chemical conversion processes. The MobiLab of FZ Jülich fulfils the necessary prerequisites for an adequate recording of the pollutant concentrations of interest.

5 Representative measurement runs under typical traffic conditions - Results

In total, three scenarios were investigated:

- Urban agglomerations, motorways and metropolitan regions i)
- ii) **Tunnels**
- "Auto-Motor und Sport (AMS)" test round in the Stuttgart area iii)

Since the residence times of a fuel cell vehicle in urban agglomerations and on motorways dominate the integral levels of exposure to traffic-borne trace substances (Talke, 2017), particular attention was paid to this scenario. For this purpose, both long-term measurements in a neighboring metropolitan region (Rhine-Ruhr region) and campaign-like studies at different seasons to investigate orographic influences (Berlin, Stuttgart) on pollutant levels were carried out.

The two other research priorities "Tunnel" and "AMS-Testrunde" could be dealt with in parallel within the framework of the measurement campaigns carried out in Berlin and Stuttgart.

In the detailed presentation of the results achieved in this project, the chronological sequence of the measurement program was deliberately omitted. It turned out that only the parallel discussion of the results from long-term measurements and from campaigns allows different aspects of seasonal changes to emerge: Temperaturedependent changes in traffic-related nitrogen oxide concentrations can be determined most clearly on the basis of long-term studies. Seasonal changes in background concentrations, on the other hand, can be determined on the basis of campaign-like windward studies of metropolitan regions.

Urban agglomerations, motorways and metropolitan regions 5.1

Two different research approaches were pursued in the investigation of pollutants in urban agglomerations:

On the one hand, campaign-like investigations were carried out in two different metropolitan regions of Germany (Berlin and Stuttgart). On the other hand, the study area in the Rhine-Ruhr metropolitan region was repeatedly probed on a fixed route over a period of more than one year.

A major objective of the campaign-like investigations was to clarify whether and to what extent different orographic conditions influence the observable pollutant levels.

We selected Berlin for a case study of a metropolis in flat terrain and Stuttgart for a city in structured terrain. The state capital Stuttgart of Baden-Württemberg is framed by low mountain ranges (Stuttgart basin). In recent years, the city of Stuttgart has made headlines as the place with the highest NO₂ annual average value for all of Germany [Landesamt für Umwelt BW, 2016], measured directly at the edge of the B14 road at Neckartor.

In the course of the project, we investigated the concentration levels at both test sites both for summer (July/August) and winter conditions (January/February).

Fig. 8 shows the measured concentration curve of NO₂ mixing ratios during east-west crossing of the Berlin city area. It can be seen that the lowest NO2 mixing ratios of approx. 45 ppb were found on the windward side of the city of Berlin in the vicinity of the city of Nauen. The wind arrow describes the wind direction prevailing on this day (northwest); the associated wind speed was low and amounted to 1.5 - 3 m/s. It should be noted that the observed windward side background value of 45 ppb or 84 μg/m³ is remarkably high, although the permissible 1-h mean value of 200 µg/m³ [39. BlmSchV] is still far above.

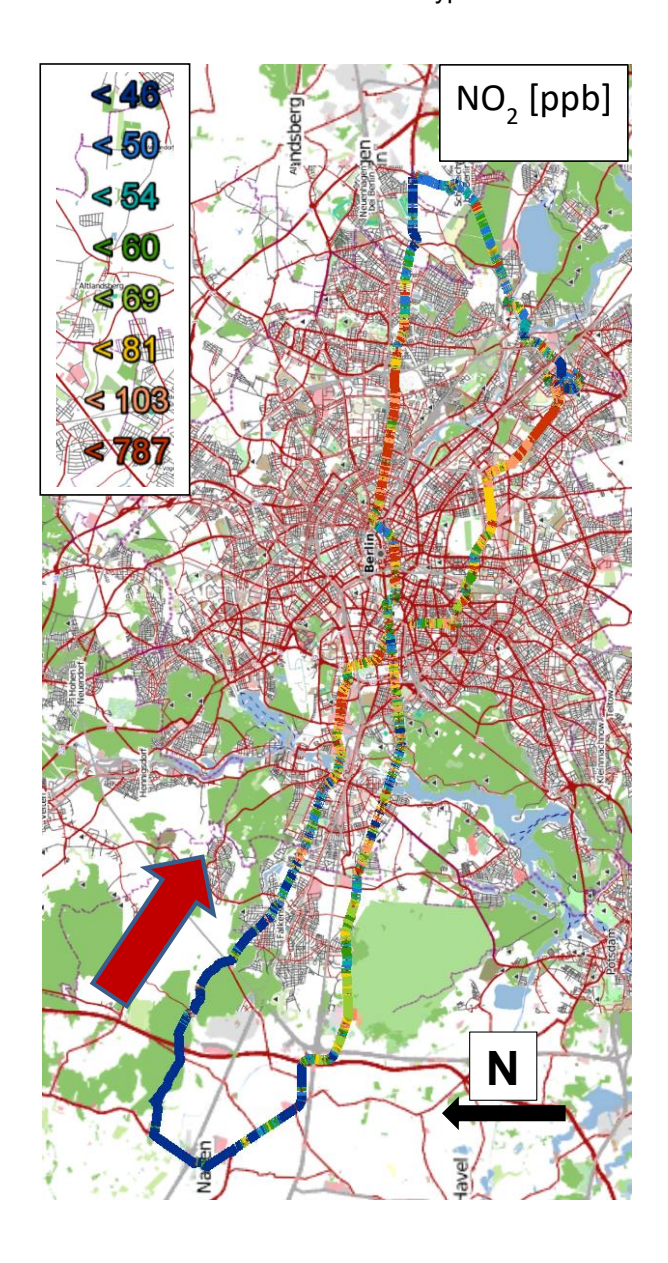


Fig. 8: Results of the NO₂ measurements (cf. color scale) when crossing the city of Berlin in east-west direction and investigations in the windward and leeward area of Berlin under winter conditions and north-west wind direction (see wind arrow). The measurements with MobiLab presented here took place on a weekday in January 2017 between 9:00 and 12:30 UTC.

Highest NO₂ mixing ratios were observed with NO₂ values of more than 100 ppb in the center of Berlin. A detailed analysis of the mean windward and leeward NO2 values in the Berlin hinterland provides an additional contribution of NO₂ by the city of Berlin of about 15 ppb in the southeastern leeward area of the city (investigation period: January 2017).

As part of another campaign, we investigated the Berlin site under summer conditions (August 2017). Fig. 9 shows the NO₂ mixing ratios measured on the illustrated route in the center of Berlin (surroundings of Ernst-Reuter-Platz). High NO₂ mixing ratios were found on main roads and at intersections. Low NO₂ values close to the local background values were observed for secondary roads and/or residential areas.

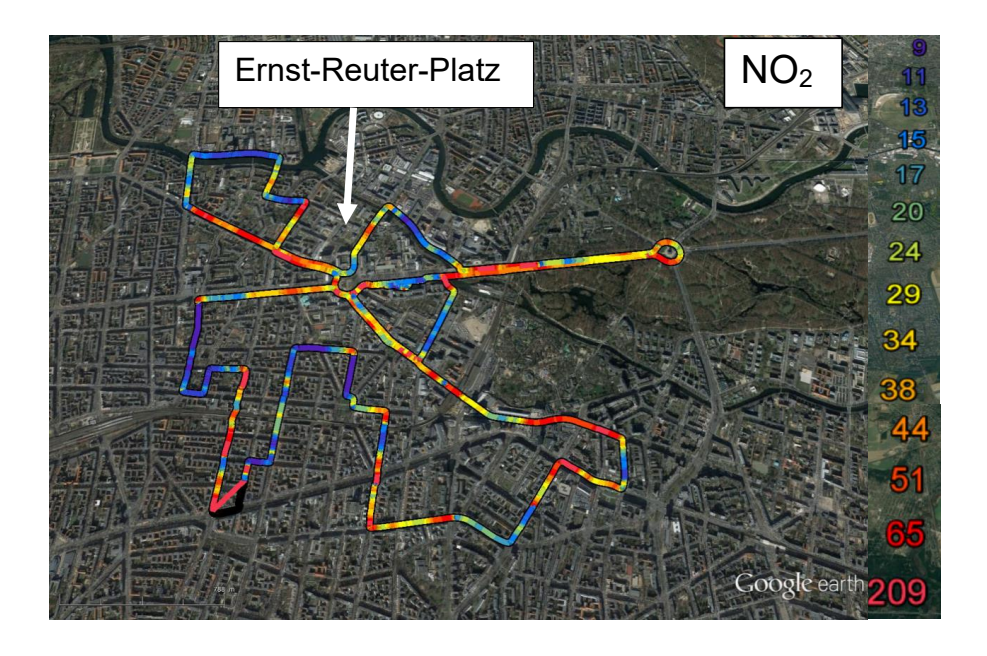


Fig. 9: Measurement drive with MobiLab-II in August 2017 in Berlin. Concentration distribution of NO₂ [ppb] in the inner city area of the city of Berlin (surroundings of Ernst-Reuter-Platz). High NO₂ mixing ratios were found on main roads and at intersections. Low NO₂ values close to local background values were observed in secondary roads and/or residential areas, cf. concentration color scale. For the typical mixing ratios and variation range of inner-city NO_x values (Berlin Neukölln, summer 2017) see also Fig. 4.

It was examined whether other NO_x sources were prominent in addition to road traffic at street level. For this purpose, we investigated the environment of the heavily used inner-city airport Berlin Tegel by passing the surrounding streets of the airport area of

Berlin Tegel several times to circle the area. The graphical representation in Fig. 10 shows the result of the measurement drive around the airport area with the mobile laboratory. On this day in August 2017 eastern inflow conditions were present (wind speed: 2 - 3 m/s). It was shown that the measured NO_x concentration was clearly "modulated" by the prevailing traffic density and traffic flow. A clear influence of the NO_x emissions from air traffic on the measured NO_x concentration levels could not be determined in the leeward area of the airport during any of the orbits with MobiLab.

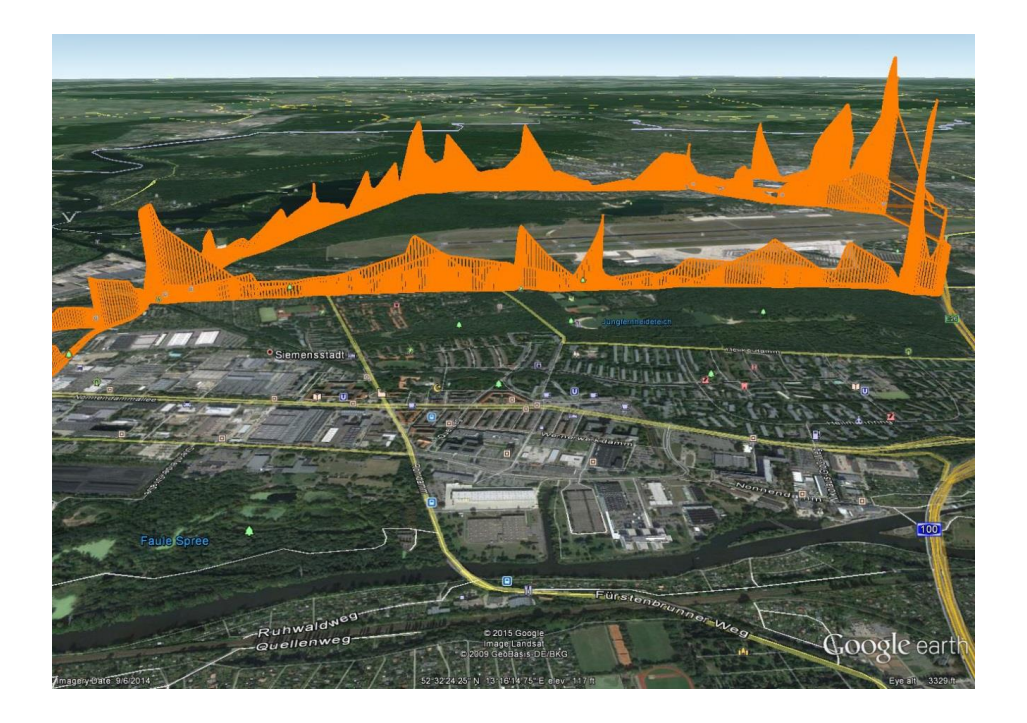


Fig. 10: Measurement drive with MobiLab in August 2017 in Berlin. Result of NO_x measurements during multiple circumnavigations of Tegel Airport with the mobile measurement laboratory. The measured NO_x concentration was clearly influenced by the prevailing road traffic density and traffic light phases. A clear influence of the NO_x emissions emitted by air traffic on the measured NO_x concentration levels could not be determined in the leeward area of the airport.

Fig. 11 shows the NO_x concentration curve during a measurement drive with MobiLab in the same measurement period in August 2017. Under western inflow conditions (period: 10:00 - 15:50 UTC, wind speed 2 - 3 m/s), both the centre and the windward hinterland of Berlin were probed. While NO_x mixing ratios of well over 100 ppb were found in the inner city area, the NO_x background values were only about 3 ppb⁶.

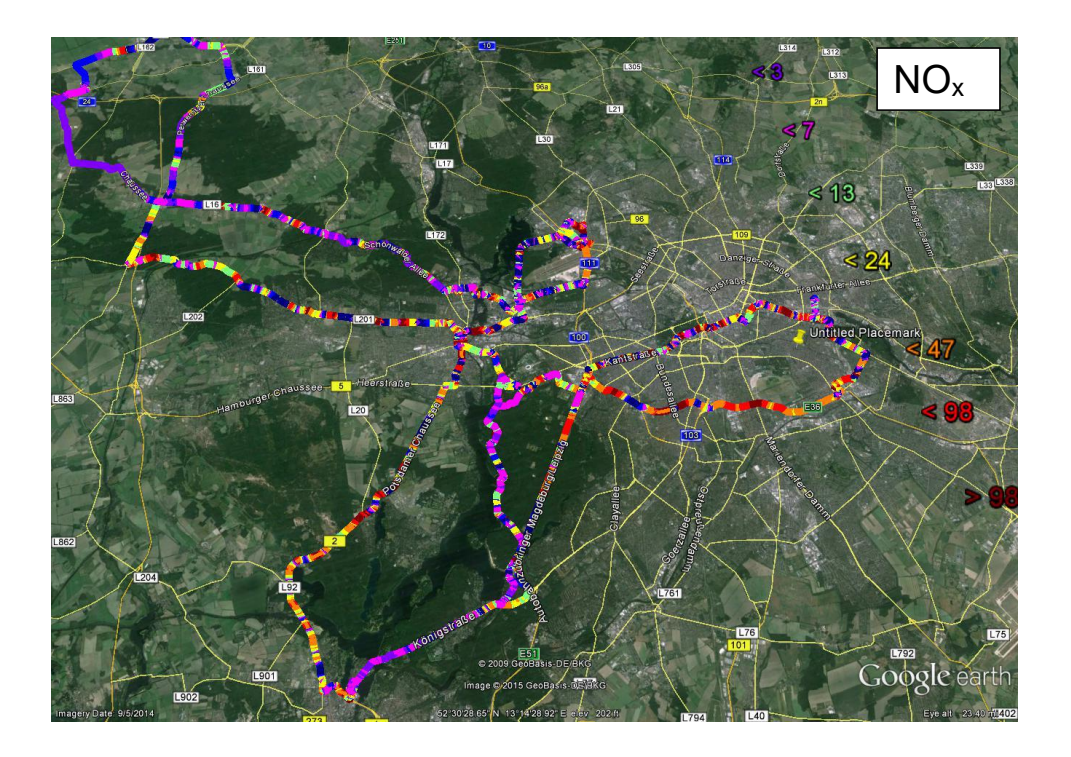


Fig. 11: Measurement drive with MobiLab-II in August 2017 in Berlin and in the windward Berlin hinterland. Maximum NO_x values were found in the inner-city area and on the inner-city motorways. In the windward Berlin hinterland the NO_x background value measured only about 3 ppb⁷.

⁶ For the daytime-dependent distribution of NO_x in NO and NO₂ away from nearby NO sources see Fig. 2.

⁷ These low summer NO_x background concentrations are in good agreement with the MobiLab results of the PEGASOS campaign in the Netherlands in summer 2012 [Ehlers, 2013, Ehlers et al., 2014], where NO_x background concentrations of 4 ppb were observed in rural areas of the Netherlands.

The same climatologically oriented approach was chosen for the second study area (metropolis with structured terrain, city of Stuttgart). As part of a campaign lasting several days, MobiLab was used for measurements under winter conditions.

Fig. 12 shows the selected route through the Stuttgart hinterland and crossing the city in February 2017. It is clearly visible that the highest NO2 mixing ratios occur in the city area of Stuttgart along the B-14, while the route sections in the outskirts of Stuttgart (Kaltental and Botnang) with about 21 ppb NO₂ are more than a factor of 5 lower than those of the inner-city area around the Neckartor.

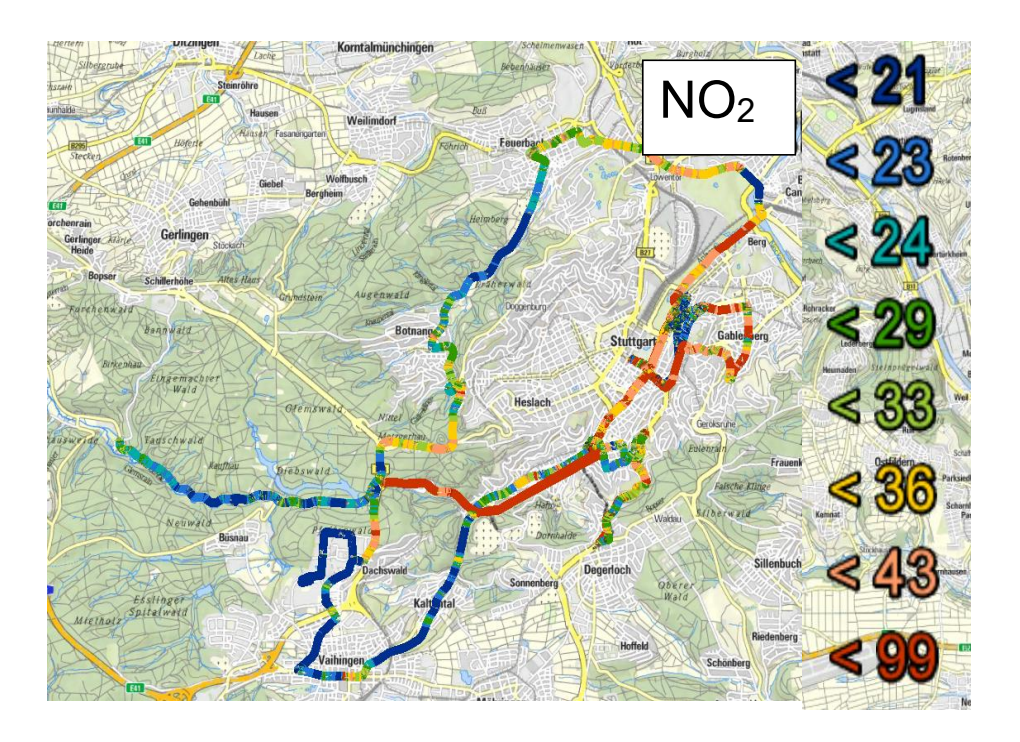


Fig. 12: NO2 mixing ratio [ppb] for 20 February 2017, measured in the Stuttgart basin and in the surrounding marginal areas (Kaltental and Botnang). Highest NO2 mixing ratios were observed in the urban area of Stuttgart along the B-14, while the travel sections in the peripheral areas of Stuttgart (Kaltental and Botnang) with about 21 ppb NO₂ are more than a factor 5 lower than those of the innercity area around the Neckartor.

In order to estimate the pollution level during city trips, the MobiLab was used to investigate the spatial extent of the Neckartor concentration "hotspot" in the Stuttgart city area under winter conditions. Fig. 13 shows a detailed view of the area around the Neckartor from a measurement drive in February 2017. For this purpose, the surroundings of the Neckartor were examined by a series of mobile investigations. Fig. 13 shows a part of the Schlosspark, the B-14 and the Neckartor in the foreground of the picture. Highest NO₂ mixing ratios were observed along the B-14. Already at a distance of 50 - 100 m the NO₂-mixture ratios decreased significantly. In the area of the Kernerplatz, the NO₂ mixing ratios of about 27 ppb were only a few ppb above the regional background values determined on the same day (c. f. Fig. 12).

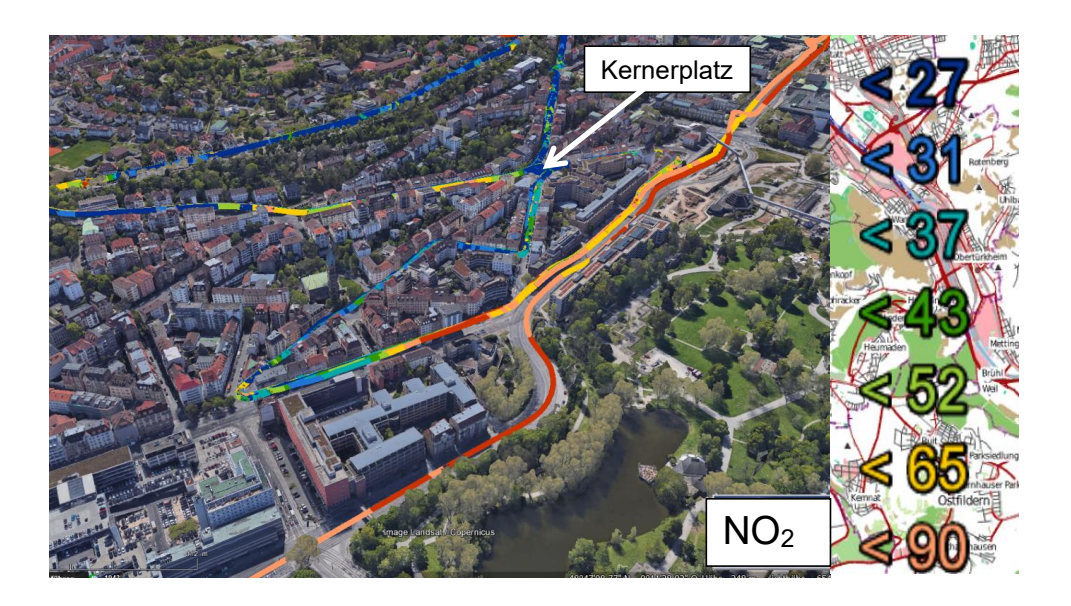


Fig. 13: NO₂ mixing ratio [ppb] for February 2017 measured in the Stuttgart basin in the Neckartor area and on the adjacent Kernerviertel at Uhlandshöhe (wind speed 2 - 3 m/s). Highest NO2 mixing ratios were observed along the B14. Already at a distance of 50 - 100 m the NO2-mixture ratios decrease significantly. In the area of the Kernerplatz, the NO₂ mixing ratios of about 27 ppb were only a few ppb above the regional background values determined on the same day (c. f. Fig. 12).

The following conclusions can be drawn from these studies in two metropolitan regions:

- The winter regional backgrounds of NO_x can be up to a factor of 10 higher than the summer regional backgrounds. Since the regional backgrounds and the contribution of the city behave additively (cf. Fig. 5), significantly higher levels of pollution⁸ are to be expected in winter than under summer conditions.
- It was found that meteorological conditions sometimes have a stronger influence on regional background concentrations than orographic conditions. Thus for the respective winter measuring periods a mean regional background for Berlin was found during a pronounced weak wind situation of 45 ppb NO₂ (January 2017), whereas the mean regional background for Stuttgart in February 2017 was only 21 ppb of NO2.

A further aspect of our long-term study dealt with the description of representative nitrogen oxide mixing ratios for various road types in the Rhine-Ruhr metropolitan region. In the course of 2015, the route network plan shown in Fig. 14 for the mobile measurements in NRW was developed. The route network covers relevant areas from less frequented country roads in the Eifel to the heavily frequented motorways in the Ruhr area.

An essential criterion for the selection of the routes was the characterization of typical routes over medium distances, such as those frequently used by commuters in the Ruhr area. For the same reason, more rural areas in the Eifel were also included in the measurement program in order to record a characteristic driving profile for rural areas. In this way, the loads acting on fuel cell vehicles can be comprehensively characterized. In the further course of the project, the routes used were repeatedly sampled so that the temperature and weather as well as the traffic situation on the roads could also be recorded representatively and included in an evaluation.

Table 3 gives an overview of the proportion of measurement time for the various road types (cf. caption to Fig. 14) on the routes of the Rhine-Ruhr measurement area covered by MobiLab.

⁸ The NO_x reduction technology (usually SCR catalytic converters) installed in EURO 6 diesel vehicles switches off at low temperatures, thus increasing the NOx emissions of the current vehicle fleet (cf. footnote 14) and thus the ambient air concentrations in the city during the cold season.

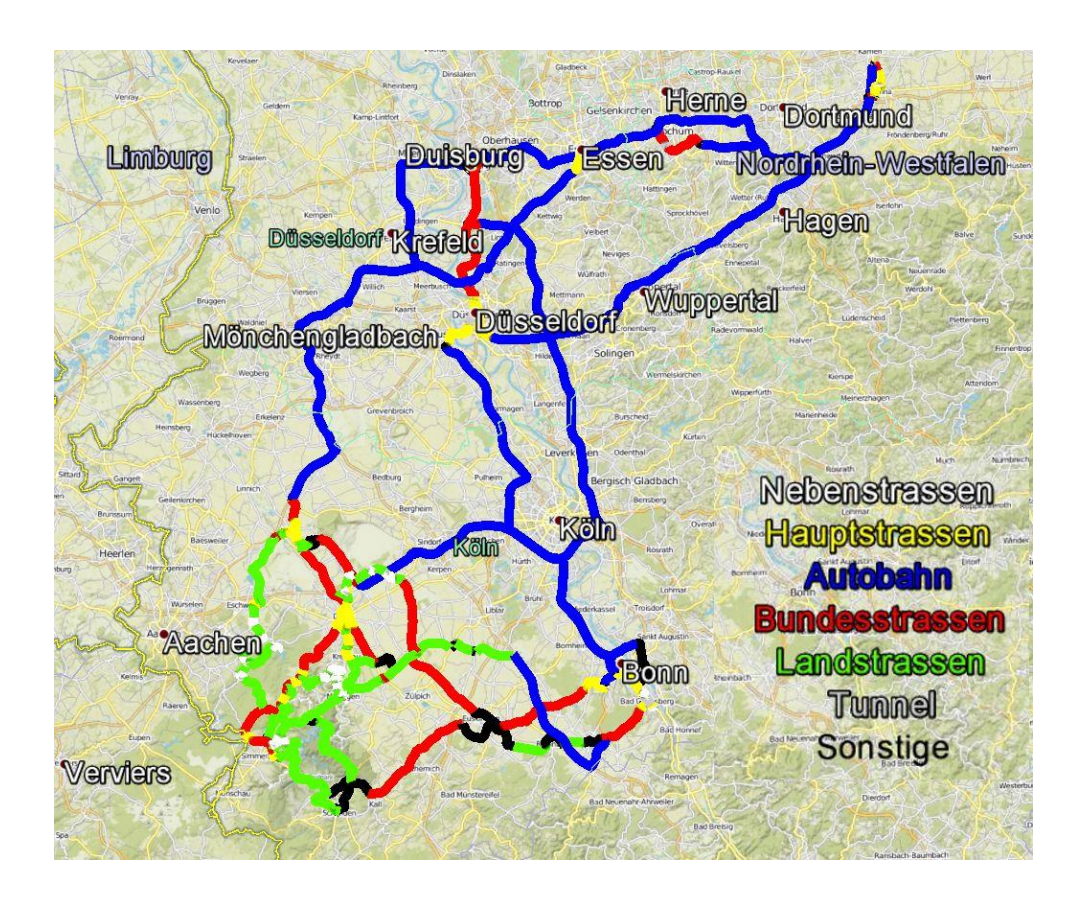


Fig. 14: Overview of the various measuring sections of the Rhine-Ruhr measuring area which we travelled with MobiLab several times in the course of 2015. In addition to the motorway sections in the Ruhr area, the routes include urban areas and rural backgrounds in the Eifel. The different areas are color coded: Autobahn (blue), trunk roads (Bundesstraßen, red), primary roads (Hauptstraßen, yellow), secondary roads (Landstraßen, green), tertiary roads (Nebenstraßen white), road tunnels (Tunnel, light grey) and small sections not classified in the previous areas (black).

Table 3: Percentage of total measuring time for the different road types (cf. explanation of Fig. 14) of the Rhine-Ruhr measuring area.

Roads Category	Contribution / %	Roads Category	Contribution / %
Autobahn	16.8	Landstraßen	10.5
Autobahn-Tunnel	0.3	Nebenstraßen	10.9
Bundesstraßen	9.0	Other (Sonstige)	18.2
Hauptstraßen	29.6	Tunnel	4.7

A comparative analysis of the various regions for nitrogen oxides showed extremely high concentrations in tunnels. The "Rheinufer" tunnel in Düsseldorf and the "Bad-Godesberg" tunnel in Bonn were included in the regular measurement plan of the Rhine-Ruhr studies, so that the high mixing ratios found could be statistically confirmed by a large number of individual passages at different times of the year.

Fig. 15 shows the mean values, medians, 25th and 75th percentiles of the MobiLab measurements for the nitrogen oxide mixture ratios of various road types in the Rhine-Ruhr measuring area. In Fig. 16 the MobiLab driving speed distribution during the measurements is depicted.

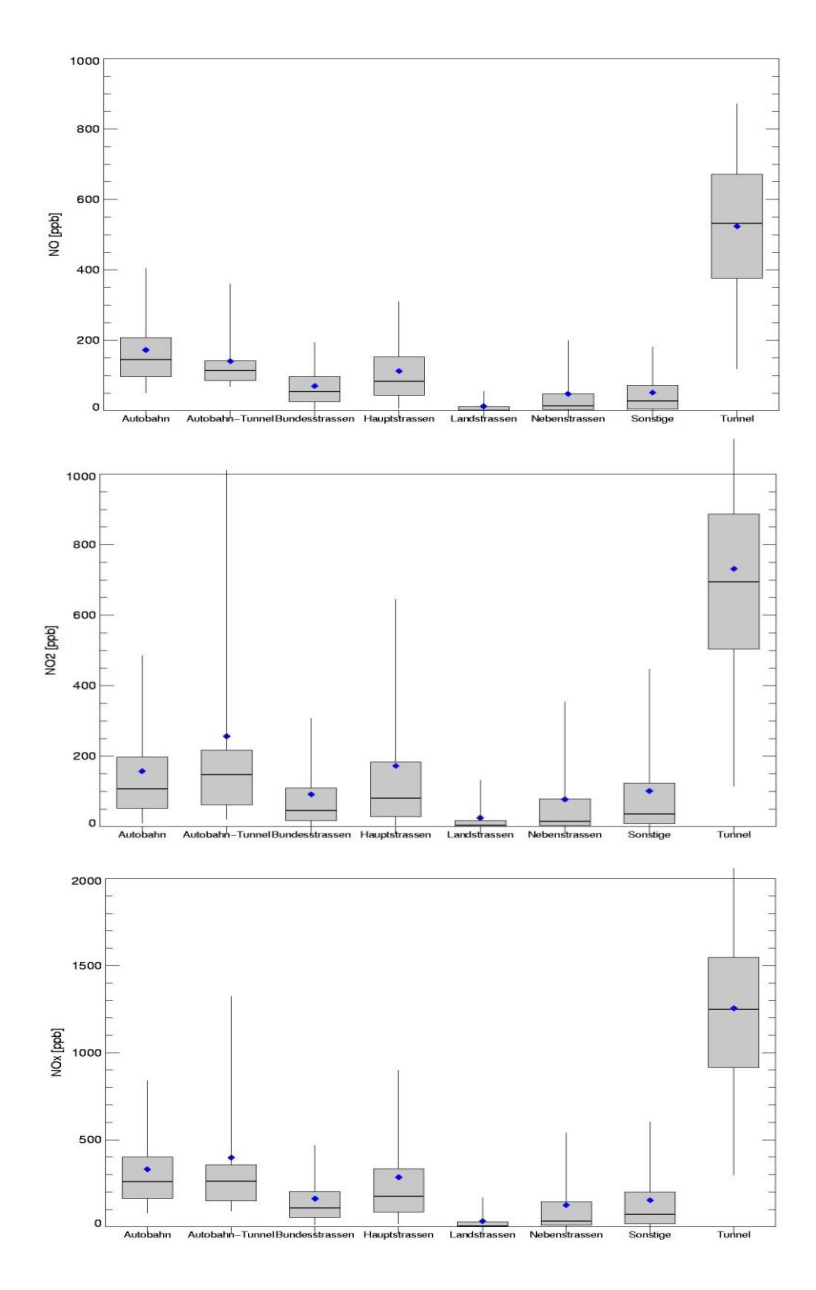


Fig. 15: Concentration overview of NO, NO₂ and total nitrogen oxides (NO_x), for the different road types (cf. classification, as indicated in Fig. 14). The black crossline indicates the respective mean value of the concentration, the blue dot indicates the median value. The grey box marks the 25^{th} to 75^{th} percentile and the vertical black lines indicate minimum and maximum values.

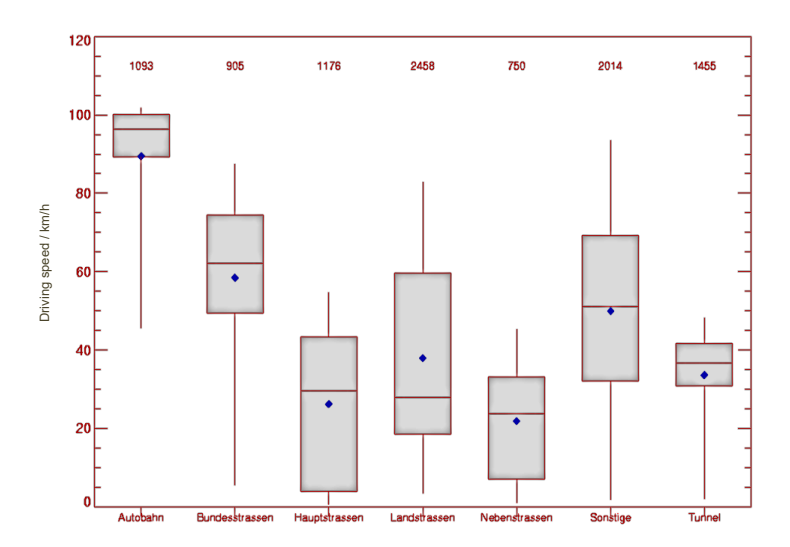


Fig. 16: Characterization of the MobiLab driving speed distribution during the measurements for the different road types (cf. classification in Fig. 14). The number values arranged above the road types indicate the respective ensemble size for the nitrogen oxides minute averages (minute averages; consisting of 20 individual measurements each + 2 background determinations). While on multi-lane road types (Autobahn, trunk roads (Bundesstraßen)) the MobiLab driving speed can be lower than that of the average car fleet due to its truck speed limitation, for single-lane road courses the given profile is a good measure for the speed profile of the entire car fleet. The black transverse line indicates the respective median value of the speed, the blue dot indicates the mean value. The grey box marks the 25th to 75th % percentile and the vertical black lines indicate minimum and maximum values.

For the primary roads (Hauptstraßen) the dependence of the total nitrogen oxide concentration (NO_x) on the outside temperature is shown in Fig. 17. For the mean concentrations there is a linear correlation with a gradient of -12.2 ppb/°C and an intercept of 457 ppb. The correlation coefficient is $R^2 = 0.619^9$.

$$t_0 = R \cdot \sqrt{\frac{n-2}{1-R^2}} = 0.78 \cdot \sqrt{\frac{21}{1-0.62}} = 5.79 > 1.714$$

⁹ With a confidence interval of 95%, a result greater than 1.714 is considered significant for the t-test with 23 degrees of freedom:

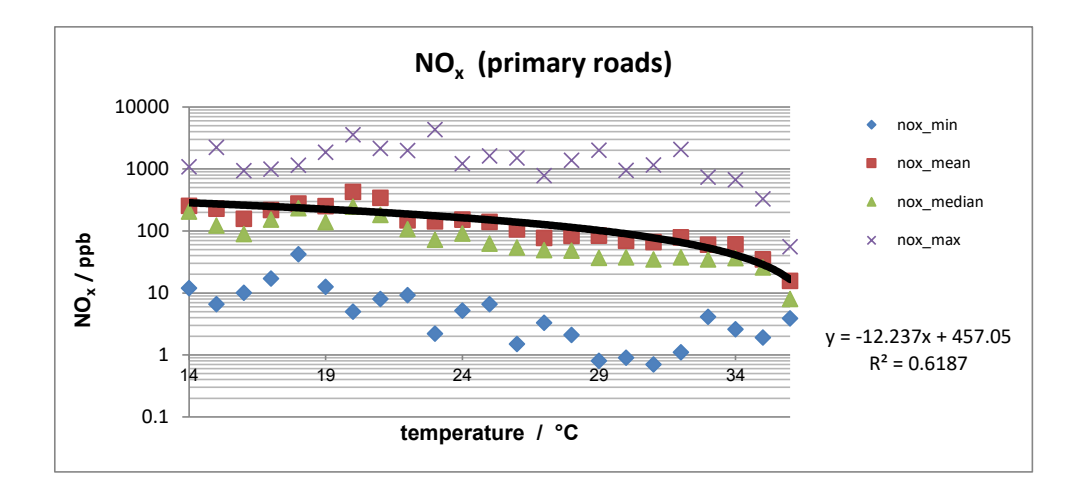


Fig. 17: Temperature dependence of the total nitrogen oxide (NO_x) concentration for measurements on primary roads (Hauptstraßen). The maximum concentrations (black), the median concentrations (blue), the mean concentrations (red) and the minimum concentrations (grey) are plotted as diamonds. The solid line shows the linear trend. For the mean concentrations (black line) there is a linear correlation with a slope of -12 ppb/°C and an intercept of 460 ppb. The correlation coefficient is $R^2 = 0.62$.

Here the significant trend in concentrations shows that the vertical mixing in the atmosphere, which also increases with rising temperatures, leads to a greater dilution of the nitrogen oxide concentrations on the main roads. A second reason for the NO_x trend increasing with decreasing temperature is the fact that the nitrogen oxide exhaust gas cleaning of new EURO 6 diesel engines is currently only insufficiently effective at low temperatures (see UBA, 26. 04. 2017) or only starts after a long warm-up phase (see e. g. [Ehlers et al., 2017]. The Handbook of Emission Factors has taken this into account in its latest version (HBEFA 3.3) [Keller et al., 25. 04. 2017] by introducing external temperature-dependent correction factors which approximate the increase in NO_x emissions from diesel cars¹⁰.

 $^{^{10}}$ The following NO_x emission increases between the standard temperature of 20 °C and the temperature of 0 °C are linearly approximated in version 3.3 of HBEFA: EURO-4: factor 1.4; EURO-5: factor 1.8; EURO-6: factor 1.9.

5.2 Tunnel studies

Fig. 18 shows the time series of NO and NO2 during the passage through the Heslacher Tunnel in Stuttgart in November 2016.

Under conditions where photochemical processes are almost negligible, the NO/NO2 ratios observed here reflect the average emission ratio of the vehicle fleet passing through the tunnel. It should be noted that such changes in the immission ratios of NO/NO₂ at the same total nitrogen oxide concentration have repercussions on the kind and extent of NO_x damage potential of a fuel cell stack¹¹ [see also literature review in: A. Talke, 2017].

¹¹ At the same initial concentration, the damaging effect of NO on a fuel cell stack occurs significantly faster than for the harmful gas NO2. Private Communication, U. Misz, ZBT, 2015.

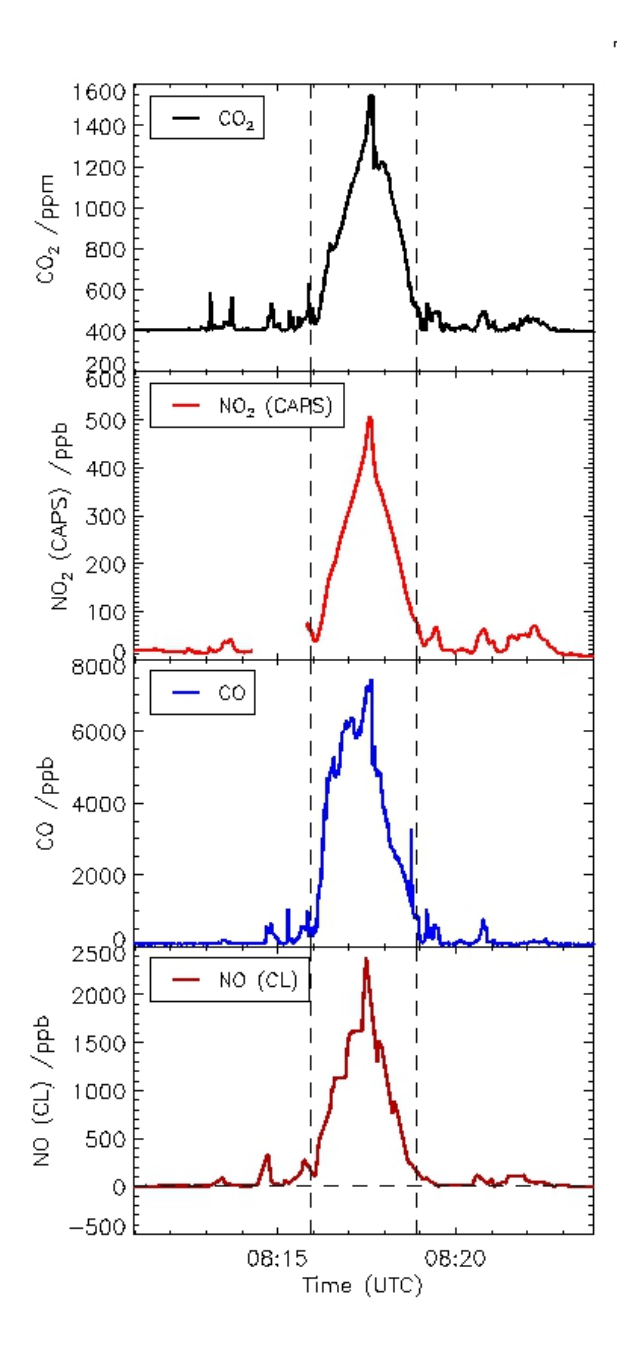


Fig. 18: Concentration patterns of CO₂, NO₂, CO and NO during the passage of the Stuttgart Heslacher Tunnel in November 2016 with MobiLab-II (tunnel passage 8:16 - 8:19 UTC). It can be seen that the NO mixing ratios [NO (CL)] measured in the tunnel are four times higher than the NO₂ mixing ratios [NO₂ (CAPS)] measured simultaneously.

It was already pointed out in the previous section that a significant "added value" of the investigations with MobiLab is that as many relevant trace substances as possible can be measured simultaneously and at a particularly high temporal resolution. However, these capacities were only available after MobiLab-II had been completed (e.g. fast NH₃ laser measuring system, fast SO₂ measuring system).

For this reason, some of the studies already carried out with MobiLab-I were supplemented by additional investigations using the extended measurement equipment of MobiLab-II. This primarily concerned the extension of the tunnel studies already carried out in the Rhine-Ruhr area by further tunnel studies in Southern Germany. It turned out that the Stuttgart Heslacher Tunnel in Stuttgart is particularly suitable for this purpose:

- The Heslacher Tunnel connects the Stuttgart motorway junction with the B-14 which runs directly through Stuttgart and therefore has an extraordinarily high traffic volume (throughput: approx. 50000 vehicles/weekday, including 2500 trucks).
- Its length of approx. 2300 m is sufficient, that atmospheric trace substances (in this case ozone) introduced by vehicle-induced turbulence have no noticeable effects on the measured nitrogen oxide content distributions.
- The changing load situations (constant speed conditions outside the rush hour times, stop-and-go conditions during the rush hour times) allow the investigation of different emission conditions of the current vehicle fleet.
- The good traffic connection of the tunnel allows a high frequency of tunnel passages by MobiLab.

The source attribution of tunnel measurements is particularly simple, as the pollutants here clearly originate from the source traffic. Characteristic parameters are the trace substance/CO2 ratios of a current transport fleet, as they represent a measure of the trace substance emission standardized to fuel consumption. Fig. 19 shows the trace gas concentrations measured for CO2, NO2, NH3 and SO2 during a crossing of the Heslacher Tunnel. In addition, two correlation plots of the measured second data of NO₂ (CAPS) vs. CO₂ and SO₂ vs. CO₂ are shown (Fig. 20), which provide

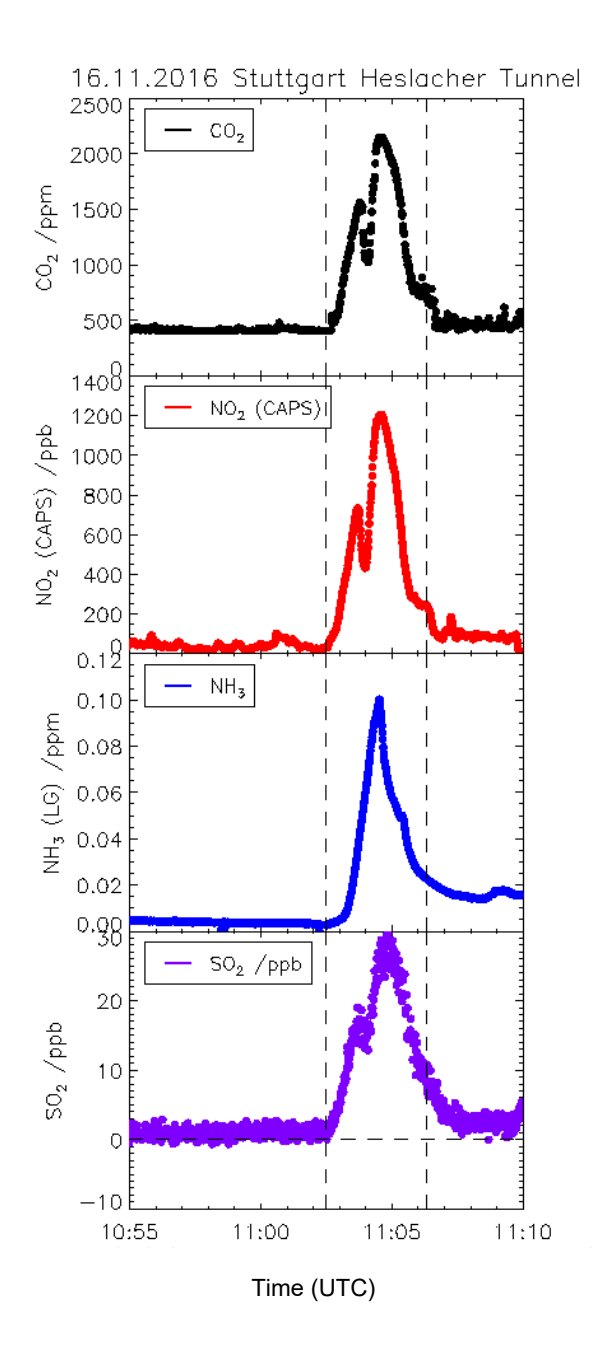


Fig. 19: Trace gas measurements of CO₂, NO₂, NH₃ and SO₂ during the passage of the Heslach Tunnel in Stuttgart on 16. 11. 2016. The trace gases rise synchronously with the measured CO2. For the NO/NO₂ ratio see also Fig. 18 from another Heslach tunnel passage on 10.11.2016.

information on the observed emission ratios of NO₂/CO₂ [ppb/ppm] and SO₂/CO₂ [ppb/ppm].

By normalizing to the simultaneously measured CO2 signal (cf. Fig. 20), emission factors of the current vehicle fleet can be tested experimentally. It has to be considered that the atmospheric CO₂ background values are not negligible compared to the CO₂ values observed in the tunnel. Still, the emission ratio can be obtained from the slope of the regression line. In the Heslacher Tunnel the following

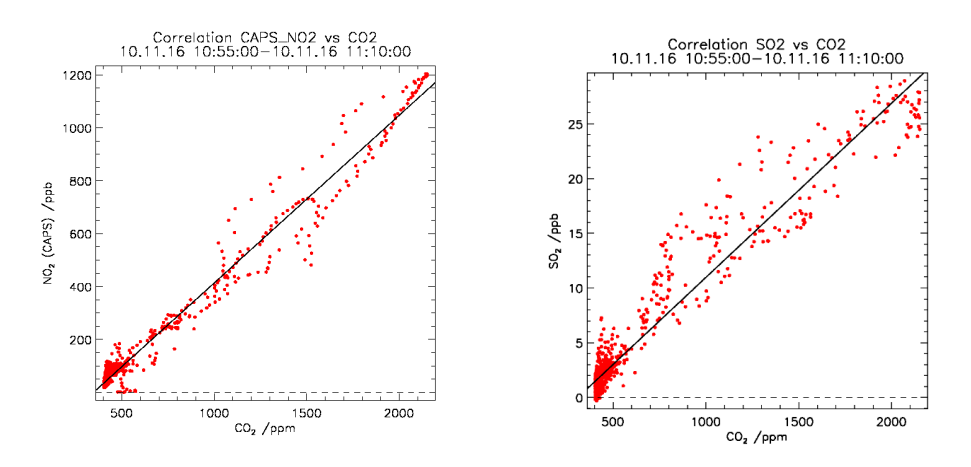


Fig. 20: Examples for correlation plots of the second data of NO₂/CO₂ and SO₂/CO₂ during the passage of the Heslacher Tunnel on 10.11.2016 10:55 - 11:10 UTC . These measurements were carried out outside the rush hour times, so that constant speed conditions (45 +- 5) km/h prevailed during these measurements. It can be seen that the CO2 second data have an offset of 400 ppm caused by the atmospheric background of the CO2.

trace emission ratios were determined:

Detailed analysis of the various tunnel passages in November 2016 on weekdays (with a truck share of about 5 %) showed:

 0.6 ± 0.2 NO₂/CO₂ [ppb/ppm]:

or with NO/NO₂ \approx 3/1(cf. Fig. 18) and NO_x = NO + NO₂

 2.5 ± 0.5 $NO_{x/}CO_2$ [ppb/ppm]:

 0.06 ± 0.01^{12} NH₃/CO₂ [ppb/ppm]:

 SO_2/CO_2 [ppb/ppm] : **0.02 ± 0.003**

Another aspect of the tunnel studies concentrated on a climatology of the NO_x/CO₂ratios of the current vehicle fleet. For these studies we used MobiLab measurements from the Tiergartentunnel in Berlin and from the Heslacher Tunnel in Stuttgart. For both locations, both summer and winter tunnel passages were available, so that the temperature dependence of the emitted NO_x/CO₂-ratios could be comprehensively studied. Fig. 21 shows the NO_x/CO₂ ratios determined on the basis of the various tunnel passages as a function of the outside temperature (mean value before/after the tunnel).

Simultaneous nitrogen oxide and CO2 measurements showed that under winter conditions the nitrogen oxide emissions of the vehicle fleet normalized to fuel consumption (i.e. CO₂) are about 50 % higher than under summer conditions¹³:

 $(NO_x/CO_2)^{summer} = 1.8 \text{ ppb/ppm}; (NO_x/CO_2)^{winter} = 2.9 \text{ ppb/ppm}.$

¹² In the course of the investigations by means of MobiLab within the scope of the BMBF-funded urban climate project 3DO (funding code (O1LP1602F)), far higher NH₃ to CO₂ ratios were observed several times behind diesel-powered EURO-6 city buses (equipped with SCR-NO_x exhaust gas cleaning) [Wegener et al., 2017]. While the NH₃/CO₂ ratios of 0.06 [ppb/ppm] in Figure 19 are primarily caused by side reactions during the conversion of nitrogen oxides to the 3-way noble metal catalysts of petrol engines, the NH₃/CO₂ ratios of about 1 [ppb/ppm] observed here are clearly attributable to the NH₃ slip of the SCR catalytic converter. Comparably high NH₃/CO₂ ratios were also observed behind EURO-6 trucks on gradients on motorways. It will be the task of further investigations to observe the possibly increasing NH₃ slip from traffic with increasing age of the SCR cats and to evaluate its significance next to the agricultural source [UBA, 2017] which has been predominant so far.

¹³ A significant influence of these proportions by the NO_x emissions of petrol-driven vehicles can be ruled out. Already for the vehicle fleet of the year 2008 (measured in the Düsseldorfer Rheinufertunnel) a share of about 80 % of the NO_x emissions could be assigned by us to the diesel-powered vehicles [Klemp et al., 2012]. Ehlers, 2013] achieved an almost equal share of diesel in NO_x emissions when measuring in the Rheinufertunnel in 2012.

The reason for this observation is the limited functionality of the catalytic converter technology used at lower outside temperatures¹⁴.

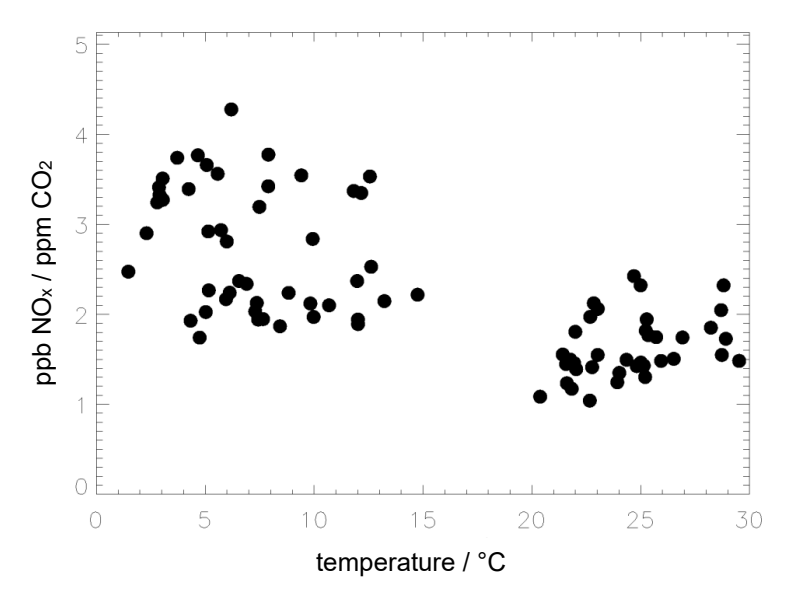


Fig. 21: NO_x/CO₂ ratios measured in the Berlin Tiergarten Tunnel and in the Stuttgart Heslach Tunnel as a function of the outside temperature (mean value before/after the tunnel).

From earlier investigations it is known (e.g. Klemp et al., 2012, Ehlers et al., 2017) that diesel vehicles with oxidation catalysts emit a considerable part of their NO_x emissions in the form of NO₂. This is due to the fact that the oxidation catalyst used, in addition to reducing CO and VOCs (depending on the catalyst temperature), converts part of the NO originally produced by the engine to NO₂ with the residual oxygen present in the diesel exhaust gas. Since the NO-to-NO₂ equilibrium responsible for this has its NO₂ maximum at several hundred degrees, the NO₂ content in diesel exhaust increases under inner-city partial load conditions with rising outside temperature (cf. Fig. 22).

In contrast, the exhaust gas from petrol engines with 3-way catalytic converters contains significantly lower nitrogen oxide concentrations than that from diesel vehicles

¹⁴ The same conclusion is reached by the editors of version 3.3 of the manual for emission factors. Taking into account the sharp increase in passenger car diesel NO_x emissions at lower operating temperatures, the average NO_x emissions of this engine type rose from 575 mg/km to 767 mg/km for the reference year 2016 [UBA, 26.04.2017].

(see footnote 16). Moreover, their NO_2 content in the NO_x emitted is low and amounts to only a few percent of their NO_x emissions.

Fig. 22 shows the NO_2 mixture ratios standardized to fuel consumption (i.e. CO_2 emissions) for the tunnel measurements.

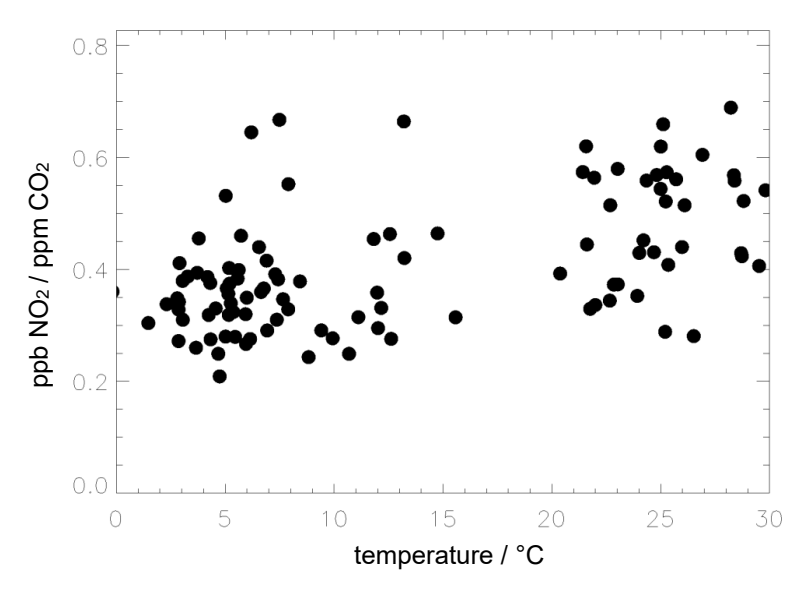


Fig. 22: NO₂/CO₂ ratios measured in the Berlin Tiergarten Tunnel and in the Stuttgart Heslach Tunnel as a function of the outside temperature (mean value before/after the tunnel).

Even though the mean values calculated from a linear regression (cf. Fig. 20) of the NO₂ concentrations normalized to the respective CO₂ output vary considerably, a significantly increasing NO₂/CO₂ ratio can be observed with increasing outdoor temperature: 0 °C < T < 10 °C: 0.37 NO₂/CO₂ [ppb/ppm]. For the temperature interval 20 °C < T < 30 °C the result is: 0.44 NO₂/CO₂ [ppb/ppm]. This observation is consistent with the assumption that a lower outside temperature leads to lower mean operating temperature of the diesel oxidation catalysts 15 used.

The comparison of the averaged results from Fig. 21 and Fig. 22 allows the determination of the averaged NO_2 content in the NO_x emissions of the 2016 vehicle fleet for summer and winter conditions:

¹⁵ The publication of a detailed analysis of the tunnel measurements including counting loop measurements is currently in preparation.

In winter, a mean share of NO₂ in the NO_x mixing ratio of 12 % was found. Under summer conditions, the proportion of directly emitted NO₂ in NO_x was twice as high at 24 %.

It has already been pointed out that the ratio of NO/NO2 at the same total nitrogen oxide concentration NO_x has repercussions on the shape and extent of the nitrogen oxides damage potential of a fuel cell stack¹⁶ [cf. literature overview in: A. Talke, 2017]. Fig. 23 shows the existing SO₂/CO₂ ratios [ppb/ppm]. It is known from the literature that SO₂ or H₂S in the cathode air lead to irreversible deactivations of the catalyst material by establishing strong bonds between active catalyst centres and the sulfur atoms [Mothadi et al., 2004]. Unfortunately, in contrast to nitrogen oxides, no sufficiently statistically verified climatology could be established for SO₂ since in the case of winter measurements only a single measured value exists so far due to measuring problems with the instrument.

¹⁶ In addition, the emission ratio of NO/NO₂ from the source traffic is also of particular interest for urban air quality considerations, since apart from the titration of NO with background ozone only direct NO2 emissions can produce an exceedance of the legally regulated NO₂ limit value of 40 µg/m³ (corresponds to a mixing ratio of 21.3 ppb). In fact, the efficiency of NO₂ generation in the oxidation cat depends not only on the catalyst temperature but also strongly on the catalyst material used (the catalyst material platinum [cf. Zellner et al., 2012] leads to significantly higher NO2 contents in the exhaust gas under otherwise identical conversion conditions (private communication, [J. Dornseiffer, 2018] as its alternative palladium.

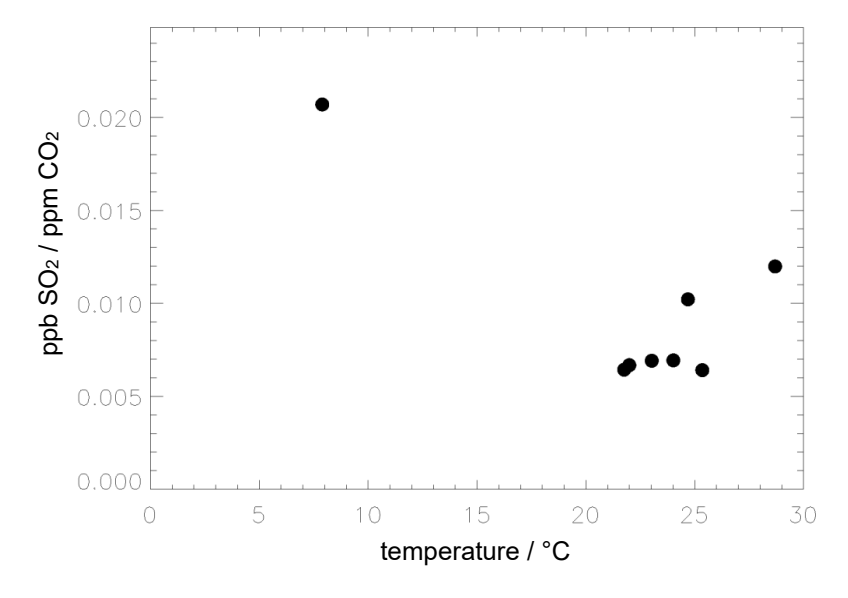


Fig. 23: SO₂/CO₂ ratios measured in the Tiergarten Tunnel (Berlin) and in the Heslacher Tunnel (Stuttgart) as a function of the outside temperature (mean value before/after the tunnel).

For the summer tunnel passages, a mean ratio of SO_2/CO_2 of: 0.0075 [ppb/ppm] was found for the temperature interval of 20 °C < T < 30 °C. The only evaluable tunnel measurement under winter conditions, however, provides an SO_2/CO_2 ratio of: 0.02 [ppb/ppm] (see also Fig. 19). It will be the subject of future investigations whether the indicated seasonal variation in the SO_2/CO_2 ratio is confirmed¹⁷.

5.3 "AMS-test track" in the Stuttgart area

In the course of the reporting period, the new MobiLab-II with its extended measurement analytics was used for comprehensive investigations of traffic-loaded areas in southern Germany. In contrast to the previous periods (in which repeated investigations of a selected measuring area in NRW to determine a "harmful gas

¹⁷ Since October 2009, an upper limit of 10 ppm/kg fuel sulfur exists for both petrol and diesel fuel (according to EN 590). In particular, there is also no indication in the fuel specifications that the seasonal change from "summer fuel" to "winter fuel" would lead to an increase in the sulfur content.

climatology" were in the focus), additional campaign-like investigations were carried out in 2016 in heavily traffic-loaded regions of southwestern Germany.

One of the focal points was the test section in the Stuttgart area (AMS round, cf. Fig. 24). This test track was selected at the suggestion of the consortium partner Daimler AG (Dr. Talke / Dr. Konrad) in order to be able to "follow" the immission behaviour found there for the fuel cell test under realistic conditions on the test bench. The distance is 93 km and contains different types of roads (city traffic, motorway, country road and federal road), the driving time is about 2 hours. The task of the Jülich MobiLab-II was to comprehensively characterize the immission behaviour of the surrounding traffic.



Fig. 24: "Auto, Motor und Sport"-measuring round [Leyrer, AMS, 2010].

Figs. 25a and 25b describe the observed ambient air concentrations of NO₂, CO, O₃ and NH₃ during the circumnavigation of the AMS measuring round. A total of 3 test rounds were completed. The dotted lines mark the passage through the Fellbach tunnel.

AMS measuring drive

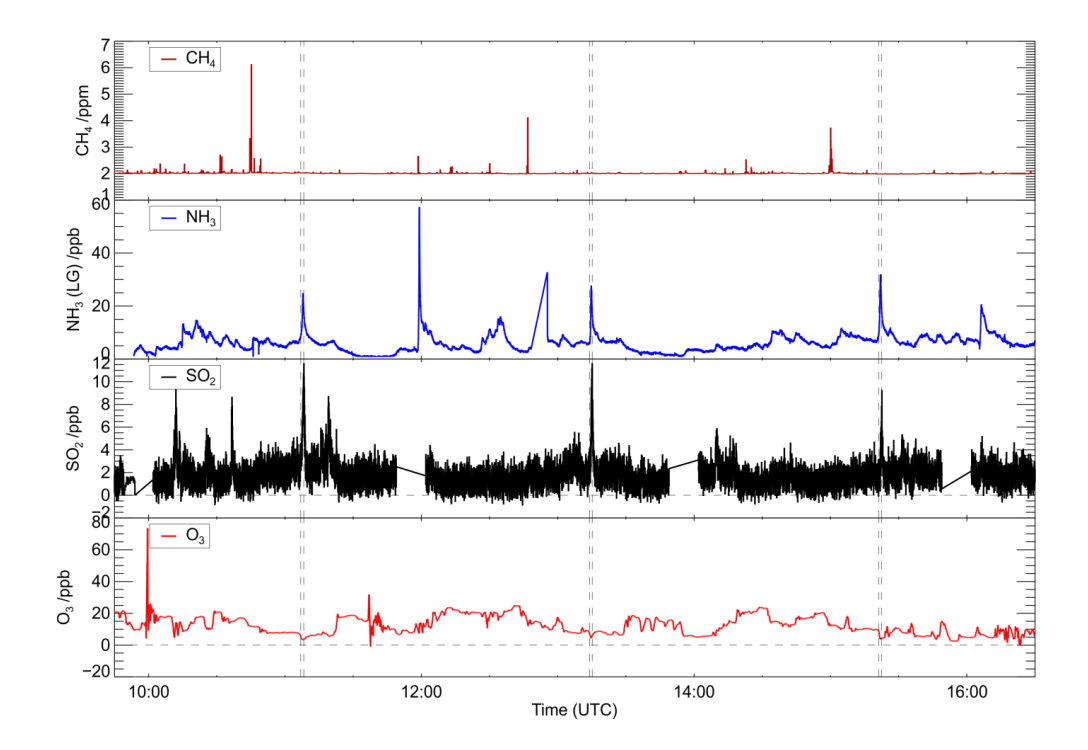


Fig. 25a: Observed concentrations of CH₄, NH₃_LosGatos, SO₂ and Ozone on the "Auto, Motor und Sport" measuring drive. The AMS test drive was passed three times by MobiLab on 9. 11. 2016. The recorded data set contains one-second data of gaseous compounds as well as one-second data of 12 size classes of particle numbers in the range of 5 nm to 10 μ m. These trace gas data are supplemented by GPS information accurate to the second and meteorological parameters. The dotted line marks the passages through the Fellbach Tunnel.



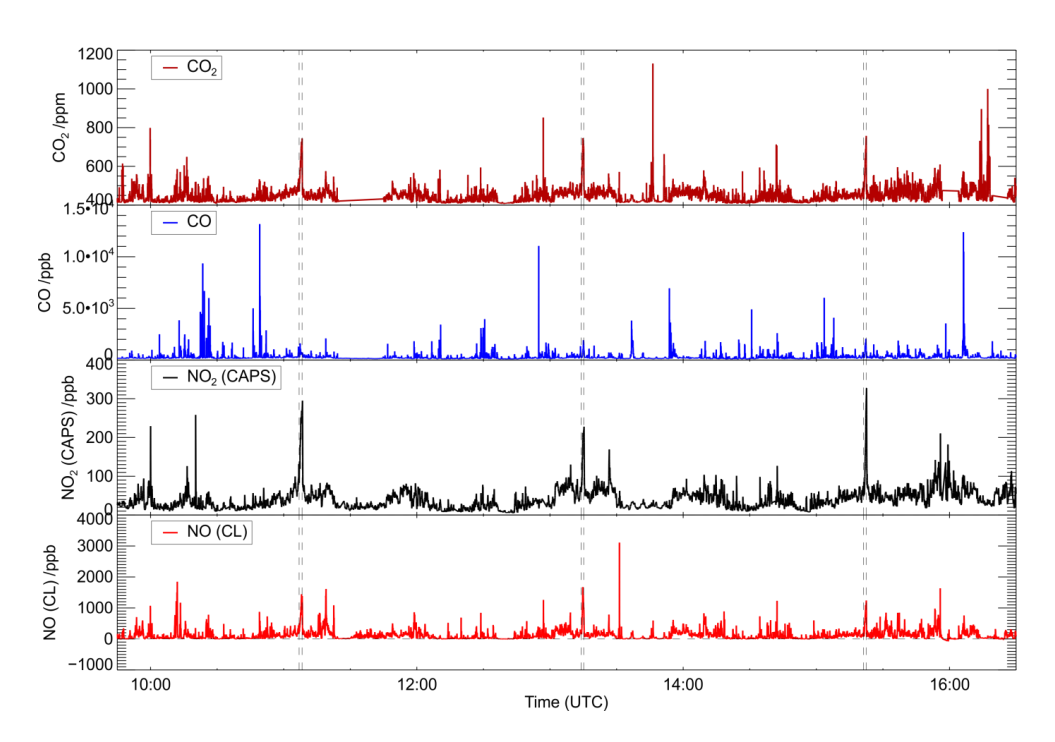


Fig. 25b: Observed concentrations of CO₂, CO, NO₂_CAPS and NO_CL on the "Auto, Motor und Sport" for the same measuring drive shown in Fig. 25a.

The measured trace gases can be classified into the following groups according to their situation-dependent concentration behaviour:

- The highest concentration peaks of CO are caused by individual motor vehicles driving ahead, although weaker peaks can also be observed during the short tunnel passages. The main causes for those emission peaks are likely to be vehicles with catalytic converters that are not yet at operating temperature or CO breakthroughs during full-load enrichment. In the case of methane, emissions from traffic are only of low importance compared to the atmospheric background (recognisable from the lack of increases in methane during the short tunnel passages).
- In the case of nitrogen oxide emissions, both NO and NO₂ show clear increases in concentration during the tunnel passages. For NO2, the relative increases of the tunnel

passages compared to the outside air passages are more pronounced than for NO. Especially during the tunnel passages, the direct emissions of NO₂ from warm diesel vehicles lead to immediate increases in NO2 concentrations. However, individual NO2 peaks are also recognisable in the outdoor air passages, which are only partially accompanied by simultaneously increased NO concentrations.

- Another (but less significant) source of increased NO2 concentrations during tunnel passages are titration effects of NO with ozone, which is carried into the tunnel passages by vehicle-induced turbulence (recognisable from the ozone minima during tunnel passages).
- The clearest increases during the tunnel passages compared to outdoor air passages can be observed for CO2, NH3 and SO2, caused by the reduced dilution of the trace gases mentioned here. However, there are also individual immission peaks for these substances during the outdoor air passages (especially in the case of NH₃), which indicate individual "large emitters" of these trace substances.

Fig. 26 a - k list the median values for the trace gases of interest, 25th and 75th percentiles, minima and maxima and the number of individual values for different route types. According to the attribution in [openstreetmap, 2018], the following route types were distinguished as different route types: Tunnel, Motorway, Trunk Road, Primary Road, Secondary Road and Tertiary Road. A detailed list of the results can be found in Table 6 in the appendix.

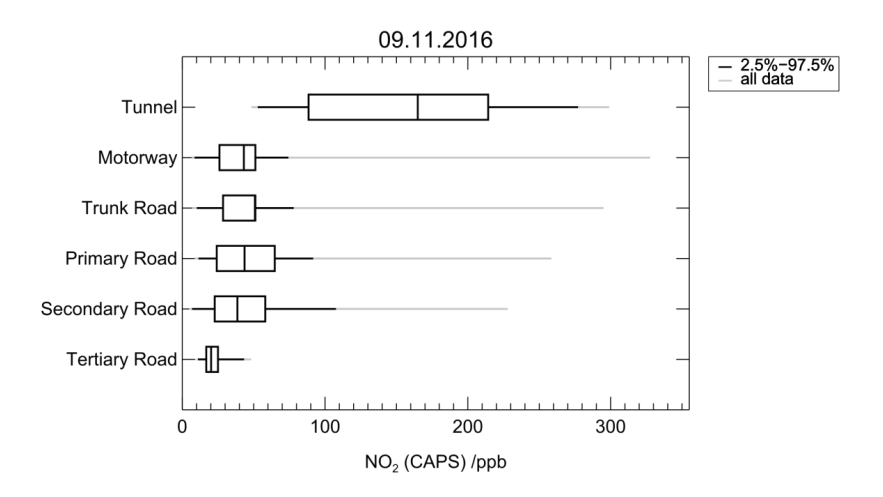


Fig. 26 a: Averaged NO2 (CAPS) concentrations for the various road types of the AMS test round, determined from the measured second data. All data in ppb.

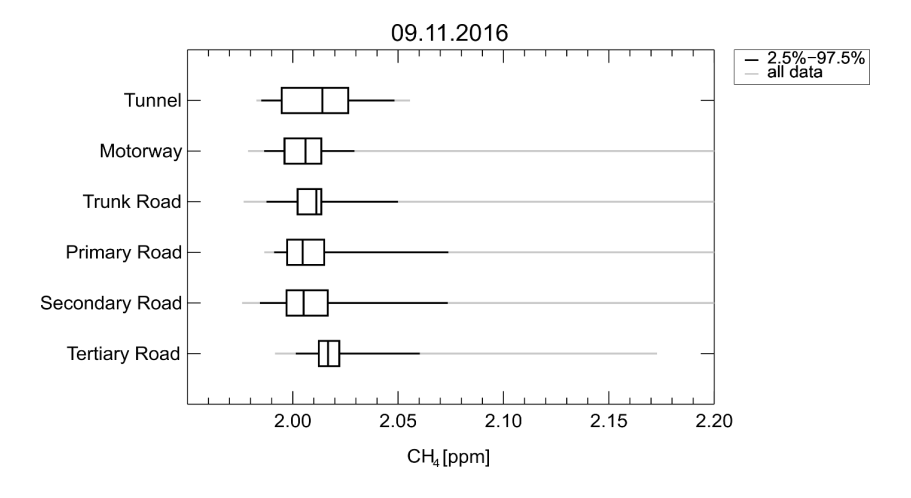


Fig. 26 b: Averaged methane concentrations for the various road types of the AMS test round, determined from the measured second data. All data in ppm.

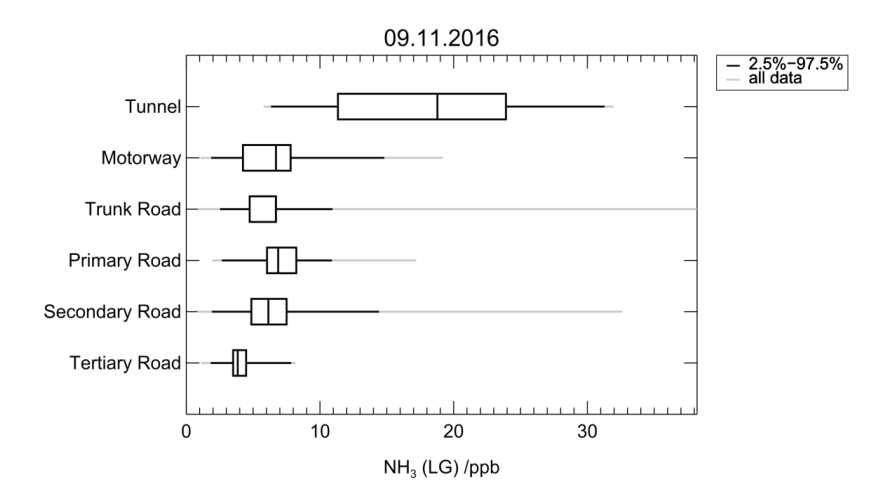


Fig. 26 c: Averaged NH₃ concentrations¹⁸ (Los Gatos Inc., OA-ICOS, Off-Axis Integrated Cavity Output Spectroscopy) for the various road types of the AMS test round, determined from the measured one-second data. All data in ppb.

1:

¹⁸ Two different optical detection techniques were used for the NH₃ measurements: IR detection using long path absorption (ICOS technique), LosGatos Inc., USA: LG_NH3 and Picarro Inc. Cavity-ringdown IR detection. The cavity-ringdown technique requires the use of an absolute filter before the cavity, since the necessary high reflectivity of the mirrors can only be maintained with extreme cleanliness. At low concentrations in the lower ppb range, the absolute filter used tends to produce noticeable "memory" effects, so that in particular the minimum values and 25th percentiles indicated for the Picarro system are significantly higher than for the LosGatos system. In addition, the high suction flow of the LosGatos ensures a considerably faster exchange time of the sample gas (suction flow LosGatos: 35 l/min, suction flow Picarro: approx. 1 l/min). However, the LosGatos system weighing more than 100 kg (unit + Scoll pump) is much more unwieldy than the 19" system from Picarro.

For the verification of higher NH₃ mixing ratios (from approx. 30 - 50 ppb, see also footnote 12), the effect described here is almost insignificant, so that in this range both systems have a good approximation of similar response behaviour.

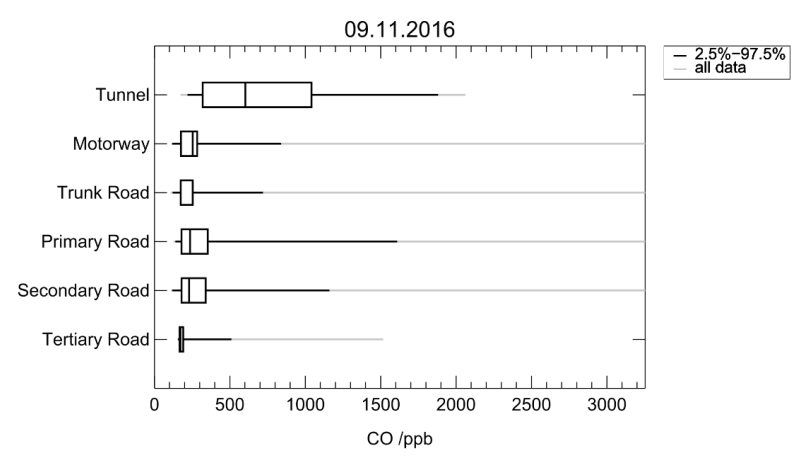


Fig. 26 d: Averaged CO concentrations for the various road types of the AMS test round, determined from the measured one-second data. All data in ppb.

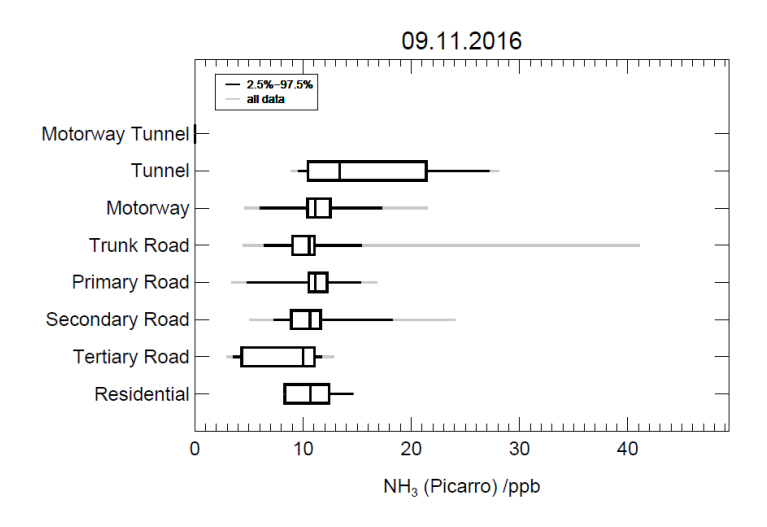


Fig. 26 e: Averaged NH₃ concentrations (Picarro Inc, cavity ringdown detection system) for the various road types of the AMS test round, determined from the measured one-second data. All data in ppb.

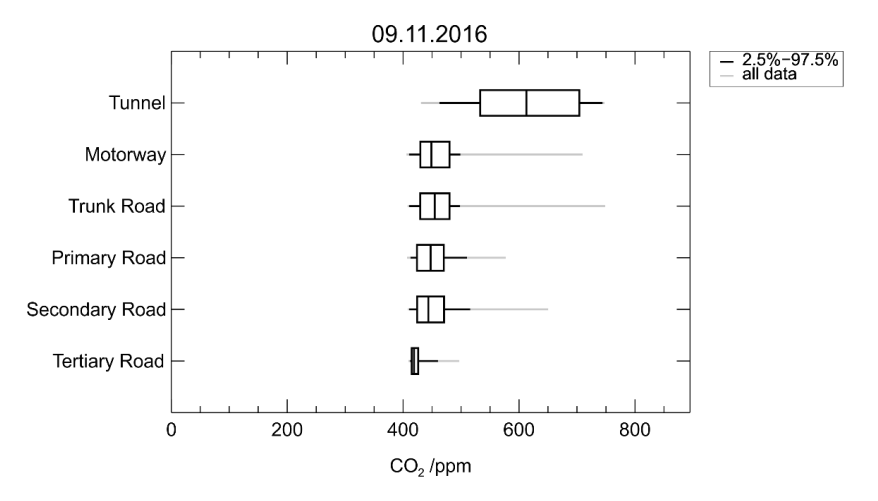


Fig. 26 f: Averaged CO₂ concentrations (Picarro Inc, cavity ringdown detection system) for the various road types of the AMS test round, determined from the measured one-second data. All data in ppm.

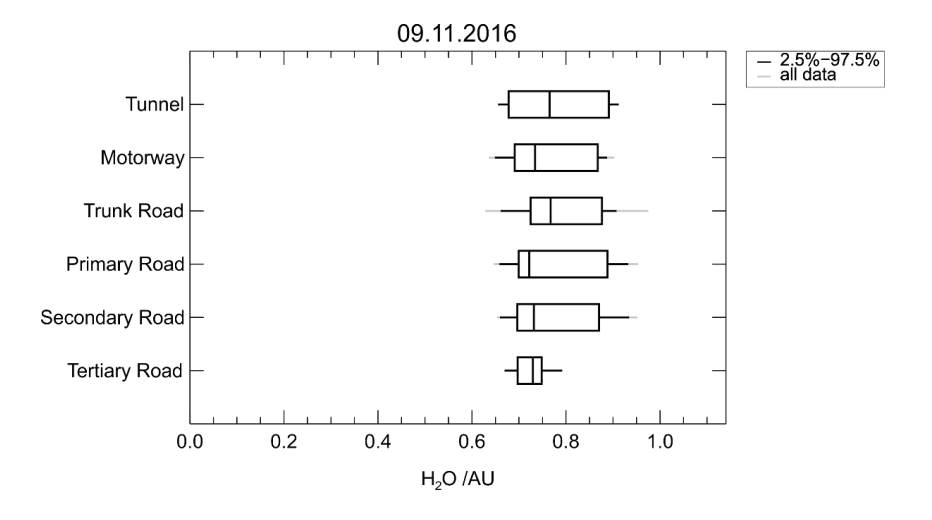


Fig. 26 g: Averaged H₂O concentrations (Picarro Inc, cavity ringdown detection system) for the various road types of the AMS test round, determined from the measured one-second data. All data in ppm * 10000.

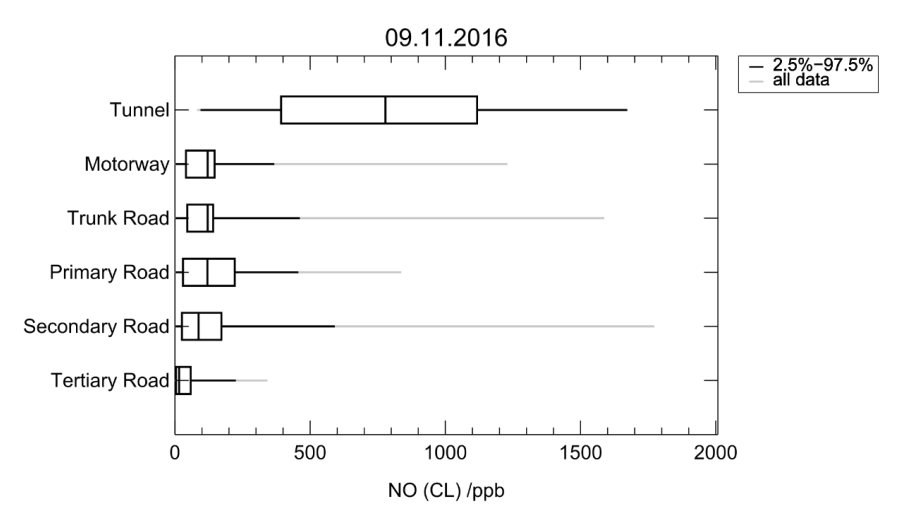


Fig. 26 h: Averaged NO concentrations (EcoPhysics) for the various road types of the AMS test round, determined from the measured one-second data. All data in ppb.

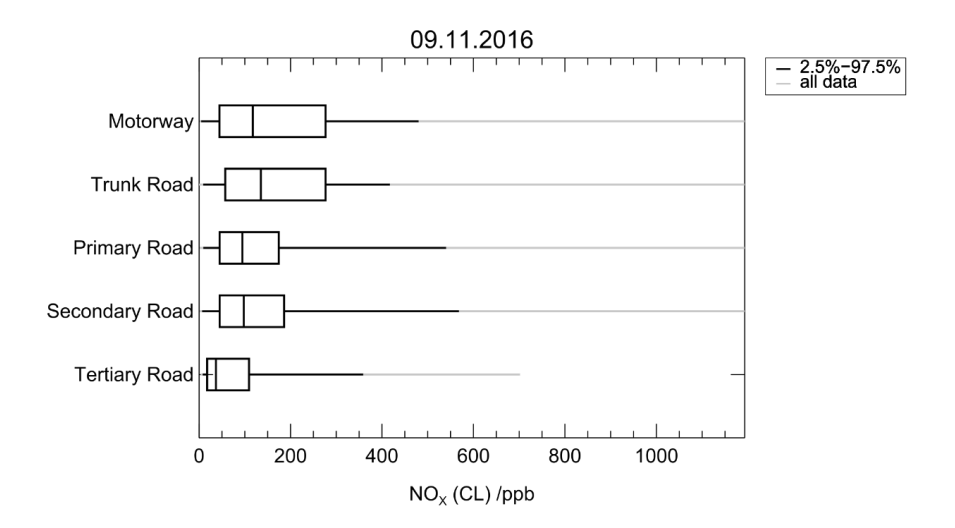


Fig. 26 i: Averaged NO_x concentrations (EcoPhysics) for the various road types of the AMS test round, determined from the measured one-second data. All data in ppb.

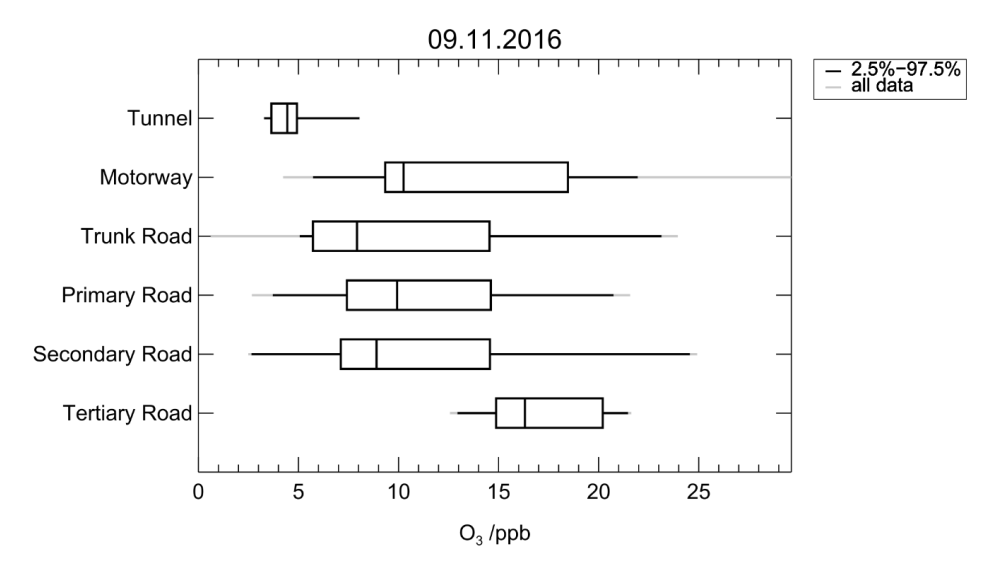


Fig. 26 j: Averaged O₃ concentrations (Environnement S. A.) for the various road types of the AMS test round, determined from the measured one-second data. All data in ppb.

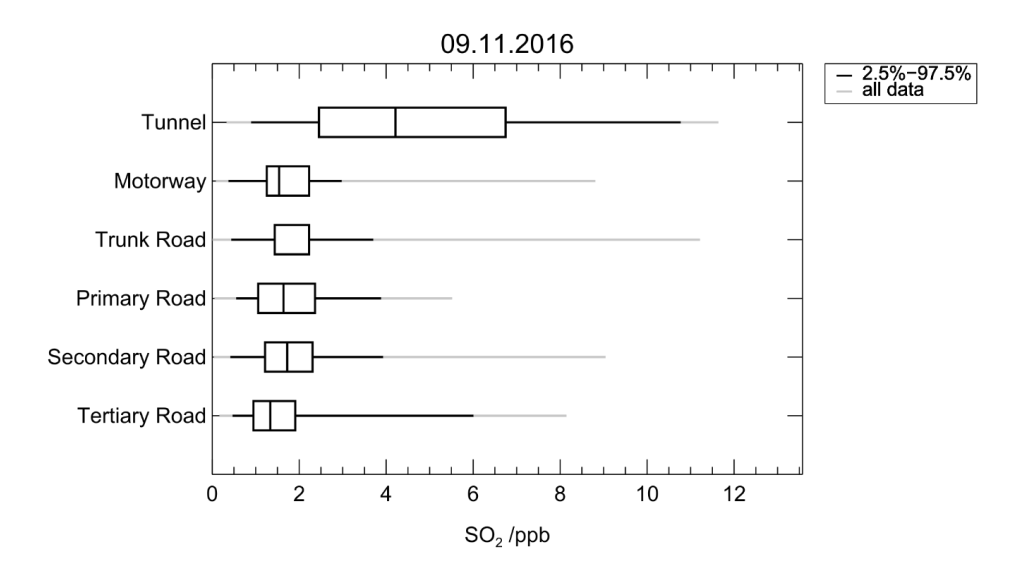


Fig. 26 k: Averaged SO₂ concentrations (ThermoFisher Inc.) for the various road types of the AMS test round, determined from the measured one-second data. All data in ppb.

5.4 Conclusions and Summary

- We found the highest concentrations of nitrogen oxides, SO₂, hydrocarbons and CO₂ in tunnels
- Seasonal influences have a particularly strong effect on short-lived trace substances with an atmospheric lifetime in the range of hours. In the case of nitrogen oxides (NO_x), differences in loads in the atmospheric background were observed with maxima under background conditions of up to an order of magnitude (summer: 2 ppb, winter: > 20 ppb).
- The seasonal differences found for inner-city pollution are significantly weaker with a factor of 2 for nitrogen oxides.
- A comparison between two metropolitan regions with different orographic conditions (Berlin and Stuttgart) showed no clear differences in concentrations. It was shown that the level of pollutant is mainly influenced by meteorological conditions (height of the inversion layer, wind speed) and local conditions (road width and height of buildings).
- In tunnels and in the immediate vicinity of traffic, the emission ratios of nitrogen oxides dominate the NO/NO₂ ratio of the investigated air masses (comparable ratios were also found in direct exhaust gas measurements). With increasing distance to the sources, the observed NO/NO2 ratio approaches more and more the photostationary state during the course of the day (see also [Ehlers et al., 2017]).
- A clear influence of the outside temperature on the NO₂/NO_x ratio can be demonstrated for the tunnel measurements. In winter, a mean share of NO₂ in the NO_x mixing ratio of 12 % was found. Under summer conditions, the proportion of directly emitted NO₂ in NO_x was twice as high at 24 %. The main source emitting NO₂ is diesel passenger cars oxidation catalysts which transform VOC and CO to CO₂, but also NO to NO2. It can be concluded that under urban conditions in cities the operating temperatures in the exhaust tract are significantly lower than in summer. This behaviour is particularly true for diesel trucks, whose oxidation catalytic converters usually require a longer heating phase than those of diesel passenger cars (see also: [Klemp et al., 2020]).
- In fact, the reduction in the exhaust gas system temperature observed on the basis of the changed NO₂ emissions also has negative effects on the efficiency of the NO_x reduction of the exhaust of diesel vehicles equipped with SCR-catalysts. Simultaneous NO_x- and CO₂-measurements showed that, under winter conditions, the NO_x

emissions of the vehicle fleet measured in the tunnel, standardized to fuel consumption (i.e. CO₂), are about 50% higher than under summer conditions¹⁹.

Based on our on-board investigations, A. Talke (Daimler AG) carried out a relative weighting of the pollutant values observed here for the various road types on the basis of statistical driving profile investigations. The pollutant levels determined from our investigations for different seasons form the basis for the calculated average load level of a fuel cell vehicle over the period of one year. Together with the damage potentials determined from the fuel cell test bench investigations [Daimler AG, 2017; ZBT, 2017] estimates of the resulting reduction in the service life of the fuel cell stack were carried out for the first time [Talke et al., 2018]. At the same time, these results form the basis for the required pollutant-dependent retention capacity of the harmful gas filters to be developed.

¹⁹ Since the diesel vehicles of the measured vehicle fleet are responsible for the vast majority of the NO_x emissions (cf. footnote 14) and the NO_x emissions of diesel vehicles without an SCR catalytic converter (i.e < EURO-6) are independent of the oxidation catalytic converter temperature (see for example: [Klemp et al., 2012]), the limited effect of the SCR catalytic converters in winter was concluded to be the main reason for the observed drastic increase in NO_x emissions.

6 Extension of the MobiLab-II analytics by integration of VOC investigations

It is known that the damaging effects of various hydrocarbons and other organic gases on the fuel cell stack vary widely [Zhai et al., 2010, Talke et al., 2015]. In order to estimate possible damage effects by organic substances on the fuel cell stack (see sections 6.1.4 – 6.1.9), volatile organic compounds (VOC) were sampled into canisters during measurement drives with MobiLab and analysed offline in Jülich laboratories. The additional financial resources from this project allowed us to intensify our longterm measurements of VOC and NOx in conurbations, so that during the course of the project the previous long-term data set could be supplemented with the latest data sets. The resulting paper is published by us in Faraday Discussions, DOI: 10.1039/C5FD00180C²⁰: [Ehlers et al., 2016].

An analysis of the individual compositions of hydrocarbon samples (Volatile Organic Compounds (VOCs)) allows conclusions to be drawn about their originators. It can be seen that the dominant sources of VOC are petrol vehicles with temporarily reduced catalyst efficiency (so-called cold-start conditions). On the other hand, diesel vehicles are the main source of nitrogen oxides from traffic. Our long-term studies carried out by means of stationary and mobile measurements showed that the ratio of VOC/NOx [ppb/ppb] had decreased by a factor of 7.5 between 1994 and 2014. This experimentally determined decrease is significantly greater than the decrease by a factor of 2.5 predicted by the German Federal Environment Agency [Federal Environment Agency (UBA), 2015]. Using box model studies, we were able to show [Ehlers et al., 2016] that the disproportionate decrease in VOCs compared to NO_x is mainly responsible for the observed reduction in summer ozone formation.

After the commissioning of our larger mobile measuring laboratory MobiLab-II in 2016, it was now possible to integrate up to 10 additional sample cylinders (Silcosteel, Restek) into the vehicle and thus episodically extend the measurement spectrum by the acquisition of cylinder samples of organic gases. In the second part of the ALASKA funding period the new measuring equipment was successfully used for the first time.

²⁰ The ALASKA project (03ET6036D) sponsored by the BMWi was thanked in acknowledgement of the publication for its support.

The long-term trends shown in [Ehlers et al., 2016] were confirmed by these investigations.

In the following, the gas chromatographic system used will be presented and the results of VOC measurements at road level and in tunnels will be described. First, an overview of the VOC mixing ratios found for different load conditions will be given. In a second part, the relation of the emitted VOC and NOx concentrations to the airchemically formed secondary pollutants as well as to the air-chemically controlled selfcleaning processes of the atmosphere is presented.

6.1 The gaschromatographic system

C2 - C12-hydrocarbons are detected and quantified by high-performance gas chromatography flame ionization detector (FID) with a cryogenic enrichment unit coupled to a quadrupol mass spectrometer (Agilent 5975) [Schmitz et al. 1997; Schmitz et al. 2000; Mittermaier und Klemp, 2004].

The analysis system "GC/MS 1 ($C_2 - C_{12}$)" is based on a commercial gas chromatograph (GC 6890, Agilent) with FID and MSD unit (cf. Fig. 27). In addition, the instrument has several programmable valves and heating zones. The entire time control of the system required for fully automatic operation is carried out via an external control unit. The gas flows during the analysis are controlled by a valve system consisting of two multi-way valves (Valco). The valves are heated to 130 °C to minimize possible losses of less volatile hydrocarbons due to interactions with the metal surface of the valve. The heating power is controlled by the programmable control loop of the GC 6890. The sample gas flow and the carrier gas (H₂) are controlled via the central valve, a 6/2-way valve. The second valve, a 4/2-way valve, separates the sample loop from the carrier gas or sample air. The suction line and all lines in contact with the sample gas are made of silanized stainless steel.

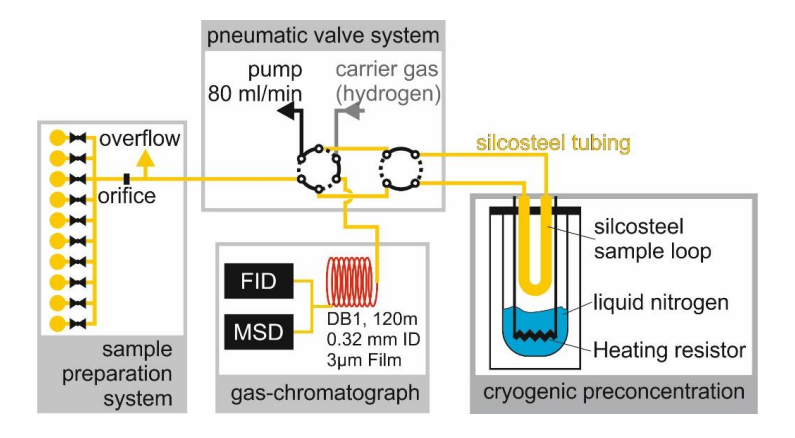


Fig. 27: Flow diagram of the GC-MS system "GC/MS 1 ($C_2 - C_{12}$)" used. Sample preparation system: A set of 10 Silco-steel cylinders previously filled with sample air can be connected to the system for analysis. Cryogenic preconcentration: Used to increase the concentration of air samples by about a factor of 1000. Gas chromatograph: Equipped with FID and MSD, column 120 m DB1, 0.32 mm ID.

The silanized material does not interact with aromatic compounds, as can be the case for stainless steel. The necessary enrichment of hydrocarbons is achieved by condensing the trace gases contained in the sample at the temperature of liquid nitrogen. This cryogenic enrichment is carried out in a U-shaped, silanized stainless steel tube (1/8", Silcosteel, Restek). The enrichment loop is located in the flange of a dewar partially filled with liquid nitrogen (TRI 11, Air Liquide) and is above the liquid level in the gas chamber. The temperature in the flange is about -170 °C to -180 °C, caused by the evaporation of the liquid nitrogen, independent of the filling level of the dewar. This temperature is still too high for an enrichment of the slightly boiling C2hydrocarbons, so that the temperature in the flange must be lowered to approx. -190 °C by additional evaporation of the liquid nitrogen. This is done with a heating resistor placed directly above the bottom of the Dewar. The heating resistor is switched on about 10 minutes before the air sample is enriched. In this way, a stream of cold nitrogen gas develops, which flows evenly around the enrichment loop. The flow through the collection loop is kept constant at 80 mL/min during the enrichment interval of 10 min by means of a mass flow controller (MFC). The enrichment loop is filled with fine glass beads (80/100 mesh; Alltech). This increases the flow resistance through the enrichment loop and also reduces the volume in which the substances are frozen to about 1 ml. The increase in the flow resistance results in a pressure gradient in the

loop, which means that the nitrogen present in the sample cannot condense at all and the oxygen can only partially condense. The remainder of the oxygen and other lightly boiling trace substances whose boiling points are significantly lower than those of ethene are separated from the sample by evacuating the loop at the end of the enrichment process. From the outside, the tube is wrapped with a heating conductor (15 Ω/m; Philips). A suitable variation of the winding density of the heating conductor ensures uniform heating of the sample inside. The injection of the sample takes place at a temperature of 130 °C. After injection, the loop is rewound with nitrogen (N₂ 5.0) and baked at a temperature of 150 °C. The sample is then injected into the loop at a temperature of 130 °C. The heating temperatures are controlled by a measuring controller (Digitemp). The sensor for this control is located at the lowest and therefore coldest point of the enrichment loop to ensure complete emptying. In addition, the enrichment temperature is monitored and recorded with a resistance thermometer (PT100). This makes it possible to check later whether the temperature during the enrichment process was sufficiently low to retain the low-boiling components.

A DB1 capillary column (J&W) with a length of 120 m, an inner diameter of 0.32 mm and a film thickness of 3 µm is used to separate the hydrocarbons. Since the stationary phase consists of a non-polar material, the retention times correlate essentially with the boiling points of the hydrocarbons to be separated. The separation performance of the column is optimized by a suitable temperature program: After the injection, the column is first operated isothermally for 8 min at -60°C and then heated to 180°C at a rate of 4°C/min and then to 220°C at 20°C/min. The column is then heated at 220 °C for 10 minutes. At the end of the analysis, the GC oven is cooled down again to the starting temperature of -60°C and a new gas chromatographic analysis is started.

The separated substances are detected with a flame ionization detector (FID) and an MSD (Agilent 5975).

Fig. 28 gives an overview of the separation performance achievable with the system and lists the retention times for the most common organic trace gases of an air sample.

a) Calibrations

The GC system was calibrated before and after the measurements using a 74component gas standard of pure hydrocarbons (Apel-Riemer Environmental, Inc., Denver CO, USA) and oxygenated substances (National Physical Laboratory (NPL), Middlesex, GB). The FID sensitivity of substances not present in the gas standard was obtained using experimentally determined Response Factors derived from the injection of known concentrations of pure organic gases and further dilution with synthetic air. The connected MSD (Agilent 5975) was used to identify the substances. The results were verified with the help of a self-made diffusion source [Konrad and Volz-Thomas, 2000]. In addition, the retention times of the individual substances were determined by injecting the pure substances and comparing them with the corresponding retention times (cf. Fig. 28) of the 74-component standard (Apel-Riemer Inc., Boulder, CO) and by comparing them with retention indices [EPA 1997].

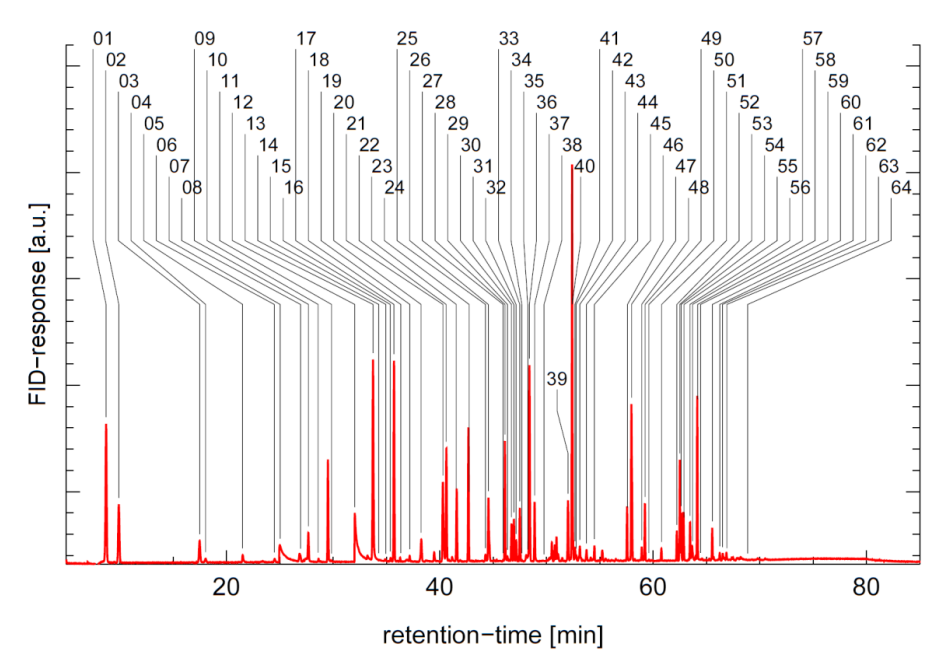


Fig. 28: Overview of the separation performance achievable with the system. Chromatogram from a petrol car under cold-start condition. The peaks are labeled as follows: 01 - Ethene; 02 - Ethane; 03 -Propene; 04 – Propane; 05 – Propyne; 06 – Methylpropane; 07 – Methanol; 08 – 1-Butene / i-Butene; 09 – n-Butane; 10 - trans-2-Butene; 11 - cis-2-Butene; 12 – Ethanol; 13 – 2-Methylbutane; 14 – Acetone; 15 - 1-Pentene; 16 - 2-Propanol; 17 - n-Pentane; 18 - Isoprene; 19 - cis-2-Pentene; 20 - 2,2-Dimethylbutane; 21 – Cyclopentane / 2,3-Dimethylbutane; 22 – 2-Methylpentane; 23 – 3-Methylpentane; 24 - n-Hexane; 25 - trans-1,3-Hexadiene; 26 - Methycyclopentane / 2,4-Diimethylpentane; 27 -Methylcyclopentene; 28 – Benzene; 29 – 1-Butanol; 30 – Cylohexane; 31 – 2-Methylhexane; 32 – 2,3-Dimethylpentane; 33-3-Methylhexane; 34 - Pentanal; 35 - 1-Heptene; 36 - 2,2,4-Trimethypentane; 37 - Heptane; 38 - 2,3-Dymethyl-2-pentene; 39 - 2,3,4-Trimethylpentane; 40 - Toluene; 41 - 2-Methylheptane; 42 - 4-Methylheptane; 43 - 3-Methylheptane; 44 - Hexanal; 45 - n-Octane; 46 -Ethylbenzene; 47 - m/p-Xylene; 48 - Styrene; 49 - o-Xylene; 50 - n-Nonane; 51 - i-Propylbenzene; 52 - n-Propylbenzene; 53 - m-Ethyltoluene; 54 - p-Ethyltoluene; 55 - 1,3,5-Trimethylbenzene; 56 - o-Ethyltoluene; 57 - Octanal; 58 - 1,2,4-Trimethylbenzene / t-Butylbenzene; 59 - Decane; 60 - 1,2,3-Trimethylbenzene; 61 – Indane; 62 – 1,3-Diethylbenzene; 63 – 1,4-Diethylbenzene / Butylbenzene; 64 - Undecane.

b) Error estimation

Experimental uncertainties in the analysis of canister samples can result from different reasons:

The influence of transport and storage on the quality of the results was investigated by parallel measurements on wet and dry samples with different storage times. Fig. 29 shows the comparison of two calibration gas samples after 8 days storage time, during which one of the samples was additionally moistened during filling.

In addition, care was taken to ensure that the VOCs were collected ozone-free in the canister samples. This was ensured by the collection process using a capillary heated to 120 °C (Silco-steel, 0.15 mm diameter). Laboratory tests on VOC calibration standards ensured that all VOCs contained in the calibration mixture were collected loss-free at this capillary temperature. By adding ozone (maximum concentration of 160 ppb) it could be proven that the ozone-degradable alkenes can also be quantitatively collected, stored and enriched in the loop without any noticeable losses. Based on the results of a test series of different VOCs, it was found that alkanes, alkenes, aromatics and terpenes differed in their mixing ratios by less than 10 % from the results of directly analyzed samples after a storage period of 4 days²¹. For alcohols, the deviations found in the time interval under consideration were less than 20 %. In addition, the accuracy of the measurements depends on the quality of the calibration standard (deviations between true and indicated mixing ratios < 5 %, Apel-Riemer Environmental Inc.). Further errors are caused by uncertainties of the mass flow meters (MKS Instruments, < 2 %) and by errors in the integration of the peak areas (< 7 %). The geometric addition of the individual errors adds up to a total error of 12

²¹ As part of the campaigns carried out, care was taken to ensure that the storage and transport time of the collected canister samples up to the measurement in Jülich never exceeded a period of 4 days.

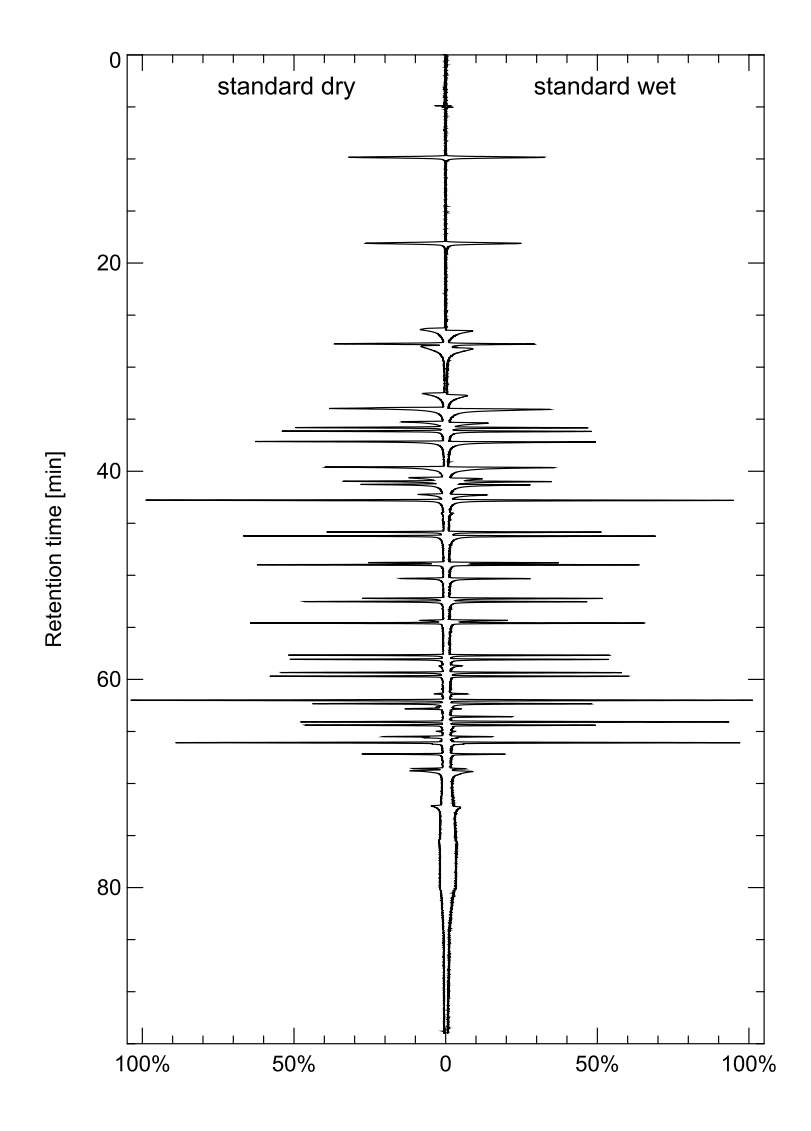


Fig. 29: Comparison of two calibration gas samples after 8 days storage time, in which one of the samples was additionally moistened during filling.

6.2 <u>Measurements of low volatile hydrocarbons</u>

The system for the determination of hydrocarbons described above is limited to the analysis of compounds with less than 13 carbon atoms. The maximum heating temperature of the sample loop of 150°C and the valve temperature of 130°C prevent

the quantitative determination of heavier hydrocarbons. For the analysis of these compounds, a GC/MS system " $GC/MS 2 (C_9 - C_{16})$ " was additionally set up in which air samples are taken at room temperature on tubes with adsorbent (Carbotrap® 300. Supleco). The samples were desorbed with a thermodesorption system (TDS®, Gerstel, Mülheim), focused with a cold feed system (KAS®, Gerstel, Mülheim) and detected with a GC/MS/FID (Agilent GC6890, MSD5975). The high desorption temperature of 350°C and a valveless design allow the analysis of compounds with up to 17 carbon atoms. However, lighter hydrocarbons <C9 are not measured quantitatively. As in section 6.1, the compounds were quantified using a calibration standard or their molecular response factor in the FID and identified using a mass spectrometer (cf. Fig.30a and Fig.30b).

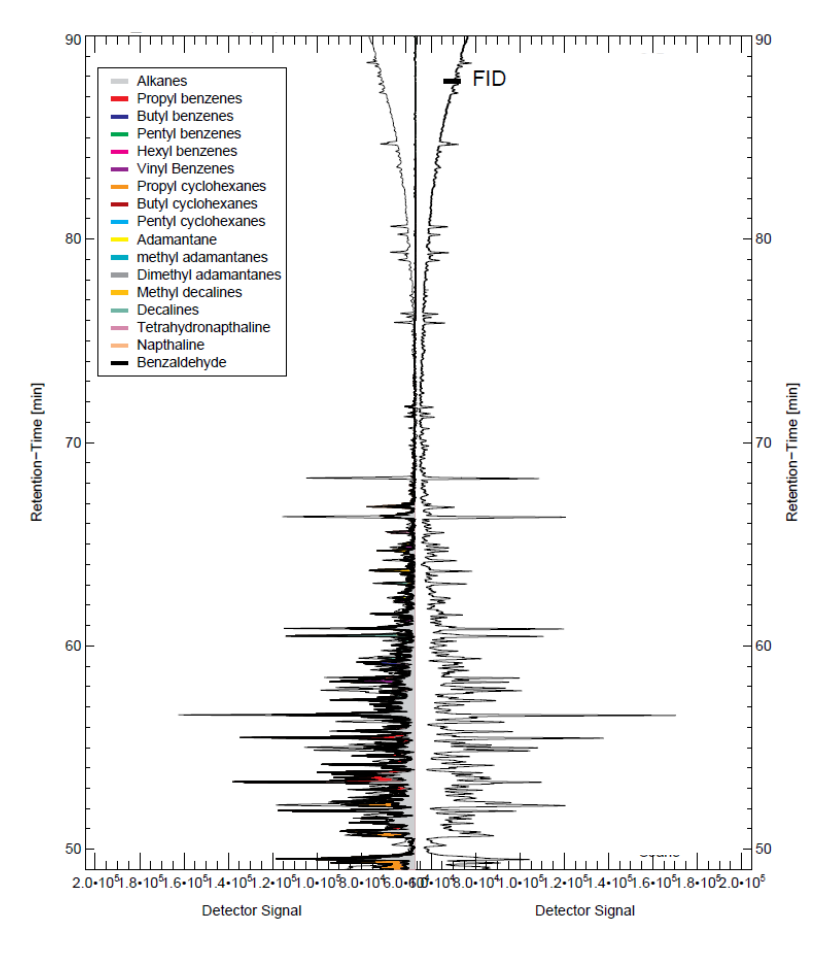


Fig. 30a: MS chromatogram (left) and FID chromatogram of a diesel exhaust sample measured with "GC/MS 2 (C9 - C16)".

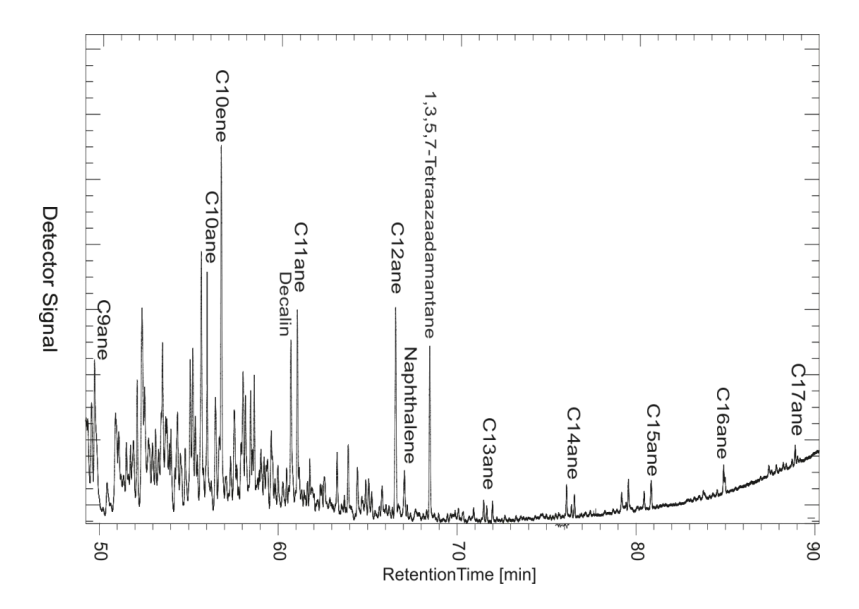


Fig. 30b: Retention times of various n-alkanes in the FID chromatogram of a diesel exhaust sample measured with "GC/MS 2 ($C_9 - C_{16}$)".

6.3 The reactivity concept

More than 90% of all VOCs in the atmosphere react with atmospheric OH radicals. The atmospheric processing of an air mass can therefore be described in good approximation by the total reactivity Rvoc with OH.

The OH reactivity R_{VOC_i} describes the velocity of a VOC_i for the reaction with OH radicals. The summation of all VOCs then provides (1):

$$R_{VOC} = \sum k_{OH+VOC_i} \times [VOC_i] \tag{1}$$

The quantity reactivity is extremely useful because it allows the local ozone production for VOC mixes of different composition to be described using a single parameter (cf. [Klemp et al., 2012]).

In the atmosphere reactions leading to ozone formation compete with reactions leading to formation HNO₃ (cf. Fig. 31). Ozone and other photooxidants are formed only via the reaction path Rvoc; the reaction path R_{NO2} converts the nitrogen oxides present in the form of NO₂ to HNO₃, which is removed from the atmosphere by wet deposition. The turnover of these reaction pathways is controlled by the ratio of the reactivities Rvoc/R_{NO2}. Fig. 31 shows these processes in a simplified scheme of the trace gas degradation of VOC and NO2 in the troposphere.

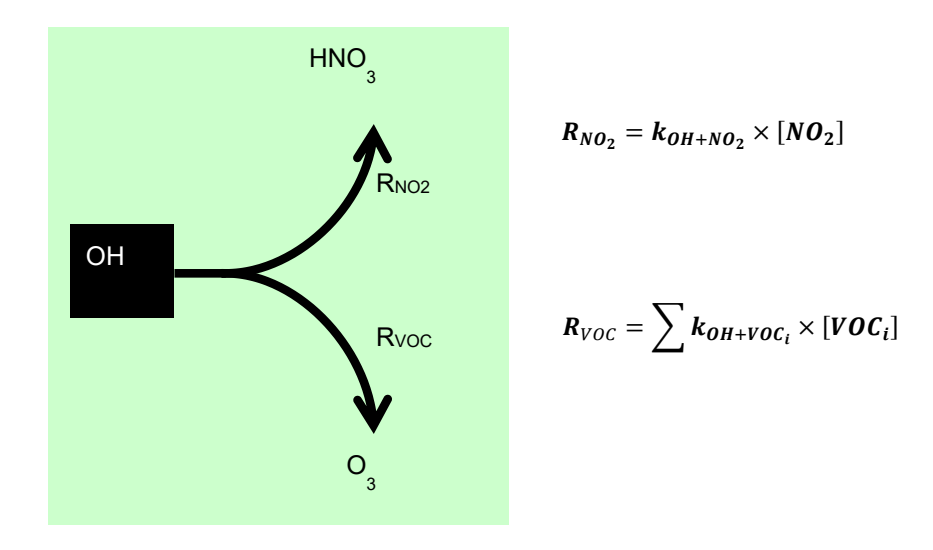


Fig. 31: Simplified scheme of the reaction paths of OH radicals in the degradation of nitrogen oxides and VOCs. Only on the reaction path R_{VOC} additional ozone is formed in the atmosphere; the reaction path R_{NO2} converts the nitrogen oxides present in the form of NO_2 to HNO_3 , which is removed from the atmosphere by leaching processes. The ratio of reactivities. R_{VOC}/R_{NO2} controls the relative importance of the two processes in the degradation of trace substances.

The formation of photooxidants (i.e. the photochemical effect) for different initial ratios of R_{VOC}/R_{NO2} can be examined with the help of a detailed reaction model (MCM, Master Chemical Mechanism [Jenkin et al., 1997]). The main advantage of this approach is that the measured input parameters (NO₂, VOC, radiation data) can be used for the description of photochemical ozone formation valid for this location. Fig. 32 shows the result of variational calculations of $P(O_3)$ -formation with MCM-3.3. The resulting local ozone production rates for different start ratios and start reactivities of VOC and NO₂ are shown as a so-called "isopleth plot".

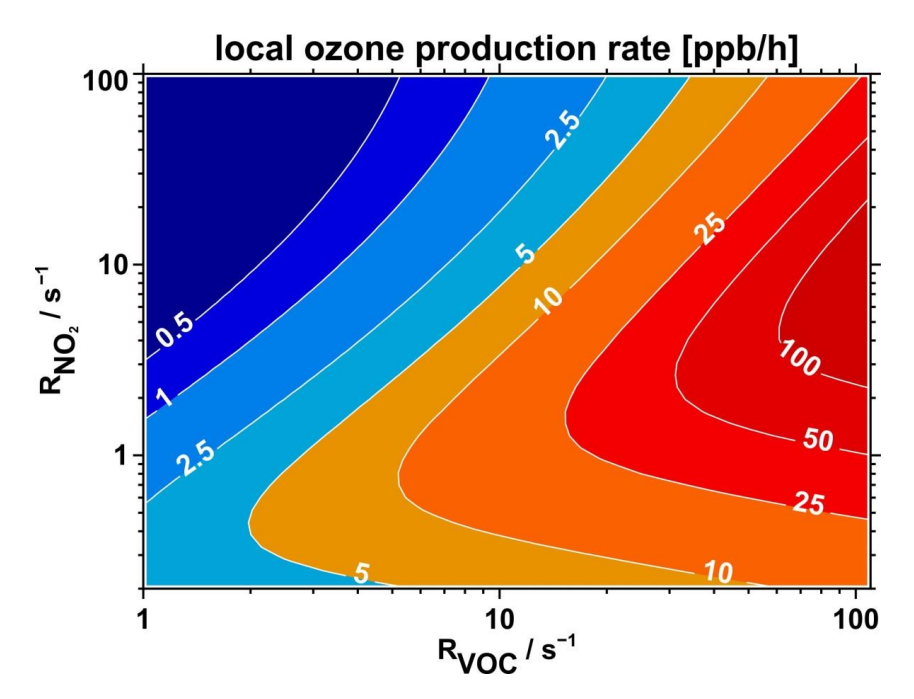


Fig. 32: Variational calculation of P(O₃) with MCM3.3 (Details: cf. [Klemp et al. 2012] for different start ratios and start reactivities of VOC and NO2. The results are presented as an isopleth plot of local ozone production rate. Boundary conditions: Latitude: 52.5° north latitude, radiation conditions: 21. 06., noon 12:00, clear sky conditions. A fast transformation between NO and NO2 occurs at noon via the photostationary equilibrium on the time scale of 1 - 2 minutes.

a) VOC limitation of the ozone formation rate

The ozone production rates in the upper left area of the isopleth diagram are characterized by small VOC/NO222 ratios, typically found in urban areas of Central Europe. A reduction of the VOCs leads to a reduction of the calculated ozone production. A reduction of the NO2 concentration, however, results in an increase of the calculated ozone formation. The reason for this is that at high NO₂ concentrations, the reaction of NO₂ with OH competes noticeably with the degradation of the VOCs by OH. The reduction of the NO₂ concentration leads to an increase in ozone production due to the increased degradation of the VOCs. In general, positive slopes of the P(O₃)isopleth with respect to NO₂ reactivity characterize the range of VOC limitation.

b) NO₂ limitation of ozone formation rate

Values in the lower right area of the P(O₃)-isopleth plot are characterized by large VOC/NO₂ ratios. This air-chemical scenario is typical for rural regions far away from anthropogenic sources, since during the transport of an air mass the nitrogen oxides are removed from the atmosphere on average faster by OH radicals than the VOCs. In the range of negative slopes of the P(O₃)-isopleth with respect to NO₂ reactivity, the reduction of NO2 leads to a reduction in ozone formation; this part of the isopleth diagram is therefore referred to as the NO2-limited range. A change in the VOC concentration, on the other hand, has only a minor influence on ozone formation. This is because the ozone formation rate is limited by the amount of NO (or NO_x available, see: footnote 22) [Madronich and Calvert, 1990]. In this range, the system does not contain sufficient NO_x to recycle the OH radicals sufficiently fast by radical reactions with NO.

²² Due to the photostationary balance between NO, NO₂, ozone and solar radiation present during the day, a fairly constant ratio of NO to NO2 of about 3:1 [ppb/ppb] is formed 1 - 2 minutes after the release of NO_x (primarily in the form of NO) away from the sources.

6.4 Results of VOC concentration measurements

Fig. 33 shows a comparison of the VOC concentration distribution ("pattern") of a tunnel measurement on the Berlin motorway ring road under congestion conditions (i.e. stop-and-go conditions) with that of a tunnel measurement under constant speed conditions (approx. 60 km/h). As already mentioned, tunnel measurements are particularly well suited for comparisons, as they allow the determination of a traffic mix undisturbed by other sources. The distribution of VOC in the tunnel resembles the distribution observed on the road. This is a clear indication of the "stability" of the VOC pattern from the source traffic.

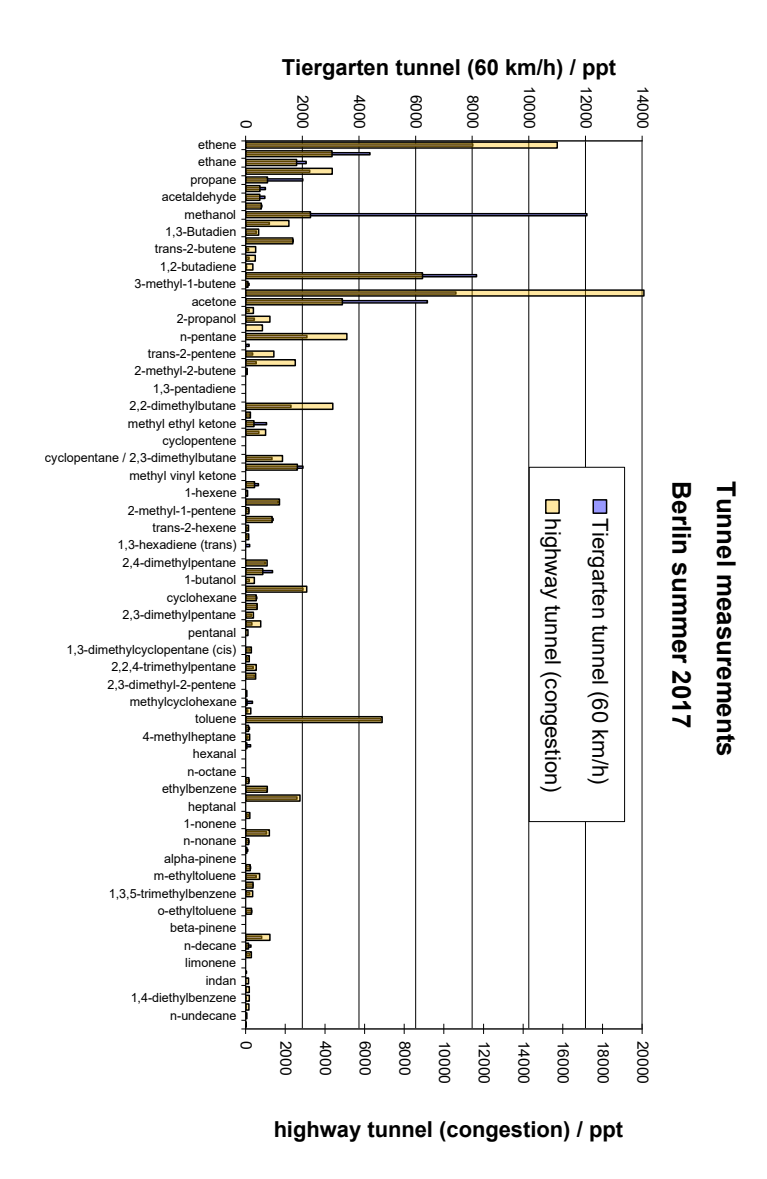


Fig. 33: Comparison of the VOC concentration distributions ("patterns" of the mixing ratios) of a tunnel measurement on the Berlin motorway ring road under congestion conditions with that of a tunnel measurement under constant speed conditions (approx. 60 km/h). The scaling for the tunnel pattern was chosen so that the aromatic toluene has equal proportions in both patterns. The relative increases occurring in the congestion pattern for the light hydrocarbons (C_2 - and C_3 -alkenes and C_5 - and C_6 -alkanes) can be inferred from increased evaporation fractions (C_5 - and C_6 -alkanes) or different conversion rates of the vehicle catalysts.

However, for light hydrocarbons, significantly higher proportions of C2- to C3-alkenes and C₅- to C₆-alkanes can be observed in the congestion pattern if both patterns are normalized to the same fraction of toluene. The relative increases occurring in the congestion pattern for the light hydrocarbons (C₂- to C₃-alkenes and C₅- to C₆-alkanes) can be inferred from increased evaporation proportions (C5- to C6-alkanes) or different conversion rates of the vehicle catalysts.

Fig. 34 shows a comparison of the observed VOC patterns from the inner city area (Berlin Neukölln, Hermannplatz, summer 2017) with a VOC sample drawn windward from Berlin (Alt Landsberg, summer 2017). Nearly all substances showed lower mixing ratios in the windward side of Berlin than in the inner city area. Even the mixing ratios of the biogenically dominated VOCs (isoprene, α -pinene) were lower in the agricultural dominated area of Alt Landsberg in August (on the harvested fields) compared to the values at Hermannplatz. The clearest differences were found for the VOCs mainly released from traffic: The ethene concentration was almost a factor of 10 lower in Alt Landsberg than at Hermannplatz, in the case of toluene the difference was a factor of seven.

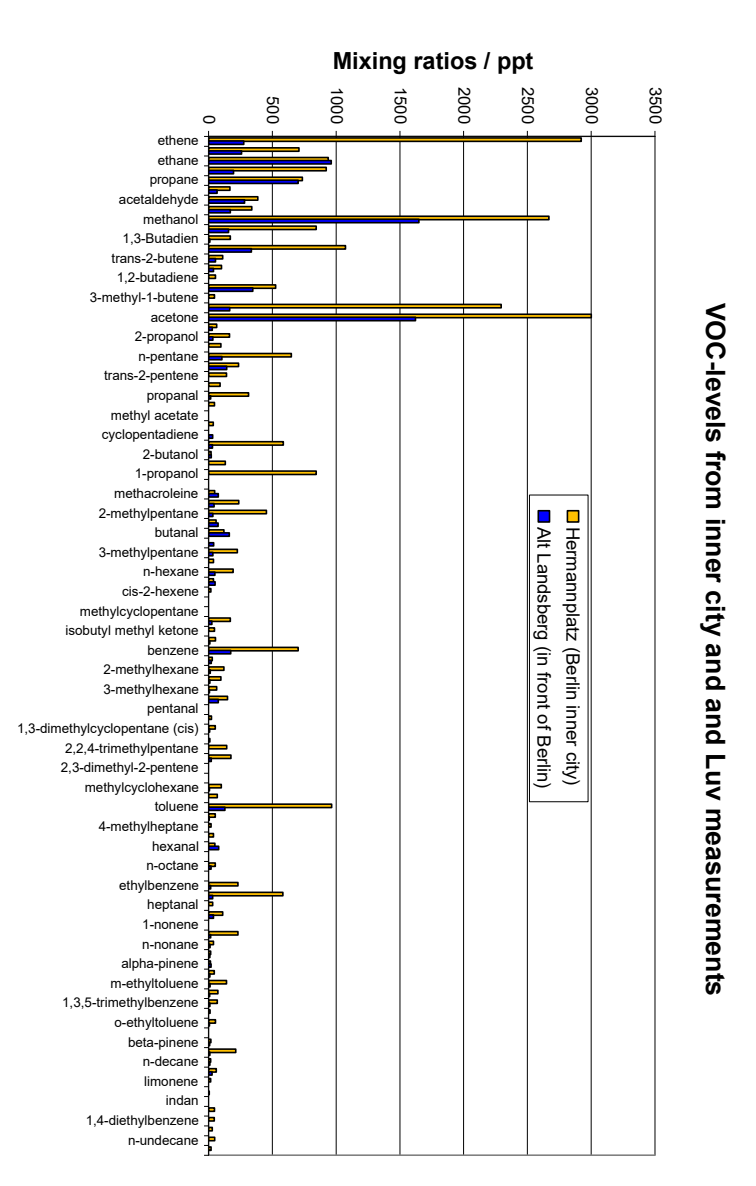


Fig. 34: Comparison of the VOC concentration distributions ("pattern" of the mixing ratios) of a VOC canister sample from the inner city area (Hermannplatz, Berlin Neukölln) with a windward drawn sample from the eastern Berlin foreland (Alt Landsberg).

6.5 Content of alcohols in the VOC profile from traffic

Fig. 35 and Fig. 36 (from: [Ehlers et al., 2016]) compare reactivity-weighted VOC profiles in the form of so-called "Rorschach plots". A current profile of our investigations from summer 2014 [Bonn et al., 2016] is compared with a profile of our measurements in Munich from 1997.

The most significant change in the current traffic profiles is the occurrence of previously non-existent alcohols in the traffic-dominated VOC profiles (resulting from the addition of 5% and 10% respectively of bioethanol to petrol, which has been taking place since 2011).

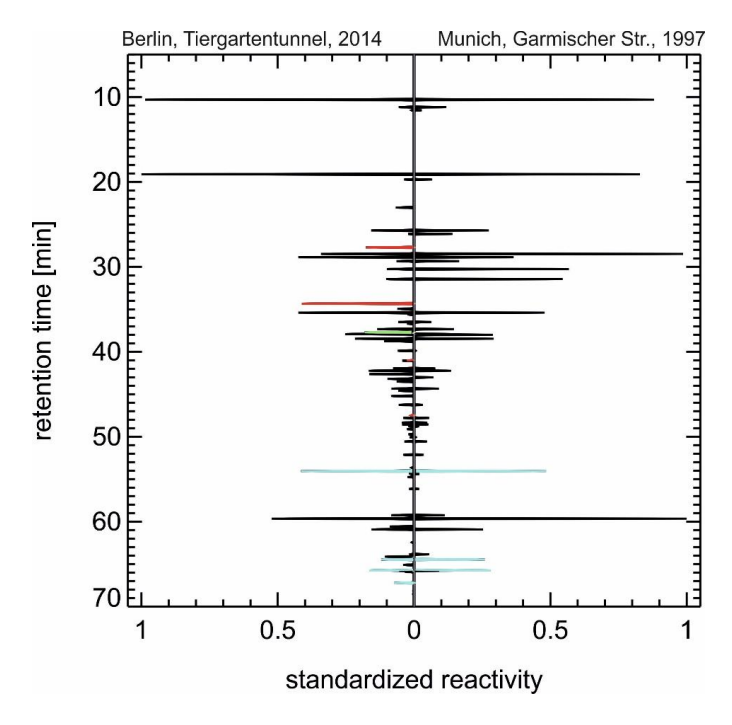


Fig. 35: Reactivity-weighted VOC profiles (so-called "Rorschach" plots) from a measurement campaign with MobiLab-I in summer 2014 [Bonn et al., 2016] and from measurements in the inner city area of Munich in 1997 (February 1997) [Kern et al., 1998]. Both VOC profiles are normalized to the most abundant species. The reactivity contributions of the alcohols (methanol, ethanol, propanol) (red) of isoprene (green) and of some aromatics (toluene, trimethylbenzenes) (mint green) are highlighted.

In Fig. 36 a current gasoline engine exhaust gas mix under cold-start conditions is compared to a mix observed in 1997 on Garmischer Straße in Munich. The similarity of the exhaust gas chromatogram with the VOC immission profile in 1997 is somewhat lower than in the case of the two immission profiles (mainly because in Fig. 36 the averaging effect due to the superposition of the many individual sources is omitted). However, the cold-start emission profile of the gasoline engine of 2015 clearly indicate the release of alcohols, which were not present in the emission pattern of 1997.

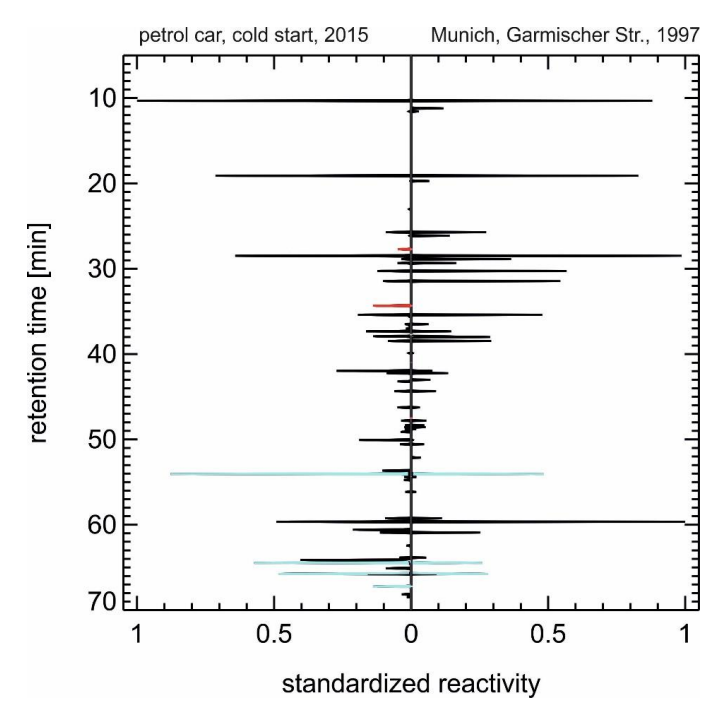


Fig. 36: Reactivity-weighted VOC profiles (so-called "Rorschach" plots) of a gasoline engine under cold-start condition from 2015 and from the inner city area of Munich from 1997 (February 1997) [Kern et al., 1998]. The reactivity fractions of the alcohols (methanol, ethanol, propanol) (red), and aromatics (toluene, trimethylbenzenes) (mint green) are highlighted. It has to be noted, that the VOC emissions from traffic have decreased by at least one order of magnitude [Ehlers et al., 2016] during the last 20 years mainly due to the shortening of the cold-start condition phases. Nevertheless, as in 1997 the cold-start emissions from gasoline cars are dominating the average VOC emissions pattern from traffic.

6.6 Relative contributions of various drive concepts

The VOC pattern of transport, which, apart from the alcohols has remained largely constant for decades, is still dominated by the same emitter class: Petrol vehicles with (not yet) working catalytic converters (catalytic converters in the so-called cold-start state). The relative shares of the various drive concepts in the VOC emissions of road traffic are shown in Fig. 37.

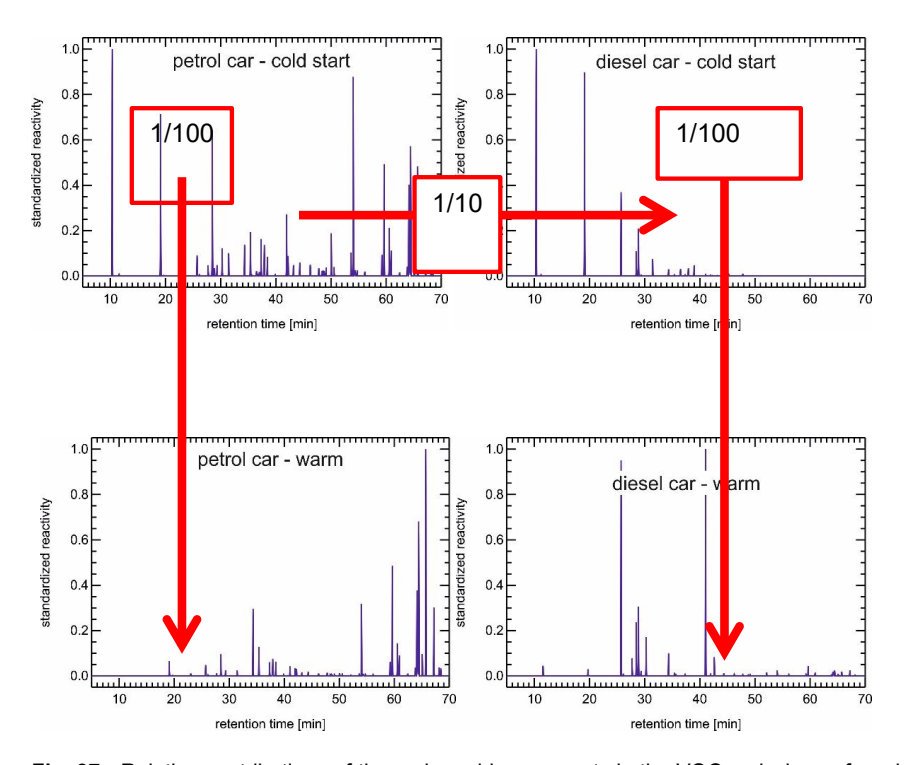


Fig. 37: Relative contributions of the various drive concepts in the VOC emissions of road traffic. The standardized OH reactivity distributions²³ calculated from the measured emission patterns for petrol engines with catalytic converters and diesel vehicles with oxidation catalytic converters²⁴ are shown.

²³ Here presented as standardized OH reactivity, i.e. only the relative change in the "reactivity-weighted VOC mix" is discernible on the basis of the VOC patterns shown, but not the factor of reduction achieved. This can only be seen from the "reduction arrows" shown.

²⁴ Starting with exhaust class EURO-2 (since Jan. 1997), all diesel passenger cars are also equipped with oxidation catalytic converters.

Petrol engines under cold-start conditions emit VOC at one order of magnitude higher quantities compared to Diesel engines under cold-start conditions. With a functioning catalytic converter. VOC emissions under warm operating conditions are reduced by about two orders of magnitude in both engine concepts.

6.7 Determination of VOC concentrations and reactivities for different air pollution scenarios

The median contributions of the VOC mixing ratios from the measurement campaign in August 2017 in Berlin are shown in Fig. 38 a - e for four different pollution situations. For a better overview, the average mixing ratios for each pollution situation ("urban background", "inner city area", "Tiergarten tunnel" and "windward area in front of the city") are listed separately in the form of subgroups for alkanes, alkenes, aromatics, biogenic VOCs (terpenes and isoprene) and oxygenated substances. A detailed presentation of the individual substances, their mean values, medians and 25th and 75th percentiles of the mixing ratios can be found in Table 7 a - d in the appendix. By comparing the share distributions of the four scenarios, the following conclusions can be drawn:

- For all four summer VOC scenarios, the group of oxigenated substances represented the largest percentage of the mixing ratios. The main reasons are firstly, the increased photochemistry under summer conditions which results in high proportions of secondary VOC degradation products and secondly, the addition of bioalcohols to the fuels.
- The proportion of aromatics decreased continuously with increasing distance from the "source". The highest values, 13 %, were found in the Tiergarten tunnel, while the proportion in the city centre dropped to 9 %. In background areas, percentages of 5 % were found (mainly caused by the long-lived components benzene and toluene).
- For the same reason, the proportion of alkanes in the VOC mix tended to increase. The long-lived alkanes had higher proportions in aged VOC mixes. On the other hand, as a result of their shorter average atmospheric lifetime, the alkene content in photochemically aged mixes tended to decrease.

The proportion of biogenically emitted VOCs strongly depends on the emission strength of the plants in the vicinity of the sampling due to the short lifetimes of these VOCs. The highest concentration shares of 7 % were found in the urban background of Berlin. On harvested fields windwards to Berlin in Alt Landsberg, the biogenic-induced shares of the total VOC concentration were only 2 %.

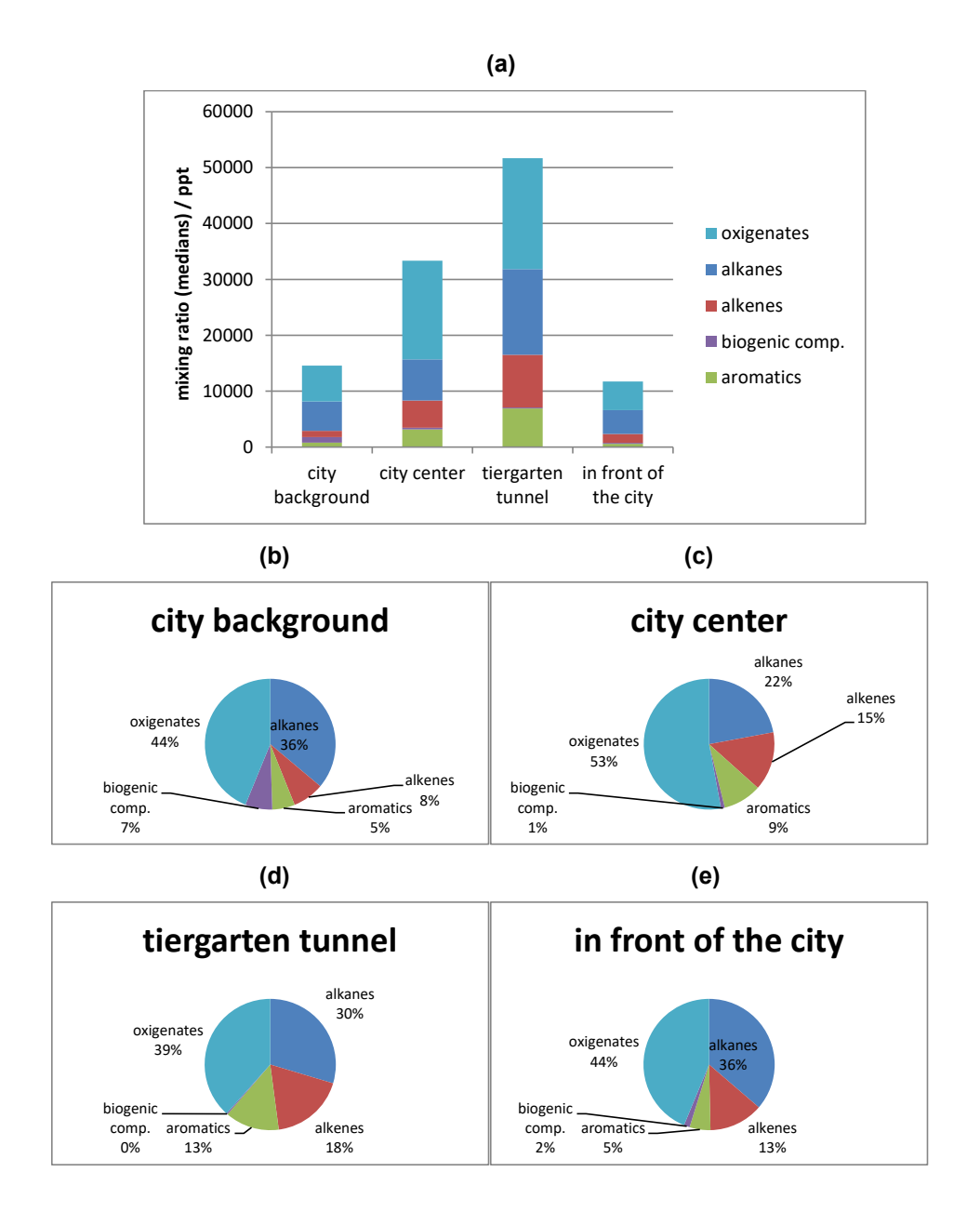


Fig. 38 a – e: (a): Cumulative mixing ratios for five different VOC subgroups; shown are the medians for the four different pollution scenarios, (b) - (e): Percentages of the mixing ratios for the sum of alkanes, alkenes, aromatics, oxigenated and biogenically emitted species (i.e. isoprene and terpenes) for different emission szenarios (city background, city center, Tiergarten tunnel, windward of the city (rural environment with agricultural use (Alt Landsberg)).

For the sample sets taken and analysed during the measurement campaign in August 2017 in Berlin (cf. Fig. 38 a - e), mean OH reactivities were determined and the relative proportion distributions of the different subgroups for the four different pollution situations were calculated. (Fig. 39 a - e). A detailed list of the individual reactivity contributions for the measured pollution scenarios can be found in the appendix (Table 8).

If CH₄ and CO were not considered the highest OH reactivity was found in the Tiergarten Tunnel (cf. Fig 39 a). Alkenes had the largest share of OH reactivity from VOC with 46 %, followed by aromatics with 19 %.

The source distributions (exclusively originating from traffic) found in the Tiergarten Tunnel were well reflected in the VOC distributions of the inner city samples (cf. Fig. 39 c and Fig. 39 d).

In the urban background of Berlin, however, biogenic reactivity dominated the VOC mix found there with almost 60 %. This circumstance reflects the high proportion of "green" in Berlin's urban background.

However, the contribution of biogenic components is strongly dependent on the activity of plant growth in the vicinity of the measurement site. On harvested fields in the Berlin area (Alt Landsberg), on the other hand, only a biogenic fraction of about 20% of the OH reactivity was found with a low OH reactivity from VOC of about 2 s⁻¹.

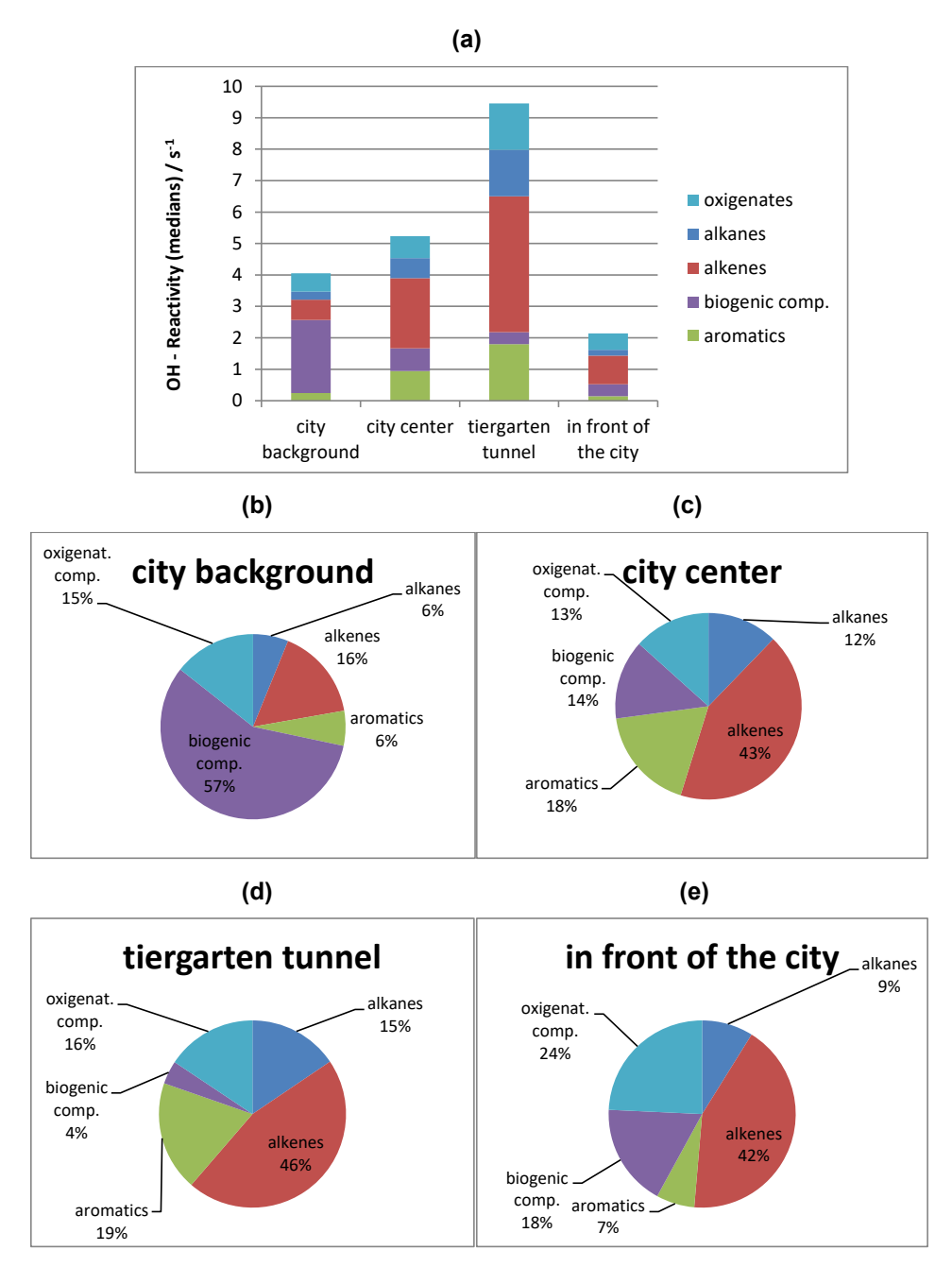


Fig. 39 a – e: (a): Cumulative reactivities for five different VOC subgroups; shown are the medians for the four different emission scenarios, (b) - (e): Reactivity contribution for the sum of alkanes, alkenes, aromatics, oxigenated and biogenically emitted species (i.e. isoprene and terpenes) for different emission scenarios (city background, city center, Tiergarten tunnel, windward of the city (rural environment with agricultural use (Alt Landsberg)).

6.8 Experimental determination of the reactivity contribution of VOCs (> C₁₂) in

traffic-loaded areas by diesel exhaust gases.

In a recent publication [Dunmore et al., 2015] it was argued that so far the emissions of large VOCs from diesel exhaust gas have been underestimated by orders of magnitude because they are difficult to detect with conventional GC systems. If the reactivity of these large VOCs in diesel exhaust gas was adequately taken into account, this contribution would account for up to 50 % of the total OH reactivity from VOC in anthropogenically dominated winter London street conditions [Dunmore et al., 2015].

If this statement was correct, several consequences would be associated with it:

- The VOC mass released from traffic would be considerably higher than previously determined with conventional GC-MS measurements.
- The release of significant quantities of high-boiling VOCs (> C₁₂) would offer a significantly higher potential for secondary particle formation than previously assumed.
- The ratio of VOC to NO_x would be higher with faster photooxidant formation than previously assumed.

We have developed a VOC detection system based on CarboSieve® and Carbotrap® adsorption tubes which allows a quantitative determination of the C9- to C16-VOCs. The GC system is based on an Agilent 6890 with MSD Agilent 5975 and an FID detector. As part of the quality assurance measures, measurements with adsorption tubes and cylinder samples were compared:

- It was found that that systems agreed better than 5% when measuring calibration gas mixtures.
- The response factors of higher compounds (>C₁₂) corresponded to the values calculated from the effective carbon number which indicates that there are no significant losses in the range up to C₁₆.
- In addition, it was ensured that even the least volatile components were transferred quantitatively (i.e. without residues) to the column (DB-1, 120 m length, 0.32 i. d.) during the heating process of the Carbotrap® collection tubes.

For the characterization of the contribution of higher hydrocarbons to VOC total reactivity, we pursued three different approaches:

Firstly, the proportion of higher hydrocarbons (> C₁₂) in the traffic-dominated air masses was determined. In order to estimate an upper limit of the contribution of higher hydrocarbons to OH reactivity, measurements were carried out in a road tunnel (cf. 6. 8. a).

Secondly, investigations on the detailed VOC composition of the diesel exhaust gas were carried out on a EURO-6 vehicle under cold-start conditions (cf. 6. 8. b).

Thirdly, the total OH reactivity of diesel exhaust gas of a EURO 6 vehicle using a was measured with LIF [Fuchs et al., 2017] and compared to the results of differentiated reactivity measurements (cf. 6. 8. c).

a) Reactivity contribution of (>C₁₂)-VOCs in a street tunnel

In 2015, adsorption tubes and cylinder samples were taken and analyzed simultaneously on several days in the Bonn road tunnel.

The hypothesis made by [Dunmore et al., 2015] could be refuted by us. Fig. 40a shows an example of the combined GC chromatogram²⁵ of canister measurement and tube measurement, simultaneously collected in the Bonn road tunnel. On average less than 2 percent of the FID signal of the whole sample was assigned to low volatile VOC components (> C₁₂).

Even with a generous estimation of an average OH reaction rate constant of 1.10⁻¹¹ cm³ s⁻¹, the reactivity contribution of the found VOC signals (> C₁₂) was less than 3 % of the total reactivity²⁶ of the VOC mix in the tunnel.

 $^{^{25}}$ The adaptation of both chromatograms was performed in the overlapping range of C_9 - C_{11} using the respective intensities of the n-alkane signals.

²⁶ For the C₂ - C₁₁-range was found an average k_{OH} of 6 · 10⁻¹² cm³ s⁻¹ [Schmitz et al., 1997].

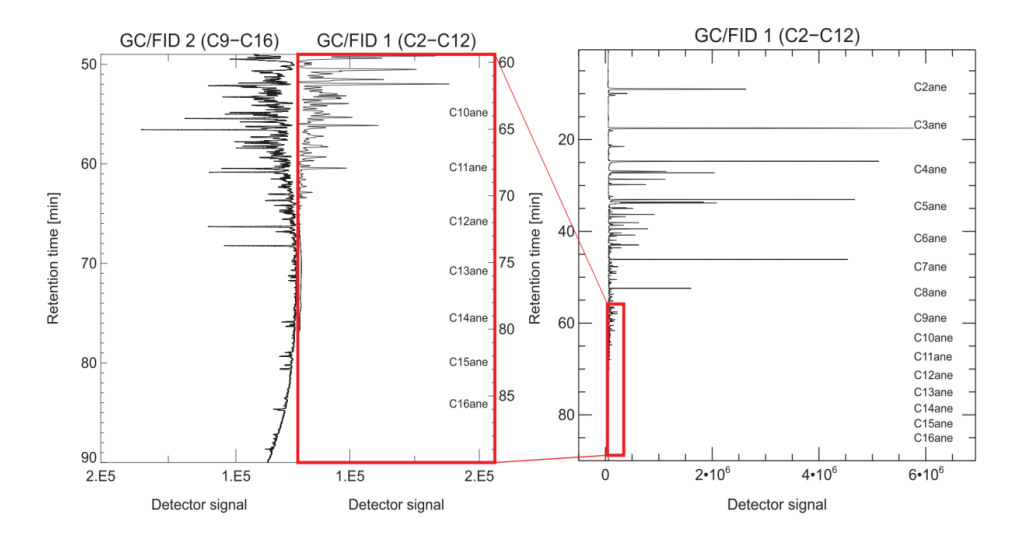


Fig. 40a: Combined chromatogram of canister measurement (GC/FID 1: range C2 - C12) and tube collection (Carbotrap® collection tubes, GC/FID 2: range C9 - C16) from simultaneous sample collections in the Bonn tunnel in autumn 2015.

b) Reactivity contribution of (>C₁₂)-VOCs in Diesel exhaust

In addition, we investigated the VOC composition in the exhaust gas of a modern diesel vehicle in cold-start conditions²⁷. For this purpose, exhaust gas of the MobiLab vehicle was collected under cold-start conditions in previously evacuated Silco Steel canisters (Restek Inc.) and then analyzed for its VOC content. Fig. 40b shows the respective reactivities of the C2 - C12-VOCs, measured in the exhaust gas of the MobiLab diesel

²⁷ The exhaust emissions of CO and VOCs from diesel vehicles have been effectively reduced in the EU for more than 20 years (cf. e.g. Klemp et al., 2012, pp. 253ff), so that only diesel vehicles under cold start conditions could make a noticeable contribution to the VOC budget (>C12). The VOC spectrum of vehicles with petrol engines (also cold start conditions) has no significant shares above C₁₁, as the good agreement found on the exhaust gas of petrol vehicles between our C2 - C12-GC system and parallel TOC measurements points out [Mittermaier et al., 2004, Klemp et al., 2012, pp. 42].

vehicle (EURO-6 with SCR catalytic converter and particulate filter, year of construction 2016).

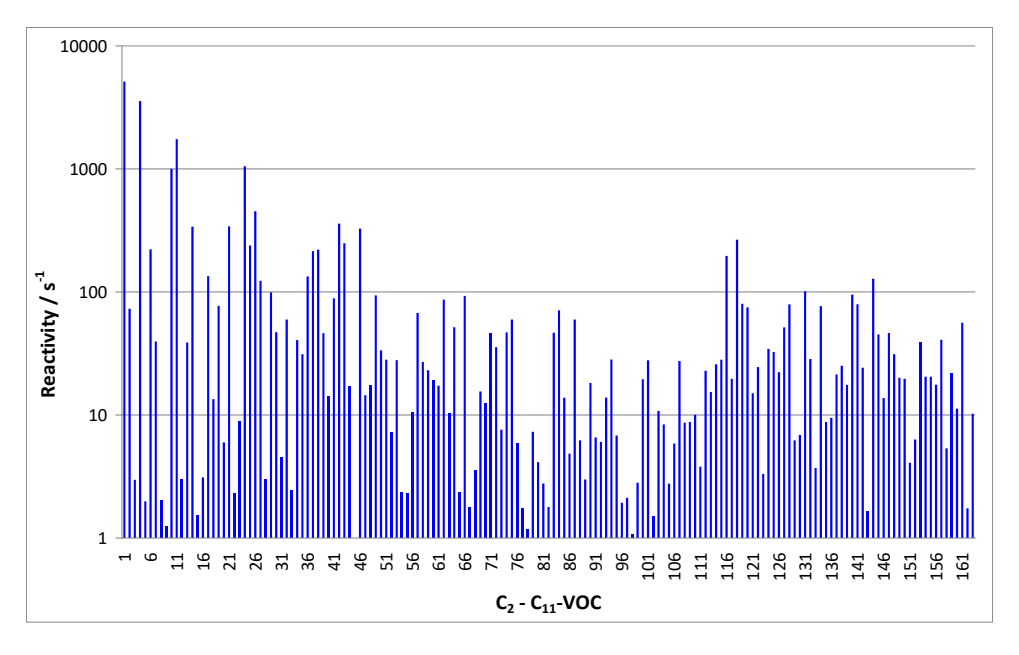


Fig. 40b: Calculated reactivities of the C2 - C12-VOCs, measured in the exhaust gas of the MobiLab diesel vehicle (EURO-6 with SCR catalytic converter and particulate filter, year of construction 2016).

1: ethene; 2: ethyne; 3: ethane; 4: propene; 5: propane, 6: cyclopropene; 7: propyne; 8: methyl nitrite; 9: isobutane; 10: acetaldehyde; 11: 1,3-butadiene; 12: butane; 13: 1-butene-3-yne; 14: trans-butene, 15: 1-butyne; 16: methylethyl-ether; 17: cis-butene; 18: 1,2-butadiene; 19: 3-methyl-1-butene; 20: ethanol; 21: acrolein; 22: isopentane; 23: acetone; 24: 1,4-pentadiene; 25: 1-pentene; 26: furan; 27: 2-methyl-1butene; 28: pentane; 29: trans-pentene; 30: cis-pentene; 31: methyl nitrate; 32: 2-methyl-2-butene; 33: methyl acetate; 34: trans-1,3pentadiene; 35: nitromethane; 36: methyl-propanal; 37: metacrolein; 38: cyclopentene; 39: 4-methyl-1-pentene; 40: 3-methyl-1-pentene; 41: 2,3-dimethylbutane; 42: methyl vinyl ketone; 43: butanal; 44: methyl ethyl ketone; 45: 3-methyl-pentane; 46: 2-methyl-1-pentene; 47: hexane; 48: trans-2-hexene; 49: 2-methylfuran; 50: 3-methylcyclopentene; 51: cis-2-hexene; 52: ethyl tertbutyl ether; 53: trans-1-3hexadiene; 54: methylcyclopentane; 55: 2-butenal; 56: butanol; 57: cis-2-methyl-3-hexene; 58: benzene; 59: 2-methyltetrahydrofuran; 60: cyclohexane; 61: 2-methylhexane; 62: pentanal; 63: 3-methylhexane; 64: cyclohexene; 65: cis-1,3-dimethylcyclopentane; 66: 1-heptene; 67: trans-1,3-dimethylcyclopentane; 68: 2,2,4-trimethylpentane; 69: methyl 3-butenoate; 70: 2-methyl-2-hexen; 71: 3,5-dimethylcyclohexene; 72: trans-2-heptene; 73: cis-2-heptene; 74: 2,3-dimethyl-2-pentene; 75: 3-ethylcyclopentene; 76: 1-ethylcyclopentene; 77: cyclopentanone; 78: cis-1,2-dimethylcyclopentane; 79: methylcyclohexane; 80: 2,5-dimethylhexane; 81: 2,4-dimethylhexane; 82: ethylcyclopentane; 83: 4methylcyclohexene; 84: cis-2-octene; 85: cis-3-octene; 86: 2,3,4-trimethylpentane; 87: toluene; 88: 2-methylheptane; 89: 4-methylheptane; 90: 2-ethyl-1-hexene; 91: 1-methylcyclohexene; 92: 3-methylheptane; 93: trans 1,4-dimethylcyclohexane: 94: 1-octene; 95: 1,1dimethylcyclohexane; 96: butyl-acetate; 97: trans-4-octene; 98: cis-1-ethyl-3-methylcyclopentane; 99: trans-1-ethyl-3-methylcyclopentane; 100: trans-3-octene; 101: octane; 102: trans-2-octene; 103: cis-1,4-dimethylcyclohexane; 104: cis-1,3-dimethylcyclohexane; 105: isopropylcyclopentane; 106: 1-propylcyclopentene; 107: 1,2-dimethylcyclohexene; 108: (E)-2-Hexen-1-al; 109: trans 3,5dimethylcyclohexene; 110: 2-methylcyclohexane; 111: cis-3,5-dimethylcyclohexene; 112: ethylcyclohexane; 113: 1,1,3-trimethylcyclohexane; 114: ethylbenzene; 115: 4-methyloctane; 116: meta and para xylene; 117: 3-methyloctane; 118: styrene; 119: o-xylene; 120: nonane; 121: 1ethyl-2-methylcyclohexane; 122: 1-ethyl-4-methylcyclohexabe; 123: isopropylbenzene; 124: 2,6-dimethylcyclohexane; 125: butylcyclopentane; 126: 1-propenylbenzene; 127: benzaldehydene; 43: butanal; 44: methyl ethyl ketone; 45: 3-methyl-pentane; 46: 2-methyl-1-pentene; 47: hexane; 48: trans-2-hexene; 49: 2-methylfuran; 50: 3-methylcyclopentene; 51: cis-2-hexene; 52: ethyl tertbutyl ether; 53: trans-1-3hexadiene; 54: methylcyclopentane; 55: 2-butenal; 56: butanol; 57: cis-2-methyl-3-hexene; 58: benzene; 59: 2-methyltetrahydrofuran; 60: cyclohexane; 61: 2-methylhexane; 62: pentanal; 63: 3-methylhexane; 64: cyclohexene; 65: cis-1,3-dimethylcyclopentane; 66: 1-heptene; 67: trans-1,3-dimethylcyclopentane; 68: 2,2,4-trimethylpentane; 69: methyl 3-butenoate; 70: 2-methyl-2-hexen; 71: 3,5-dimethylcyclohexene; 72: trans-2-heptene; 73: cis-2-heptene; 74: 2,3-dimethyl-2-pentene; 75: 3-ethylcyclopentene; 76: 1-ethylcyclopentene; 77: cyclopentanone; 78: cis-1,2-dimethylcyclopentane; 79: methylcyclohexane; 80: 2,5-dimethylhexane; 81: 2,4-dimethylhexane; 82: ethylcyclopentane; 83: 4methylcyclohexene; 84: cis-2-octene; 85: cis-3-octene; 86: 2,3,4-trimethylpentane; 87: toluene; 88: 2-methylheptane; 89: 4-methylheptane; 90: 2-ethyl-1-hexene; 91: 1-methylcyclohexene; 92: 3-methylheptane; 93: trans 1,4-dimethylcyclohexane: 94: 1-octene; 95: 1,1dimethylcyclohexane; 96: butyl-acetate; 97: trans-4-octene; 98: cis-1-ethyl-3-methylcyclopentane; 99: trans-1-ethyl-3-methylcyclopentane; 100: trans-3-octene; 101: octane; 102: trans-2-octene; 103: cis-1,4-dimethylcyclohexane; 104: cis-1,3-dimethylcyclohexane; 105: isopropylcyclopentane; 106: 1-propylcyclopentene; 107: 1,2-dimethylcyclohexene; 108: (E)-2-Hexen-1-al; 109: trans 3,5dimethylcyclohexene; 110: 2-methylcyclohexane; 111: cis-3,5-dimethylcyclohexene; 112: ethylcyclohexane; 113: 1,1,3-trimethylcyclohexane; 114: ethylbenzene; 115: 4-methyloctane; 116: meta and para xylene; 117: 3-methyloctane; 118: styrene; 119: o-xylene; 120: nonane; 121: 1ethyl-2-methylcyclohexane; 122: 1-ethyl-4-methylcyclohexabe; 123: isopropylbenzene; 124: 2,6-dimethylcyclohexane; 125: butylcyclopentane; 126: 1-propenylbenzene; 127: benzaldehyde; 128: cyclooctatetraene; 129: propylbenzene; 130: 3,6-dimethyloctane; 131: 3-ethyltoluen; 132: 4-ethyltoluene; 133: trans-pinane; 134: mesitylene; 135: 1-propenylbenzene; 136: 1,1,2,3-tetramethylcyclohexane; 137: 2-ethyltoluene; 138: 1-decene; 139: tert-butylbenzene; 140: 1,2,4-trimethylbenzene; 141: decane; 142: 1,3-methyl-isopropylbenzene; 143: 1,2-methylisopropylbenzene; 144: 1,2,3-trimethylbenzene; 145: indane; 146: 1,3-diethylbenzene; 147: 1,3-methyl-propylbenzene; 148: 1-4diethylbenzene; 149: butylbenzene; 150: 1,2-methyl-propylbenzene; 151: 1,2-diethylbenzene; 152: 1,3-dimethyl-4-ethylbenzene; 153: 1,2dimethyl-4-ethylbenzene; 154: 1,3-dimethyl-2-ethylbenzene; 155: 1,3-dimethyl-2-ethylbenzene; 156: 1-ethenyl-3-ethylbenzene; 157: undecane; 158: (1-methylbutyl)-benzene; 159: 1,2,4,5-tetramethylbenzene; 160: 1,2,3,4-tetramethylbenzene; 161: 1,2,3,5tetramethylbenzene; 162: dodecane; 163: naphthalene.

Figure 40c lists the concentrations and reactivities found in the exhaust gas from MobiLab and compares the respective fractions of C₂ - C₁₂ VOCs (measured with GC/FID-1) with the $>C_{11}$ fractions (measured with GC/FID-2).

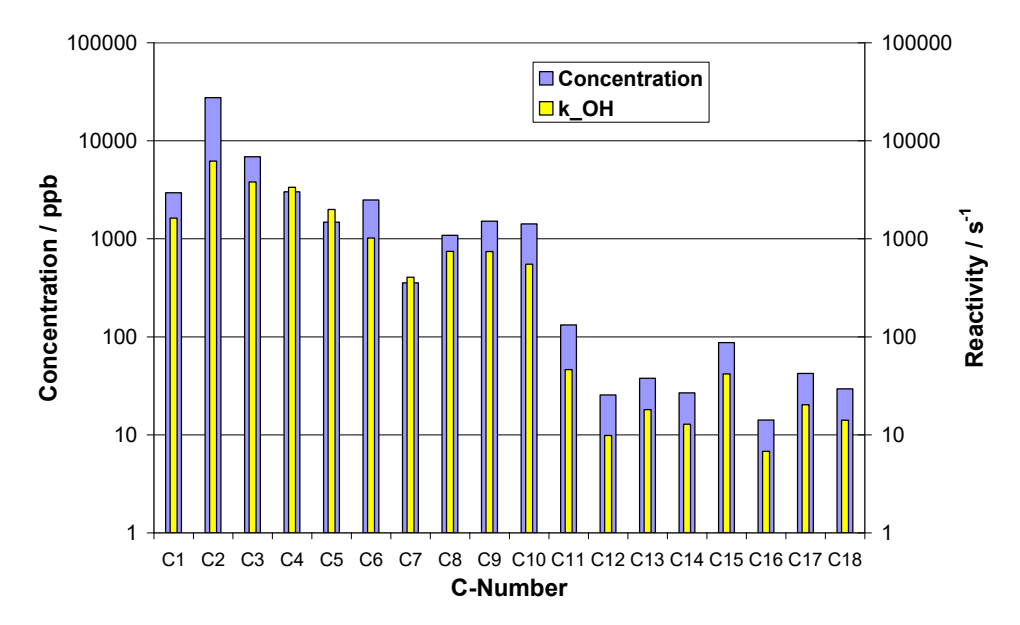


Fig. 40c: VOC concentration and reactivity fractions in the exhaust gas of the MobiLab vehicle under cold-start conditions (MobiLab: year of construction 2016, EURO 6 diesel, 6 cylinders, 212 hp, manufacturer: Daimler AG). The C₁ - C₁₁ range was measured with the GC/FID-1 system. The C₁ components listed were supplemented by the methane mixing ratio (9 ppm or 1.5 s-1) and by the respective formaldehyde mixing ratio (7.7 ppm or 1550 s⁻¹), both measured with cavity-ringdown systems (Picarro Inc.). The range C₁₂ - C₁₈ was covered by the GC/FID-System-2 (see also Fig. 30b). The necessary harmonization of both GC systems was performed on the basis of the adjustment of the range of the $C_9 - C_{12}$ components accessible for both systems.

The investigation of the exhaust gas behaviour of a modern diesel vehicle (MobiLab) under cold-start conditions leads to the following conclusions:

- More than 99% of the measured OH reactivity from VOC is distributed over the range C₁ - C₁₂. The range of heavy VOCs (C₁₃ - C₁₈) contributes to only one percent to the measured OH reactivity²⁸.
- The C₂ components have the highest reactivity contribution with 6200 s⁻¹ to the complete VOC-reactivity (C₁ - C₁₈), which is in total 21650 s⁻¹. This is primarily due to the high concentration contribution of ethylene, which accounts for 84 % of the concentration contribution of the C2 components. Moreover, the reaction constant of ethylene with OH is more than one order of magnitude higher than that of the other two components (ethane and ethyne), so that the reactivity contribution of ethylene represents more than 98% of the C₂ components.
- Also in the case of the C₁ components, a substance (formaldehyde) with a proportion of more than 97 % dominates the associated reactivity contribution. The second important component (methane), on the other hand, has a contribution of only 1 per mille measured in HCHO reactivity at a similar mixing ratio due to its reaction constant of the reaction with OH.

²⁸ In contrast to the tunnel measurements (road tunnel Bonn, cf. 6. 1. 8a), the VOC samples were not directly transferred to the adsorption tubes, but the exhaust gas was first collected in a Silco-steel canister. Due to the high initial concentrations, the waste gas had to be first diluted with synthetic air and enriched cryogenically (C2 - C12-VOCs, GC/FID-1) or sampled on adsorption tubes (C9 - C18-VOCs, GC/FID-2) and then measured. One could suspect that the low proportion of low-volatility components in the diesel exhaust gas under investigation is caused by the low-volatility components condensing on the cylinder walls and thus not being measured.

This suspicion could be refuted experimentally: In a series of preliminary tests, mixtures of C₁₅ - C₁₈alkanes in synthetic air in the high ppb range were produced by precise syringe injection and measured with the GC/FID-2. For the range of C₁₅ to C₁₇ components, the result of the GC analyses provided a recovery rate of more than 90 %. Only for the C₁₈ alkane did the recovery rate drop below 50 %. The associated underestimation of the contribution of low-volatility VOCs proves to be insignificant for the overall VOC-budget, especially since in polluted city air the tendency of VOCs to condense on particles increases significantly with increasing boiling temperature of the VOCs.

c) Comparison of direct k_{OH}-measurements with reactivity calculations derived from concentration measurements of Diesel exhaust

An independent method for determining the reactivity of a diesel exhaust gas mix is to compare direct koh measurements with the reactivity calculations from individual measurements of CO, NOx and VOCs. However, the lower the VOC contribution to the total reactivity of the exhaust gas mix, the more uncertain it is to draw conclusions about the contribution of heavy VOCs to the total VOC budget. In a pilot study, the exhaust gas of a diesel vehicle was therefore investigated under cold-start conditions (i.e. before start of exhaust aftertreatment), during which VOC emissions are typically one order of magnitude higher than under warm operating conditions (cf. Fig. 37).

The concept of total reactivity measurement (koh)

As already mentioned, the OH radical is the major oxidant during daytime. The oxidation of NO, NO2, VOCs by OH radicals leads to the conversion to oxidized compounds, which contribute to aerosol formation. Therefore, the complete description of the OH reactants is essential to analyze the degradation of freshly emitted pollutants and the formation of secondary pollution.

OH reactivity (koh) represents the pseudo first-order reaction rate constant of OH radical. It is a measure of the sum of sink terms due to OH radical reactants Xi, which depends on their ambient concentration [Xi] and their rate coefficient with OH radical. Mathematically, koh equals to the inverse of ambient OH radical lifetime.

The OH reactivity is the sum of all OH reactants times their reaction rate constants versus OH radicals (2).

$$k_{OH} = \sum_{n} k_{xi+OH} \times [X_i]$$
 (2)

The use of OH reactivity allows different VOC compositions to be evaluated by a single quantity. In particular, the concept of OH reactivity is useful to estimate the instantaneous ozone production of an air mass for which both NO2- and VOC- reactivity are known after setting the photostationay state (cf. Fig. 32). On the other hand, the measurement method of direct determination of OH reactivity of a VOC mix directly provides its total OH-reactivity. The comparison of this quantity with the results of

differentiated measurements therefore allows to draw conclusions about components that might not be detected in differentiated measurements.

The OH reactivity can be measured directly with multiple techniques, namely by laserphotolysis - laser-induced fluorescence [Calpini et al., 1999; Sadanaga et al., 2005; Lou et al., 2010; Edwards et al., 2013], flow tube technique with laser-induced fluorescence [Kovacs et al., 2003; Sadanaga et al., 2004; Ingham et al., 2009] and by the comparative reactivity method [Williams et al., 2016; Yang et al., 2017; Michoud et al., 2015].

Within our investigations, the OH reactivity measurement was conducted by a homebuilt instrument using laser photolysis technique with laser-induced fluorescence. The description of the instrument can be found in [Fuchs et al., 2017] and references therein. A brief introduction is given below:

Sampling air is passed (flow rate ~25.5 L min⁻¹) through a flow tube (volume 1 L, length 48 cm, diameter 4 cm). A small fraction of this air flow (1.0 L min⁻¹) is drawn into an OH fluorescence detection cell. A large concentration of OH radicals (~ 109 molecules cm⁻³) is produced in the flow tube by flash photolysis of O₃ with subsequent reaction of O¹D with water vapor. As there are no noticeable ozone concentrations in the air samples of car exhaust gases, ozone is artificially generated by an ozonizer with synthetic air (flow rate 0.2 L min⁻¹). The ozone flow is mixed into the main flow resulting in a mixing ratio of about 50 ppb O₃ entering the flow tube. The marginal dilution (1%) of the main flow was corrected in the evaluation of the measured OH reactivity. Radiation was provided by a quadrupled Nd: YAG laser pulse at 266 nm, which was operated at a low repetition rate of 1 Hz. The monoexponential pseudo first-order decay of the OH radicals was directly observed with the LIF instrument.

The background loss of OH in the instrument is (2 ± 0.2) s⁻¹ which was tested by sampling pure synthetic air without OH reactants. The zero decay value was subtracted from the sample measurements. During the lab experiments, each sample is measured for about 5 minutes to obtain statistically representative results²⁹.

²⁹ Under the selected investigation conditions, it was ensured that the NO concentrations were so low that the internally generated HO₂ radicals (and their subsequent reaction with NO) had no noticeable influence on the OH decay. The presence of these conditions was ensured by the observation of a simple OH-decay according to pseudo-first order.

The $k_{\rm OH}$ instrument is located in a laboratory with air-conditioning. The room temperature is adjusted to around (25 ± 0.2) degree C. So, all results are referring to 25 degree C (298 K).

Results of the differentiated exhaust gas measurements

It has already been pointed out that the diesel exhaust gas had to be mixed down in a series of dilution steps before total OH reactivity can be measured. Some problems had to be solved in this context:

- 1. Since the diesel exhaust gas contains considerable amounts of oxygen, the almost pure NO originally present in the concentrated samples reacts with O2 within minutes to form NO₂. The NO/NO₂-ratio in the cylinder was constant after subsequent dilution steps with synthetic air. As there is a 30% difference between rate coefficient values of NO and NO2 for their reactions with OH radicals (k_(NO2+OH)>k_(NO+OH)), the ratio was carefully taken into account to perform accurate reactivity calculations.
- 2. For the detection of errors associated with the dilution process the accuracy of the dilution factors for the different species were independently verified by accompanying CO₂ measurements.
- 3. The required dilution range of several orders of magnitude made it necessary to use different measuring techniques. Nitrogen oxides were measured using two different instruments: Firstly, a UV absorption spectrometer (advance Optima: Limas 11, ABB Ltd.) for mixing ratios between 1 to 5000 ppm and secondly a chemiluminescence (CLD 780TK, Eco Physics AG, Switzerland) to detect nitrogen oxides at ppb-levels.

For the whole dilution range both the dilution factors and the remaining CO₂ levels agree within 2 %. Also CO was detected using two different detection methods. For high CO mixing ratios above 10 ppm a URAS-14 (ABB Ltd.) was used. Its calibration was checked by means of a CO reference cell that could be folded into the beam path. Lower CO mixing ratios in the diluted exhaust gas samples were detected with a cavity ringdown system (Picarrro Inc.) using the absorption of a reference-free CO-IR transition of known line strengths. Methane and HCHO were only measured in the diluted samples using cavity ringdown detection. Exhaust mixing ratios of these compounds had to be deduced by extrapolation.

Table 4 a-b lists the trace gases contributing to OH reactivity in the exhaust gas of a modern diesel vehicle and compares the results of the concentration measurements during cold (Table 4a) and warm (Table 4b) operating conditions with the results of the total OH reactivity measurements.

Table 4 a: Diesel exhaust composition - cold-start conditions (MobiLab, year of construction 2016, EURO 6 diesel, 6 cylinders, 212 hp, manufacturer: Daimler AG). Listed are relevant OH-reactive species that were measured with different techniques, their corresponding rate coefficients ($K_{(X+OH)}$) for 298 K, their concentrations (in ppb) and calculated OH reactivity values in s⁻¹. The comparison of the sum of the trace gas measurements with the total OH-reactivity investigation yields a discrepancy of 23 %, with the total OH-reactivity investigation value exceeding that of the sum of the individual trace gas measurements.

Species	$\mathbf{k}_{(x+OH)}$	Concentration	OH reactivity	Calculated koh
	cm³ s-1 molec-1	ppb	s ⁻¹	%
со	2.30E-13	1.16E+06	6.55E+03	13.7
NO	7.47E-12	1.15E+04	2.12E+02	0.44
NO ₂	1.07E-11	7.45E+04	1.96E+04	41.0
VOCs (C ₂ -C ₁₂)	-	5.79E+04	1.99E+04	41.6
CH₄	6.37E-15	9.02E+03	1.41E+00	0.0029
нсно	8.37E-12	7.67E+03	1.58E+03	3.31
Sum			4.78E+04	
Result of Total				
reactivity			6.19E+04	
investigation				
Discrepancy	_	_	1.41E+04	22.8

Table 4 b: Same as Table 4 a, but for warm operating conditions. The comparison of the sum of the trace gas measurements with the result of the total OH-reactivity investigation yields a discrepancy of 21 %, with the total OH-reactivity investigation value exceeding that of the sum of the individual trace gas measurements.

Species	pecies $k_{(x+OH)}$		OH reactivity	Calculated koh
	cm³ s ⁻¹ molec ⁻¹	ppb	s ⁻¹	%
CO	2.30E-13	5.13E+02	2.90E+00	0.02
NO	7.47E-12	9.31E+02	1.71E+02	1.20
NO ₂	1.07E-11	4.65E+04	1.22E+04	85.3
VOCs (C ₂ -C ₁₂)	-	8.60E+03	1.56E+03	10.9
CH₄	6.37E-15	2.94E+03	4.61E-01	0.0032
нсно	8.37E-12	2.00E+03	4.13E+02	2.89
Sum			1.43E+04	
Result of Total				
reactivity			1.81E+04	
investigation				
Discrepancy			0.38E+04	21.0

Various remarks are to be made on the emission behaviour of the diesel vehicle investigated:

- i) Comparison of reactivity components for cold and warm operating conditions
- 1. Under cold operating conditions, nitrogen oxides and C2 C12-VOCs each accounted for more than 40 % of the sum of calculated OH reactivities.
- 2. Under warm operating conditions, the reactivity of the exhaust gas mix was reduced by more than a factor of three compared to that under cold-start conditions.
- 3. Under warm operating conditions, NO2 alone caused more than 85% of total OH reactivity. The share of C₂ - C₁₂-VOCs in the total exhaust gas reactivity only contributed to about 10 % of the total OH reactivity. The absolute VOC emission was even reduced compared to that under cold operating conditions by one order of magnitude.
- 4. The largest reduction factor was observed in the case of CO: the average OH reactivity of this substance was reduced by more than a factor of 2000 under warm operating conditions by the oxidation catalyst.

- 5. Overall, the average reaction rate constant of the mix towards OH was reduced by half when comparing cold and warm operating conditions. This is because the cleaning efficiency of the oxidation catalyst is generally higher for short-lived alkenes than for more long-lived alkanes. However, it is noteworthy that under warm operating conditions the mean OH reactivity of the sum of all VOCs (C2 -C₁₂) was reduced three times more than that of HCHO. Two explanations are conceivable: Either the HCHO content in the raw exhaust gas was significantly higher under warm operating conditions than under cold operating conditions. or the cleaning efficiency of the oxidation catalyst was lower for HCHO than for the average VOC mix. In any case, the relative contribution of HCHO to ozone production increased significantly under warm operating conditions.
- ii) Conclusions from the comparative reactivity studies regarding the contribution of large VOCs ($> C_{12}$)
- 1. The (C₂ C₁₂)-OH reactivity of the diesel exhaust gas mix derived from concentration measurements in warm operating conditions dropped to 8 % of the total OH reactivity under cold operating conditions. The oxidation catalyst also reduced the amount of larger VOCs (> C12) emitted during the warm operating state accordingly, so that only diesel emissions from the cold operating state contribute noticeably to the inner-city OH reactivity.
- 2. Under cold operating condition, the sum of calculated OH reactivity (Rvocs (Czc₁₂₎ + R_{CO} + R_{NO} + R_{NO2} + R_{CH4} + R_{HCHO}) was 23 % lower than what was measured by LIF (cf. Table 4a). Assuming that the discrepancy between the two methods was entirely caused by the reactivity of undetected VOCs, the contribution of the OH reactivity from VOC in diesel exhaust would increase from 42 % to about 55 % at maximum.
- 3. [Dunmore et al., 2015] considered the VOC contributions of petrol and diesel vehicles in winter urban traffic in London and claimed that under these conditions 50% of the OH reactivity from VOC was caused by heavy VOCs (> C₁₂) from diesel engines that are usually not detected. For the range of (C₂ -C₁₂)-VOCs it was shown that cold-start emissions dominate VOC emission of

both engine systems by far [Ehlers et al., 2016]. In the context of CMB analyses in the Düsseldorf road tunnel³⁰, we found VOC mass emission fractions of 77 % for cold-start petrol engines, 11 % for cold-start diesel engines and 8 % for petrol engines during warm-up at a recovery rate of 96 % [Urban, 2010]. For cars under cold-start conditions, test bench tests for petrol vehicles showed even an average OH reactivity contribution³¹ for VOC more than 10 times higher for $(C_2 - C_{12})$ -compounds than for diesel vehicles [Klemp et al., 2012]. If the VOC immission contributions of large VOCs (> C₁₂) from diesel exhaust gases were actually to account for 50 % of the OH reactivity found in city centres, their share would have to be of the same order of magnitude as that of petrol engines under cold-start conditions. Since the reactivity contributions of diesel engines under typical inner-city conditions were about one order of magnitude lower than these of gasoline engines if the $(C_2 - C_{12})$ -VOCs were considered exclusively, the contribution of the VOCs (> C₁₂) from diesel exhaust gases predicted by [Dunmore et al., 2015] should provide the corresponding reactivity share. However, the experimentally observed difference between the two methods of reactivity determination is only 23% and would lead to a maximum increase of the VOC contribution to the total koH reactivity from 42% to 55%). This shows that the maximum reactivity contribution of the >C₁₂ components in diesel exhaust is significantly lower than that of the $(C_2 - C_{12})$ -VOCs.

³⁰ The average share of heavy goods vehicles (trucks and buses) was 6%, the diesel passenger car contribution was 31 %. In fact, an increased share of heavy goods traffic only slightly changes the VOC mass proportion distributions found here. Recent work [Update for Emission factors for EURO5- and EURO6-vehicles, 2013] shows that diesel cars in city centre traffic (average speed: approx. 25 km/h) have typical VOC cold start mass emissions of 100 mg/km. For heavy-duty vehicles (EURO-6), significant differences between cold start and warm operating conditions are observed only for the smallest load conditions (Fig. 37 in: "Update for Emission factors for EURO5- and EURO6-vehicles", 2013]). For an average speed of 25 km/h, the upper limit for EURO 5 and EURO 6 heavy-duty vehicles (40 tons, 50 % load condition) is typical VOC mass emissions of 200 - 250 mg/km. Thus even a doubling of the share of heavy commercial vehicles from 6% to 12% would only lead to an increase in the diesel VOC mass contribution from 11% to approx. 15 - 16%.

³¹ The range of C₂ - C₁₂-VOCs was used for these investigations using GC analyses.

iii) Uncertainty analysis

From the error propagation, a total uncertainty of 14 % is estimated for the k_{OH} measurement, which results from the geometric addition of the errors of the koh measurement (< 10 %), those of the mass flow meter (< 2% deviation, MKS Instruments, Wilmington, MA, USA) and from the errors (< 6 %) due to a number of dilution steps of the exhaust gas. Thus the determined kon-reactivity value is afflicted with an uncertainty of $(6.19 \pm 0.87) \cdot 10^4 \, \text{s}^{-1}$.

In the case of differentiated reactivity measurements, the error of the GC analyses is dominant and can therefore be regarded as the lower limit for the uncertainty of this method. The measurement accuracy depends on the quality of the calibration standard (< 5% between true and declared gas concentrations, Apel-Riemer Environmental Inc.) and of the mass flow controller used for diluting the calibration gas (< 2% deviation, MKS Instruments, Wilmington, MA, USA). The linear regression calculated across a number of dilution steps carries a relative uncertainty of < 6 % for the individual species. Uncertainties of the peak areas are caused by their reproducibility (known to lie < 5%), and by an integration uncertainty estimated at < 6%. Geometric addition of all these factors yielded an overall experimental uncertainty of 12%.

Thus, the error measure for the reactivity value determined from the differentiated measurements is $(4.8 \pm 0.6) \cdot 10^4 \text{ s}^{-1}$.

iv) Conclusion

Within the scope of their calculated uncertainties the koh total reactivity measurements and the differentiated reactivity investigations provide consistent results. Since only C₁ - C₁₂-VOCs were considered in the differentiated reactivity tests, the high reactivity contribution of VOC > C₁₂ postulated by Dunmore et al., 2015 can be contradicted. Furthermore, the results of the reactivity tests on a modern diesel vehicle are in complete agreement with the results of the adsorption tube measurements.

In general, the OH reactivity calculated from the individual contribution was slightly lower than the directly measured OH reactivity. This is to be expected, since at least the reactivity contributions³² of unmeasured HONO [cf. Kessler and Platt, 1984] were not taken into account.

In summary, the total OH reactivity measurements in combination with a simultaneous NO₂ measurement could be a versatile alternative for determining the local ozone formation potential of an air mass.

³² HONO was detected in diesel exhaust gas in low concentration ratios (approx. 2 % of the respective NO₂ values). The reaction rate constant of HONO versus OH is half of NO₂. Thus, the contribution of HONO to k_{OH} is about 1% of NO₂.

Influence of VOCs and NO_x on summer ozone formation 6.9

The isopleth plot in [Ehlers et al., 2016] shows the ozone formation at midsummer (21.06.) as a function of the precursor OH reactivities R_{NO2} and R_{VOC} (incl. R_{CO} and R_{CH4}). The isopleth plot with the 1994 and 2014 trends is taken from our publication [Ehlers et al., 2016, Fig. 25]. The mean values of the reactivities from the 5 pollution scenarios are shown (see Table 5). The results of the Berlin summer measurement campaigns (yellow circles) for both high and low reactivities are grouped quite well around the trend for 2014. [Ehlers et al., 2016] describes the principal behaviour of an air mass during processing during transport from the city to biogenically dominated areas.

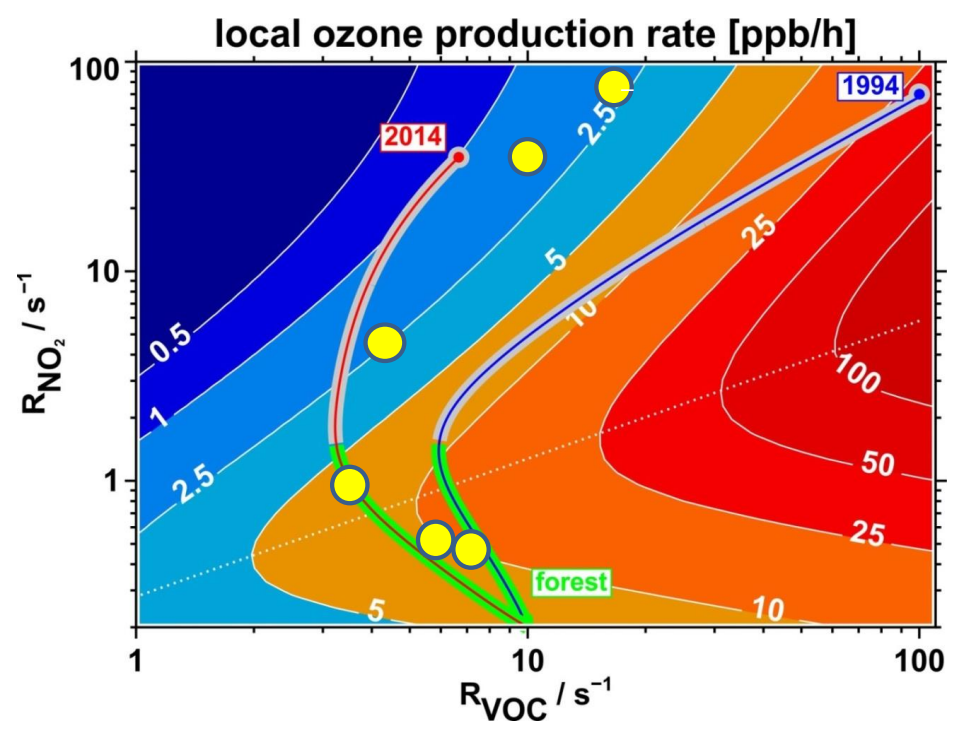


Fig. 41: Results (yellow circles) of the Berlin summer measurement campaigns (August 2016 and July/August 2017) in the isopleth plot. Isopleth plot with 1994 trend and 2014 trend: [Ehlers et al., 2016, Fig. 25). The mean values of the reactivities from the 5 pollution scenarios are shown (see Table 5). The red line from: [Ehlers et al., 2016] describes the basic behaviour of an air mass from 2014 during transport and photochemical processing from the city to biogenically dominated areas. For all 5 scenarios the respective averages group quite well around the dilution and processing course assumed for 2014 [Ehlers et al., 2016]. The trend indicated in Ehlers et al. is also supported by the measurements for the range of low NO2 values.

Table 5: Mean values of the NOx, VOC, CO and CH4 measurements for the associated OH reactivities of the various exposure scenarios (Berlin summer measurement campaigns).

Berlin campaigns	NO [ppb]	NO ₂ [ppb]	NO ₂ * ³³ [s ⁻¹]	VOC ³⁴ [s ⁻¹]	CH ₄ + CO [s ⁻¹]
City centre	102	53	34.4	8.04	2.3
Tiergarten tunnel	180	77	73	11.6	6.4
City background	5.4	12.2	3.9	4.05	0.9
"windwards of the city" ³⁵ (easterly winds)	1	4	0.9	2.76	0.75
" windwards of the city "36 (westerly winds)	0.5	2	0.55	4.65	0.7
" windwards oft the city " ³⁷ (westerly winds)	0.4	1.7	0.46	5.58	0.75

33 When calculating the respective relevant NO₂ reactivity (NO₂*), the setting of the photostationary state with a ratio of NO₂/NO ≈ 3 / 1 was assumed.

³⁴ A certain contribution to total reactivity is also provided by HCHO, a substance that we have not measured in our campaign. For polluted conditions we have observed a contribution of about 3 - 4 % of the measured nitric oxide concentration in the past [Klemp et al., 2002]. [Benning and Wahner, 1998] report atmospheric HCHO concentrations from photochemical VOC degradation in unpolluted areas of about 2 ppb. The resulting reactivity contribution of HCHO is therefore estimated at 0.5 - 1 s⁻¹, so that there were no significant changes in the position of the measuring points on the isopleth plot (Fig. 41). In the future, however, HCHO detection technology will also be integrated into MobiLab. In particular, it is to be investigated whether the increased alcohol content in the fuel leads to altered HCHO proportions.

³⁵ Alt Landsberg, August 2016, eastern inflow conditions.

³⁶ Grunewald, Pfaueninsel, August 2016, western inflow conditions.

³⁷ Grunewald, Sacrow, July 2017, western inflow conditions; results from BMBF project "Stadtklima im Wandel", summer campaign Berlin, Grant: (O1LP1602F).

The following conclusions can be drawn from this first comparison of the current ALASKA data sets with the long-term trend studies based on older data sets [Ehlers et al., 2016]:

- The [Ehlers et al., 2016] ratio of Rvoc/Rno2 can be reproduced in good approximation by the ALASKA measurements. This can be interpreted as confirmation of the trend given in [Ehlers et al., 2016].
- The ALASKA canister samples from less contaminated environments confirm the trend of the 2014 processing / dilution curve.
- The location of the starting ratios of R_{VOC}/R_{NO2} in Fig. 41 also shows that the associated reduction in the local ozone production rate compared to 1994 continues in full.
- From the course of the 2014 processing and dilution curve presented in [Ehlers et al., 2016] it can be seen that current photochemical ozone formation in the source regions is decreasing and shifting more and more to the background regions.
- In any case, due to the constant introduction of new exhaust gas cleaning technologies and the associated changes in emission conditions, a continuous review of the air chemistry framework is essential.

Further usability of our results from the ALASKA project 7

For the first time, we have compiled a representative data set of energy-related emissions of gaseous trace substances from polluted areas of Germany³⁸. It was shown that as expected the high concentrations of trace substances measured on traffic routes are almost exclusively caused by emissions from road traffic. The compilation of a climatology of these concentrations of trace substances provided in part significant differences between summer and winter conditions. These differences are caused both by meteorological processes (e.g. change in the inversion layer height) and by engine measures (e.g. by switching off the SCR catalytic converters in modern diesel vehicles or by the longer warm-up time of the exhaust gas purification system under cold-start conditions).

In addition, the aspect of faster daytime photochemical processes (photostationary state) was discussed and their influence on the NO/NO2 ratio was described.

To detect further potential sources of interference in the operation of mobile fuel cell systems we also carried out extensive VOC measurements on reactive organic gases. For this purpose, VOC canister samples were taken and analyzed for their content of C₂ - C₁₁ hydrocarbons and oxigenated substances.

As part of a further measurement campaign, a newly developed VOC detection system was successfully used for the first time to determine less volatile VOCs. We were able to show that the proportion of C₁₂ - C₁₈-VOCs contributed only little (< 2 %) to the total VOC mass in traffic-polluted air.

The data set generated in this project is of considerable relevance beyond the actual project objectives of ALASKA:

1. Near source trace gas measurements in tunnels reflect the emission conditions of the current vehicle fleet. The quality of existing emission models of road traffic³⁹ can be tested experimentally by normalizing them to the CO₂ increase in the tunnel measured simultaneously with high time resolution.

³⁸ A publication of the results is in preparation.

³⁹ It has been shown that in the past considerable deviations between predicted and experimentally observed VOC/NO_x ratios were found [Ehlers et al., 2016].

- 2. First steps for further applications have already been outlined in the appendix. Since more than 90 % of all VOCs react with OH during the day, the application of the reactivity concept for $R_{VOC} = \sum (k_{OH+VOC}, x [VOC_i])$ and $R_{NO2} = k_{OH+NO2} x [NO2]$ allows a direct comparison between different emission mixes with regard to their ozone formation. On the basis of the reactivity concept, comparisons were made with a current emission calculation model (MCM 3.3). The reactivity-weighted Rvoc/RNo2 ratio allows a direct comparison of the ozone formation rates between the different mixes based on the results of a photochemical box model. The data sets obtained in the ALASKA project confirm the trend we found in earlier campaigns.
- 3. As a further direct application of this concept, the contribution of biogenically emitted VOCs to ozone formation can be directly estimated by comparing the location of the (R_{VOC}/R_{NO2}) ratio on the isopleth plot (cf. Fig. 41) with and without biogenic Rvoc reactivity contributions together with the respective resulting ozone formations.
- 4. In addition, the current emission data sets obtained here can be used for extensive chemistry and transport modeling, so that reliable information on the atmospheric residence time of the introduced trace substances can also be derived.
- 5. Within the framework of the ALASKA project, an IR spectrometer for the detection of atmospheric NH₃ concentrations could be procured. The emission ratio of NH₃/CO₂ in the exhaust gas of petrol vehicles could be determined to a value of approx. 0.05 [ppb/ppm] on the basis of tunnel studies. In the BMBFfunded urban climate project 3DO (funding code (O1LP1602F)), which was worked on in the following, this analysis showed that diesel-powered EURO-6 vehicles (city buses equipped with SCR-NO_x exhaust gas cleaning) can emit much higher NH₃ to CO₂ ratios⁴⁰ of approx. 1 [ppb/ppm] under load conditions [Wegener et al., 2017]. Within the framework of future long-term investigations, this newly occurring input of NH₃ from SCR cat vehicles will be quantified and its significance for secondary particle formation estimated.

⁴⁰ Comparable increases in the emitted NH₃/CO₂-ratios were observed by us on motorway gradients behind trucks (e.g. motorway A-8 behind Karlsruhe in the direction of Stuttgart).

- 6. It is planned to make the temporally and spatially high-resolved data sets generated within ALASKA accessible for epidemiological studies on health effects when staying in traffic-loaded areas. In particular, it could be investigated whether the concentration peaks observed by us (cf. Fig. 4) may cause adverse health effects in addition to the continuous pollutant impacts.
- 7. Further applications of the generated data sets are feasible in the field of filter development. It is well conceivable that the filters developed in this project will not only be used for fuel cell operation, but also to protect the car by filtering the intake external air. The data records generated in ALASKA can be used to reliably dimension the necessary filter effect. First test measurements of the efficiency of conventional vehicle cabin air filters in real traffic were successfully carried out with the MobiLab measuring system. The filter efficiency for different trace gases with a resolution of seconds was determined from the difference between outside air trace gas concentrations and parallel measured cabin air concentrations in the MobiLab passenger cell.

8 Appendix

A: AMS test round: Concentration tables for different trace gases

Table 6 lists the median values for the trace gases of interest, 25th and 75th percentiles, minima and maxima and the number of individual values for different route types. According to the attribution in [openstreetmap, 2018], the following route types were distinguished as different route types: Tunnel, Autobahntunnel, Autobahn, Hauptstraße, Wohngebiet, Nebenstraße, Nebenstraße 2 and Landstraße. In addition, time-weighted mean values x_t according to the following regulation (cf. (3)) have been formed for all measured variables; the time step t_i is one second:

$$x_t = \frac{\sum route \ type_i * t_i}{\sum t_i}$$
 (3)

Table 6 a: Statistical parameters for the measured methane (CH4) concentrations for the various road types of the AMS test round, determined from the measured second data. All data in ppm.

CH4 [ppm]	Tunnel	Autobahntunnel	Autobahn	Hauptstraße	Wohngebiet	Nebenstraße	Nebenstraße2	Landstraße	Time- averaged Mean x _t
Mean	2.01	0.00	2.00	2.00	2.00	2.01	2.00	2.01	2.01
Median	2.01	0.00	2.00	2.01	2.01	2.01	2.01	2.00	2.00
25%- percentil	2.00	0.00	1.99	2.00	1.99	2.00	1.98	1.98	1.98
75%- percentil	2.01	0.00	2.01	2.01	2.01	2.01	2.01	2.01	2.01
Min	1.99	0.00	1.98	1.98	1.98	1.98	1.98	1.98	
Max	2.25	0.00	2.20	2.15	2.02	3.68	2.01	2.01	
Duration t _i	220.0	0.00	2676.0	2453.0	72.0	5649.0	983.0	12805.0	2458.0

Table 6 b: Statistical parameters for the measured carbon monoxide (CO) concentrations for the various road types of the AMS test round, determined from the measured second data. All data in ppb.

CO [ppb]	Tunnel	Autobahntunnel	Autobahn	Hauptstraße	Wohngebiet	Nebenstraße	Nebenstraße2	Landstraße	Time- averaged Mean x _t
Mean	747.81	0.00	262.77	342.56	517.05	352.98	201.96	239.86	281.97
Median	603.07	0.00	185.53	217.79	230.00	233.58	170.67	171.81	195.80
25%- percentil	319.56	0.00	170.67	170.68	146.7	182.85	168.71	170.67	174.61
75%- percentil	1041.45	0.00	279.59	333.11	331.24	349.58	185.19	249.58	288.48
Min	172.45	0.00	111.55	127.00	116.43	110.21	150.51	108.42	
Max	2062.45	0.00	3419.41	6166.14	2942.85	13104.26	1516.98	5891.03	
Duration t _i	220.0	0.0	2676.0	2453.0	72.0	5649.0	983.0	12805.0	24858.0

Table 6 c: Statistical parameters for the measured ammonia (NH₃) concentrations (LosGatos Inc.) for the various road types of the AMS test round, determined from the measured second data. All data in ppb.

LG_NH ₃ [ppb]	Tunnel	Autobahntunnel	Autobahn	Hauptstraße	Wohngebiet	Nebenstraße	Nebenstraße2	Landstraße	Time- averaged Mean x _t
Mean	9.75	0.00	7.38	7.21	6.84	6.76	5.16	6.55	6.73
Median	8.44	0.00	6.90	6.90	6.46	6.55	6.48	6.68	6.70
25%- percentil	7.57	0.00	6.62	6.60	5.17	5.24	2.25	5.47	5.55
75%- percentil	11.24	0.00	8.18	8.06	8.25	7.44	6.69	6.69	7.20
Min	6.12	0.00	1.43	1.91	4.71	0.50	0.62	0.45	0.78
Max	22.18	0.00	23.84	12.31	8.62	22.85	8.64	40.80	30.55
Duration t _i	220.0	0.0	2676.0	2453.0	72.0	5649.0	983.0	12805.0	24858.0

Table 6 d: Statistical parameters for the measured ammonia (NH₃) concentrations⁴¹ (Picarro Inc.) for the various road types of the AMS test round, determined from the measured second data. All data in ppb.

Pic_NH3 [ppb]	Tunnel	Autobahntunnel	Autobahn	Hauptstraße	Wohngebiet	Nebenstraße	Nebenstraße2	Landstraße	Time- averaged Mean x _t
Mean	15.50	0.00	11.22	11.26	10.91	10.77	8.42	10.44	10.65
Median	13.38	0.00	11.11	11.13	10.69	10.63	10.02	10.58	10.71
25%- percentil	10.47	0.00	10.40	10.53	8.33	8.92	4.32	9.01	9.11
75%- percentil	21.39	0.00	12.51	12.23	12.39	11.61	11.04	11.04	11.54
Min	8.91	0.00	4.57	3.40	8.31	5,06	2.93	4.41	
Max	28.13	0.00	21.51	16.82	14.64	24.07	12.84	41.12	
Duration t _i	220.0	0.0	2676.0	2453.0	72.0	5649.0	983.0	12805.0	24858.0

Table 6 e: Statistical parameters for the measured carbon dioxide (CO₂) concentrations (Picarro Inc.) for the various road types of the AMS test round, determined from the measured second data. All data in ppm.

CO2 [ppm]	Tunnel	Autobahntunnel	Autobahn	Hauptstraße	Wohngebiet	Nebenstraße	Nebenstraße2	Landstraße	Time- averaged Mean x _t
Mean	419.07	0.00	457.75	435.49	450.72	439.20	434.62	448.27	445.18
Median	417.20	0.00	434.18	434.97	443.09	432.07	434.18	434.19	433.66
25%- percentil	411.43	0.00	430.07	426.14	436.64	419.25	430.52	434.00	129.15
75%- percentil	424.55	0.00	465.34	438.44	457.84	445.43	440.01	459.84	453.94
Min	407.47	0.00	408.61	408.59	427.70	407.89	423.24	408.53	
Max	465.57	0.00	847.08	716.70	565.89	976.75	443.58	1097.45	
Duration t _i	220	0.0	2676.0	2453.0	72.0	5649.0	983.0	12805.0	24858.0

⁴¹ The differences in the NH₃ results (with higher values for the Picarro cavity ringdown measurement system) are due to longer response times and stronger memory effects for the Picarro system. Laboratory comparisons with NH₃-calibration gas mixtures between the two systems under steady-state conditions showed an agreement of better than 5 % in the range of 2 - 100 ppb. Subsequent optimization of the NH₃ inlet section led to a much better agreement in the transient behavior of both NH₃ measuring systems (see: Klemp et al., Energy and Environment, volume 497, ISBN 978-3-95806-465-2, pp. 60 ff).

Table 6 f: Statistical parameters for the measured water vapor (H₂O) concentrations (Picarro Inc.) for the various road types of the AMS test round, determined from the measured second data. All data in %-mixing ratio [10000 * ppm].

H2O [%]	Tunnel	Autobahntunnel	Autobahn	Hauptstraße	Wohngebiet	Nebenstraße	Nebenstraße2	Landstraße	Time- averaged Mean x _t
Mean	0.78	0.00	0.76	0.78	0.79	0.77	0.76	0.78	0.78
Median	0.77	0.00	0.74	0.73	0.74	0.73	0.74	0.77	0.75
25%- percentil	0.68	0.00	0.69	0.70	0.73	0.70	0.71	0.72	0.71
75%- percentil	0.89	0.00	0.86	0.88	0.86	0.87	0.86	0.86	0.86
Min	0.66	0.00	0.64	0.65	0.70	0.65	0.67	0.63	
Max	0.91	0.00	0.90	0.95	0.86	0.95	0.86	0.98	
Duration t _i	220	0.0	2676.0	2453.0	72.0	5649.0	983.0	12805.0	24858.0

Table 6 g: Statistical parameters for the measured nitric oxide (NO) concentrations (EcoPhysics) for the various road types of the AMS test round, determined from the measured second data. All data in ppb.

NO [ppb]	Tunnel	Autobahntunnel	Autobahn	Hauptstraße	Wohngebiet	Nebenstraße	Nebenstraße2	Landstraße	Time- averaged Mean x _t
Mean	786.55	0.00	96.04	150.17	167.71	139.69	43.51	99.41	113.65
Median	778.30	0.00	56.69	120.05	145.53	106.03	5.53	42.41	67.96
25%- percentil	392.66	0.00	65.63	19.33	26.44	34.02	32.67	18.98	29.56
75%- percentil	1330.30	0.00	155.38	234.77	175.38	190.54	39.97	152.97	170.21
Min	172.62	0.00	44.12	14.10	13.67	16.09	18.94	12.45	
Max	1551.14	0.00	1237.65	976.86	361.43	1389.33	342.32	1587.48	
Duration t _i	220	0.0	2676.0	2453.0	72.0	5649.0	983.0	12805.0	24858.0

Table 6 h: Statistical parameters for the measured nitrogen dioxide (NO2) concentrations (Aerodyne Inc.) for the various road types of the AMS test round, determined from the measured second data. All data in ppb.

NO2_CAPS [ppb]	Tunnel	Autobahntunnel	Autobahn	Hauptstraße	Wohngebiet	Nebenstraße	Nebenstraße2	Landstraße	Time- averaged Mean x _t
Mean	248.65	0.00	60.44	70.24	75.37	68.34	39.57	59.55	63.62
Median	256.70	0.00	52.99	59.84	69.38	62.01	39.42	52.99	57.02
25%-percentil	139.43	0.00	42.14	41.22	65.29	38.12	29.14	42.51	41.74
75%-percentil	328.62	0.00	74.51	98.11	86.68	89.99	52.99	75.98	82.53
Min	75.97	0.00	11.12	11.94	49.52	17.64	17.03	19.54	
Max	454.49	0.00	497.85	393.31	121.04	347.14	75.65	448.63	
Duration t _i	220	0.0	2676.0	2453.0	72.0	5649.0	983.0	12805.0	24858.0

Table 6 i: Statistical parameters for the measured NO_x (=NO+NO₂) concentrations (EcoPhysics) for the various road types of the AMS test round, determined from the measured second data. All data in ppb.

NOx [ppb]	Tunnel	Autobahntunnel	Autobahn	Hauptstraße	Wohngebiet	Nebenstraße	Nebenstraße2	Landstraße	Time- averaged Mean x _t
Mean	393.44	0.00	112.81	13047	134.18	148.35	70.76	107.82	119.48
Median	248.72	0.00	60.43	81.97	115.05	105.50	60.43	60.43	73.69
25%- percentil	151.81	0.00	44.76	49.25	81.09	49.66	23.82	51.82	49.63
75%- percentil	810.83	0.00	134.63	167.27	151.80	192.16	62.62	123.26	144.69
Min	6.79	0.00	42.22	31.09	33.85	22.36	19.03	14.33	
Max	995.11	0.00	1347.10	1412.32	361.83	1367.48	702.62	1915.18	
Duration t _i	87.0	0.0	2676.0	2453.0	72.0	5649.0	983.0	12805.0	24725.0

Table 6 j: Statistical parameters for the measured O₃ concentrations (EcoPhysics) for the various road types of the AMS test round, determined from the measured second data. All data in ppb.

O3 [ppb]	Tunnel	Autobahntunnel	Autobahn	Hauptstraße	Wohngebiet	Nebenstraße	Nebenstraße2	Landstraße	Time- averaged Mean x _t
Mean	7.38	0.00	15.52	11.94	7.98	10.74	17.56	13.99	13.21
Median	7.32	0.00	17.86	10.64	7.09	8.87	18.14	14.65	13.34
25%- percentil	6.56	0.00	9.97	7.55	6.80	6.90	15.38	8.11	8.25
75%- percentil	8.93	0.00	18.89	17.51	10.77	14.30	18.89	18.89	17.60
Min	3.59	0.00	3.61	2.65	6.56	2.49	12.57	7.61	
Max	9.83	0.00	73.58	21.57	10.94	24.92	21.63	23.95	
Duration t _i	220.0	0.0	2676.0	2453.0	72.0	5649.0	983.0	12805.0	24858.0

Table 6 k: Statistical parameters for the measured sulfur dioxide (SO₂) concentrations (ThermoFisher) for the various road types of the AMS test round, determined from the measured second data. All data in ppb.

SO2 [ppb]	Tunnel	Autobahntunnel	Autobahn	Hauptstraße	Wohngebiet	Nebenstraße	Nebenstraße2	Landstraße	Time- averaged Mean x _t
Mean	4.83	0.00	1.50	1.80	1.88	1.92	1.68	1.70	1.76
Median	4.21	0.00	1.38	1.70	1.92	1.79	1.32	1.37	1.52
25%- percentil	2.45	0.00	1.11	1.13	1.42	1.27	1.11	1.11	1.16
75%- percentil	6.75	0.00	1.81	2.19	2.33	2.45	2.15	2.17	2.24
Min	0.33	0.00	0.08	0.05	0.72	0.04	0.16	0.01	
Max	11.64	0.00	8.81	5.52	3.21	905	8.15	11.22	
Duration t _i	220.0	0.0	2676.0	2453.0	72.0	5649.0	983.0	12805.0	24858.0

B: <u>Determination of VOC concentrations for different load scenarios</u>

Table 7 a: City background, Berlin-campaign, August 2017

Species	Mean	25%-Quartile	Median	75%-Quartile
Alkanes				
Ethane	2813	1758	2575	3352
Propane	892	587	728	921
2-Methylpropane	257	182	206	278
n-Butane	759	294	346	611
2-Methylbutane	361	320	392	423
n-Pentane	167	124	162	167
2,2-Dimethylbutane	60	52	63	82
Cyclopentane / 2,3-Dimethylbutane	80	58	74	93
2-Methylpentane	191	142	163	182
3-Methylpentane	60	42	58	77
n-Hexane	71	51	65	74
Methylcyclopentane	0	0	0	0
2,4-Dimethylpentane	44	33	40	49
Cyclohexane	35	24	30	35
2-Methylhexane	31	23	32	36
2,3-Dimethylpentane	16	10	13	21
3-Methylhexane	91	79	85	104
1,3-Dimethylcyclopentane (cis)	13	2	11	14
2,2,4-Trimethylpentane	28	18	27	35
Heptane	33	27	31	37
Methylcyclohexane	20	12	19	29
2,3,4-Trimethylpentane	28	15	15	19
2-Methylheptane	21	15	23	26
4-Methylheptane	9	0	6	17
3-Methylheptane	11	5	10	17
n-Octane	28	14	25	39
n-Nonane	22	18	21	25
n-Decane	18	14	19	21
n-Undecane	16	3	13	30
n-Dodecane	6	1	5	10
n-Tridecane	0	0	0	0
Alkenes				
Ethene	251	170	243	305
Acetylene	254	197	250	297
Propene	196	162	189	224
Propyne	67	47	67	91
1-Butene / i-Butene	111	99	107	116
1,3-Butadiene	20	5	26	32
trans-2-Butene	27	22	27	33
cis-2-Butene	23	20	24	26

Mixing ratios [ppt], City ba	ackgroun	d		
Species	Mean	25%-Quartile	Median	75%-Quartile
1,2-Butadiene	0	0	0	0
3-Methyl-1-butene	25	0	3	35
1-Pentene	29	16	27	38
2-Methyl-1-butene	4	0	0	0
Isoprene	853	403	931	1135
trans-2-Pentene	11	0	4	20
cis-2-Pentene	2	0	0	0
2-Methyl-2-butene	0	0	0	0
1,3-Pentadiene	4	0	0	0
Cyclopentadiene	290	9	42	53
Cyclopentene	0	0	0	0
1-Hexene	65	22	92	98
2-Methyl-1-Pentene	0	0	0	0
trans-2-Hexene	28	15	31	39
cis-2-Hexene	7	0	3	7
1,3-Hexadiene (trans)	0	0	0	0
Cyclohexene	0	0	0	0
1-Heptene	0	0	0	0
2,3-Dimethyl-2-pentene	0	0	0	0
Octene	0	0	0	0
1-Nonene	0	0	0	0
Aromatics				
Benzene	171	138	161	178
Toluene	265	188	220	321
Ethylbenzene	55	39	55	71
m/p-Xylenes	106	88	112	128
Styrene	30	28	32	35
o-Xylene	48	32	45	67
i-Propylbenzene	9	5	8	14
n-Propylbenzene	14	12	15	16
m-Ethyltoluene	23	17	23	32
p-Ethyltoluene	21	19	21	24
1,3,5-Trimethylbenzene	19	19	19	21
o-Ethyltoluene	41	13	39	69
1,2,4-Trimethylbenzene / t-Butylbenzene	37	26	39	43
1,2,3-Trimethylbenzene	13	5	12	19
1,3-Diethylbenzene	7	4	7	9
1,4-Diethylbenzene	5	1	5	7
Butylbenzene	3	0	2	5
Manatarnanaa				
Monoterpenes a-Pinene	252	24	32	75
Sabinene	1	0	0	0
beta-Pinene	13	2	12	19

Mixing ratios [ppt], City background					
Species	Mean	25%-Quartile	Median	75%-Quartile	
Limonene	0	0	0	0	
Indane	12	0	0	11	
Oxigenated compounds					
Acetaldehyde	403	323	365	476	
Methanol	2569	1867	2475	3241	
Ethanol	598	238	312	366	
Acetone	2588	2403	2484	2876	
2-Propanol	40	33	42	52	
Propanal	39	22	44	50	
2-Butanol	25	24	25	27	
Methyl ethyl ketone	177	159	175	193	
1-Propanol	22	0	0	0	
Methacrolein	137	92	105	166	
Methyl vinyl ketone	151	104	138	208	
Butanal	73	0	0	157	
Isobutyl methyl ketone	29	23	26	29	
1-Butanol	36	30	35	39	
Pentanal	1	0	0	0	
Hexanal	132	98	105	146	
Heptanal	77	43	45	66	
Octanal	0	0	0	0	
Eucalyptol	5	0	0	8	

Table 7 b: City center, Berlin-campaign, August 2017

City center						
Species	Mean	25% Quartile	Median	75% Quartile		
Alkanes						
Ethane	1995	814	938	2648		
Propane	943	601	735	1181		
2-Methylpropane	286	260	305	321		
n-Butane	1100	837	1073	1349		
2-Methylbutane	1345	871	903	1598		
n-Pentane	434	327	534	591		
2,2-Dimethylbutane	397	303	500	542		
Cyclopentane / 2,3-Dimethylbutane	251	228	236	266		
2-Methylpentane	465	451	453	474		
3-Methylpentane	202	190	210	217		
n-Hexane	2216	204	216	3228		
Methylcyclopentane	0	0	0	0		
2,4-Dimethylpentane	145	132	144	157		
Cyclohexane	257	84	119	361		
2-Methylhexane	90	71	96	112		
2,3-Dimethylpentane	84	45	63	113		
3-Methylhexane	136	101	148	176		
1,3-Dimethylcyclopentane (cis)	17	0	0	26		
2,2,4-Trimethylpentane	128	121	137	139		
Heptane	162	111	175	220		
Methylcyclohexane	65	48	52	75		
2,3,4-Trimethylpentane	59	54	55	62		
2-Methylheptane	54	38	52	69		
4-Methylheptane	36	16	19	47		
3-Methylheptane	34	25	38	46		
n-Octane	46	41	52	54		
n-Nonane	27	22	25	31		
n-Decane	29	19	21	35		
n-Undecane	110	26	47	163		
n-Dodecane	92	9	18	138		
n-Tridecane	39	0	0	58		
Alkenes						
Ethene	2025	1577	2540	2731		
Acetylene	560	486	549	628		
Propene	561	380	549	732		
<u>'</u>						
Propyne 1 Butons / i Butons	132	115	141	154		
1-Butene / i-Butene 1,3-Butadiene	458 92	265 53	364 62	116		

Mixing ratios [ppt], City center

Species	Mean	25% Quartile	Median	75% Quartile
trans-2-Butene	72	52	62	86
cis-2-Butene	79	68	73	87
1,2-Butadiene	18	0	0	27
3-Methyl-1-butene	30	22	45	45
1-Pentene	59	57	62	62
2-Methyl-1-butene	190	67	95	265
Isoprene	375	180	234	500
trans-2-Pentene	104	86	99	120
cis-2-Pentene	73	64	74	82
2-Methyl-2-butene	68	54	63	79
1,3-Pentadiene	12	0	0	18
Cyclopentadiene	0	0	0	0
Cyclopentene	18	0	0	27
1-Hexene	34	0	0	51
2-Methyl-1-Pentene	22	14	28	33
trans-2-Hexene	70	26	37	97
cis-2-Hexene	16	9	17	24
1,3-Hexadiene (trans)	0	0	0	0
Cyclohexene	7	0	0	11
1-Heptene	5	0	0	8
2,3-Dimethyl-2-pentene	9	0	0	14
Octene	0	0	0	0
1-Nonene	0	0	0	0
Association				
Aromatics	441	240	200	F.4F
Benzene		310	388	545
Toluene	1063	1009	1053	1113
Ethylbenzene	178	152 366	187 581	933
m/p-Xylenes Styrene	672 62	38	52	81
o-Xylene	161	127	192	210
i-Propylbenzene	16	13	152	19
n-Propylbenzene	37	33	45	45
m-Ethyltoluene	142	102	139	180
p-Ethyltoluene	57	49	60	66
1,3,5-Trimethylbenzene	73	54	68	89
o-Ethyltoluene	40	32	54	55
1,2,4-Trimethylbenzene / t-Butylbenzene	158	132	182	197
1,2,3-Trimethylbenzene	58	45	59	72
1,3-Diethylbenzene	38	33	41	43
1,4-Diethylbenzene	27	18	24	34
Butylbenzene	26	22	28	32
				<u></u>
Monoterpenes				
a-Pinene	47	28	41	63
	ļ			

Mixing ratios [ppt], City center

Species	Mean	25% Quartile	Median	75% Quartile
Sabinene	7	4	8	10
beta-Pinene	15	9	18	23
Limonene	10	7	13	15
Indane	4	0	0	7
Oxigenated compounds				
Acetaldehyde	345	325	381	383
Methanol	2547	2299	2668	2855
Ethanol	2018	318	526	2973
Acetone	11756	7674	13160	16540
2-Propanol	5140	107	164	7685
Propanal	770	247	314	1065
2-Butanol	27	24	30	31
Methyl ethyl ketone	173	105	131	219
1-Propanol	281	0	0	422
Methacrolein	86	57	66	105
Methyl vinyl ketone	112	73	88	138
Butanal	40	0	0	60
Isobutyl methyl keton	57	40	45	69
1-Butanol	403	44	54	588
Pentanal	0	0	0	0
Hexanal	16	0	0	24
Heptanal	27	25	28	29
Octanal	0	0	0	0
Eucalyptol	4	0	0	6

Table 7 c: Tiergarten tunnel (weekday traffic, Mean velocity: 40 – 60 km/h, Berlin campaign, August 2017

Species	Mean	25% Quartile	Median	75% Quartile
Alkanes				
Ethane	2623	2418	2536	2744
Propane	1143	860	999	1197
2-Methylpropane	730	362	542	572
n-Butane	1290	1209	1245	1318
2-Methylbutane	3917	2686	3447	5028
n-Pentane	1121	866	1006	1461
2,2-Dimethylbutane	928	718	803	1128
Cyclopentane / 2,3-Dimethylbutane	847	420	613	896
2-Methylpentane	1382	840	1328	1950
3-Methylpentane	591	402	433	738
n-Hexane	491	348	386	588
Methylcyclopentane	55	-	-	-
2,4-Dimethylpentane	350	224	294	504
Cyclohexane	207	154	161	236
2-Methylhexane	263	132	184	356
2,3-Dimethylpentane	112	71	97	133
3-Methylhexane	242	218	226	231
1,3-Dimethylcyclopentane (cis)	74	50	62	106
2,2,4-Trimethylpentane	179	136	146	229
Heptane	152	95	118	173
Methylcyclohexane	127	89	119	131
2,3,4-Trimethylpentane	106	79	90	110
2-Methylheptane	96	47	80	127
4-Methylheptane	69	68	74	76
3-Methylheptane	70	42	50	69
n-Octane	68	50	69	99
n-Nonane	94	70	101	113
n-Decane	81	57	82	88
n-Undecane	16	13	14	19
n-Dodecane	7	3	7	9
n-Tridecane	0	0	0	0
Alkenes				
Ethene	5261	4031	4891	5773
Acetylene	2008	1274	1442	2179
Propene	1491	1080	1196	1949
Propyne	309	185	220	350
1-Butene / i-Butene	635	481	534	773
1,3-Butadiene	242	220	230	342
trans-2-Butene	110	87	102	122

Species	Mean	25% Quartile	Median	75% Quartile
cis-2-Butene	115	90	107	133
1,2-Butadiene	6	0	0	0
3-Methyl-1-butene	89	94	101	114
1-Pentene	69	65	70	88
2-Methyl-1-butene	80	0	0	125
Isoprene	121	29	153	192
trans-2-Pentene	219	151	195	236
cis-2-Pentene	174	137	204	216
2-Methyl-2-butene	54	0	19	65
1,3-Pentadiene	8	0	0	0
Cyclopentadiene	5	0	0	0
Cyclopentene	40	0	0	0
1-Hexene	31	0	0	0
2-Methyl-1-Pentene	68	31	47	96
trans-2-Hexene	51	40	48	62
cis-2-Hexene	64	37	43	79
1,3-Hexadiene (trans)	41	0	0	82
Cyclohexene	0	0	0	0
1-Heptene	27	0	13	47
2,3-Dimethyl-2-pentene	8	0	0	0
Octene	2	0	0	0
1-Nonene	0	0	0	0
Aromatics				
Benzene	1362	1163	1442	1467
Toluene	2636	1794	2042	3277
Ethylbenzene	508	332	449	706
m/p-Xylenes	2205	650	1158	1712
Styrene	109	96	109	125
o-Xylene	410	308	338	489
i-Propylbenzene	47	37	45	56
n-Propylbenzene	90	53	76	118
m-Ethyltoluene	222	111	176	323
p-Ethyltoluene	192	124	203	247
1,3,5-Trimethylbenzene	1218	97	126	296
o-Ethyltoluene	144	89	126	196
1,2,4-Trimethylbenzene / t-Butylbenzene	439	357	378	522
1,2,3-Trimethylbenzene	96	65	109	135
1,3-Diethylbenzene	53	17	47	65
1,4-Diethylbenzene	48	16	40	70
Butylbenzene	49	24	48	64
Monoterpenes				
a-Pinene	0	0	0	0
Sabinene	0	0	0	0

Mixing ratios [ppt], Tiergarten tunnel				
Species	Mean	25% Quartile	Median	75% Quartile
beta-Pinene	0	0	0	0
Limonene	1	0	0	0
Indane	20	0	6	18
Oxigenated compounds				
Acetaldehyde	516	448	490	639
Methanol	6621	5563	6636	7477
Ethanol	7005	2995	5877	10245
Acetone	4921	3215	4843	6615
2-Propanol	400	220	270	353
Propanal	843	232	301	360
2-Butanol	105	68	96	140
Methyl ethyl ketone	498	355	460	645
1-Propanol	302	267	327	415
Methacrolein	0	0	0	0
Methyl vinyl ketone	0	0	0	0
Butanal	241	170	248	332
Isobutyl methyl ketone	315	150	195	272
1-Butanol	231	73	107	125
Pentanal	9	0	0	0
Hexanal	38	0	0	41
Heptanal	0	0	0	0
Octanal	0	0	0	0
Eucalyptol	5	0	0	4

Table 7 d: "In front of the city" (regional background for easterly flows, Berlin campaign, August 2017

Species	Mean	25% Quartile	Median	75% Quartile
Alkanes				
	0004	4057	0000	0450
Ethane	2094	1957	2006	2158
Propane	876	693	715	1018
2-Methylpropane	226	165	171	268
n-Butane	648	388	451	686
2-Methylbutane	228	177	217	252
n-Pentane	152	109	152	176
2,2-Dimethylbutane	72	36	39	60
Cyclopentane / 2,3-Dimethylbutane	59	43	47	57
2-Methylpentane	52	33	54	59
3-Methylpentane	48	31	47	69
n-Hexane	75	60	72	83
Methylcyclopentane	5	0	0	0
2,4-Dimethylpentane	34	29	33	38
Cyclohexane	25	16	21	35
2-Methylhexane	20	12	16	21
2,3-Dimethylpentane	8	5	8	9
3-Methylhexane	126	64	75	106
1,3-Dimethylcyclopentane (cis)	3	0	0	7
2,2,4-Trimethylpentane	14	0	8	18
Heptane	28	21	24	33
Methylcyclohexane	21	9	19	34
2,3,4-Trimethylpentane	15	13	14	19
2-Methylheptane	11	8	10	15
4-Methylheptane	5	2	7	8
3-Methylheptane	2	0	0	2
n-Octane	29	17	18	34
n-Nonane	16	11	14	19
n-Decane	10	8	11	13
n-Undecane	8	6	7	10
n-Dodecane	2	0	0	4
n-Tridecane	0	0	0	0
Alkenes				
Ethene	292	210	248	309
Acetylene	225	204	223	245
Propene	224	194	197	263
Propyne	60	56	56	65
1-Butene / i-Butene	620	195	610	755
1,3-Butadiene	31	16	29	40

Species	Mean	25% Quartile	Median	75% Quartile
trans-2-Butene	40	32	42	47
cis-2-Butene	34	24	32	40
1,2-Butadiene	0	0	0	0
3-Methyl-1-butene	0	0	0	0
1-Pentene	32	29	29	29
2-Methyl-1-butene	0	0	0	0
Isoprene	176	122	138	183
trans-2-Pentene	11	0	0	26
cis-2-Pentene	0	0	0	0
2-Methyl-2-butene	3	0	0	0
1,3-Pentadiene	0	0	0	0
Cyclopentadiene	36	26	33	41
Cyclopentene	11	0	0	12
1-Hexene	53	26	39	45
2-Methyl-1-Pentene	2	0	0	0
trans-2-Hexene	32	5	16	38
cis-2-Hexene	0	0	0	0
1,3-Hexadiene (trans)	0	0	0	0
Cyclohexene	0	0	0	0
1-Heptene	19	9	14	17
2,3-Dimethyl-2-pentene	0	0	0	0
Octene	0	0	0	0
1-Nonene	4	0	0	0
Aromatics				
Benzene	177	168	176	186
Toluene	263	169	237	279
Ethylbenzene	27	24	27	31
m/p-Xylenes	41	29	35	47
Styrene	26	25	27	35
o-Xylene	31	18	20	29
i-Propylbenzene	16	0	8	13
n-Propylbenzene	8	7	8	9
m-Ethyltoluene	11	7	11	13
p-Ethyltoluene	8	7	8	9
1,3,5-Trimethylbenzene	11	6	8	10
o-Ethyltoluene	16	7	15	24
1,2,4-Trimethylbenzene / t-Butylbenzene	15	10	15	22
1,2,3-Trimethylbenzene	12	6	8	16
1,3-Diethylbenzene	2	0	0	4
1,4-Diethylbenzene	1	0	0	0
Butylbenzene	1	0	0	0
Monoterpenes				
a-Pinene	18	9	23	28
Sabinene	2	0	0	0
Capitotic	11	4	8	U

Mixing ratios [ppt], In fron	t of the c	ity		
Species	Mean	25% Quartile	Median	75% Quartile
Limonene	3	0	0	0
Indane	1	0	0	0
Oxigenated compounds				
Acetaldehyde	327	290	304	364
Methanol	2731	1905	2312	2916
Ethanol	212	162	203	233
Acetone	2249	1629	1705	1763
2-Propanol	43	39	46	47
Propanal	98	18	29	44
2-Butanol	23	16	25	31
Methyl ethyl ketone	117	62	74	86
1-Propanol	42	0	0	0
Methacrolein	65	53	56	68
Methyl vinyl ketone	81	63	74	82
Butanal	170	119	162	215
Isobutyl methyl ketone	29	9	10	11
1-Butanol	32	24	33	39
Pentanal	0	0	0	0
Hexanal	224	52	78	106
Heptanal	22	0	19	25
Octanal	1	0	0	0
Eucalyptol	6	5	7	8

C: OH-Reactivity determinations for the considered pollution scenarios

Table 8 a: City background, Berlin campaign, August 2017

Species	Mean	25% Quartile	Median	75% Quartile
Alkanes				
Ethane	0.018	0.012	0.016	0.022
Propane	0.025	0.017	0.020	0.026
2-Methylpropane	0.014	0.010	0.011	0.015
n-Butane	0.046	0.018	0.021	0.037
2-Methylbutane	0.033	0.029	0.036	0.039
n-Pentane	0.017	0.012	0.016	0.017
2,2-Dimethylbutane	0.004	0.003	0.004	0.005
Cyclopentane / 2,3-Dimethylbutane	0.010	0.008	0.010	0.012
2-Methylpentane	0.025	0.018	0.021	0.024
3-Methylpentane	0.008	0.006	0.008	0.010
n-Hexane	0.010	0.007	0.009	0.010
Methylcyclopentane	0.000	0.000	0.000	0.000
2,4-Dimethylpentane	0.006	0.004	0.005	0.006
Cyclohexane	0.006	0.004	0.005	0.006
2-Methylhexane	0.005	0.004	0.005	0.006
2,3-Dimethylpentane	0.002	0.002	0.002	0.003
3-Methylhexane	0.016	0.014	0.015	0.018
1,3-Dimethylcyclopentane (cis)	0.003	0.000	0.002	0.003
2,2,4-Trimethylpentane	0.003	0.002	0.002	0.003
Heptane	0.006	0.005	0.005	0.006
Methylcyclohexane	0.005	0.003	0.005	0.007
2,3,4-Trimethylpentane	0.005	0.003	0.003	0.003
2-Methylheptane	0.004	0.003	0.005	0.005
4-Methylheptane	0.002	0.000	0.001	0.004
3-Methylheptane	0.002	0.001	0.002	0.004
n-Octane	0.006	0.003	0.005	0.008
n-Nonane	0.005	0.005	0.005	0.006
n-Decane	0.005	0.004	0.005	0.006
n-Undecane	0.005	0.001	0.004	0.010
n-Dodecane	0.002	0.000	0.002	0.004
n-Tridecane	0.000	0.000	0.000	0.000
Alkenes				
Ethene	0.049	0.033	0.048	0.060
Acetylene	0.005	0.004	0.005	0.006
Propene	0.138	0.114	0.134	0.158
Propyne	0.010	0.007	0.010	0.014
1-Butene / i-Butene	0.071	0.064	0.068	0.074
1,3-Butadiene	0.032	0.009	0.041	0.052

Species	Mean	25% Quartile	Median	75% Quartile
trans-2-Butene	0.042	0.033	0.042	0.051
cis-2-Butene	0.032	0.027	0.033	0.036
1,2-Butadiene	0.000	0.000	0.000	0.000
3-Methyl-1-butene	0.019	0.000	0.002	0.028
1-Pentene	0.022	0.013	0.021	0.029
2-Methyl-1-butene	0.006	0.000	0.000	0.000
Isoprene	2.073	0.986	2.261	2.754
trans-2-Pentene	0.019	0.000	0.007	0.034
cis-2-Pentene	0.003	0.000	0.000	0.000
2-Methyl-2-butene	0.003	0.000	0.000	0.000
1,3-Pentadiene	0.009	0.000	0.000	0.000
Cyclopentadiene	0.657	0.020	0.096	0.120
Cyclopentene	0.000	0.000	0.000	0.000
1-Hexene	0.059	0.020	0.084	0.089
2-Methyl-1-Pentene	0.000	0.000	0.000	0.000
trans-2-Hexene	0.045	0.025	0.050	0.064
cis-2-Hexene	0.011	0.000	0.005	0.011
1,3-Hexadiene (trans)	0.000	0.000	0.000	0.000
Cyclohexene	0.000	0.000	0.000	0.000
1-Heptene	0.000	0.000	0.000	0.000
2,3-Dimethyl-2-pentene	0.000	0.000	0.000	0.000
Octene	0.000	0.000	0.000	0.000
1-Nonene	0.000	0.000	0.000	0.000
Aromatics	2 225	0.004	2 225	0.005
Benzene	0.005	0.004	0.005	0.005
Toluene	0.036	0.026	0.030	0.044
Ethylbenzene	0.009	0.007	0.010	0.012
m/p-Xylenes	0.049	0.041	0.052	0.059
Styrene	0.043	0.040	0.046	0.050
o-Xylene	0.016	0.011	0.015	0.023
i-Propylbenzene	0.001	0.001	0.001	0.002
n-Propylbenzene	0.002	0.002	0.002	0.002
m-Ethyltoluene	0.010	0.008	0.011	0.015
p-Ethyltoluene	0.006	0.005	0.006	0.007
1,3,5-Trimethylbenzene	0.027	0.026	0.027	0.029
o-Ethyltoluene	0.012	0.004	0.011	0.020
1,2,4-Trimethylbenzene / t-Butylbenzene	0.017	0.012	0.018	0.020
1,2,3-Trimethylbenzene	0.010	0.004	0.010	0.015
1,3-Diethylbenzene	0.002	0.001	0.002	0.003
1,4-Diethylbenzene	0.001	0.000	0.001	0.002
Butylbenzene	0.001	0.000	0.000	0.001
Manadamana				
Monoterpenes	1			

OH reactivity [s ⁻¹], City ba	ckground	j		
Species	Mean	25% Quartile	Median	75% Quartile
Sabinene	0.000	0.000	0.000	0.000
beta-Pinene	0.025	0.004	0.022	0.036
Limonene	0.000	0.000	0.000	0.000
Indane	0.003	0.000	0.000	0.002
Oxigenated compounds				
Acetaldehyde	0.155	0.124	0.140	0.184
Methanol	0.060	0.044	0.058	0.077
Ethanol	0.048	0.019	0.025	0.030
Acetone	0.014	0.013	0.014	0.016
2-Propanol	0.005	0.004	0.005	0.006
Propanal	0.019	0.011	0.021	0.024
2-Butanol	0.000	0.000	0.000	0.000
Methyl ethyl ketone	0.000	0.000	0.000	0.000
1-Propanol	0.003	0.000	0.000	0.000
Methacrolein	0.093	0.063	0.071	0.113
Methyl vinyl ketone	0.069	0.048	0.063	0.094
Butanal	0.042	0.000	0.000	0.090
Isobutyl methyl ketone	0.000	0.000	0.000	0.000
1-Butanol	0.063	0.054	0.062	0.070
Pentanal	0.001	0.000	0.000	0.000
Hexanal	0.105	0.078	0.084	0.116
Heptanal	0.058	0.016	0.040	0.055
Octanal	0.000	0.000	0.000	0.000
Eucalyptol	0.001	0.000	0.000	0.002

 $\sum R_{voc} / s^{-1}$ 4.94 2.25 4.05 5.22

Table 8 b: City center, Berlin campaign, August 2017

Species	Mean	25% Quartile	Median	75% Quartile
Alkanes				
Ethane	0.012	0.005	0.006	0.017
Propane	0.026	0.017	0.020	0.033
2-Methylpropane	0.015	0.014	0.016	0.017
n-Butane	0.066	0.050	0.064	0.081
2-Methylbutane	0.122	0.079	0.082	0.145
n-Pentane	0.043	0.032	0.053	0.058
2,2-Dimethylbutane	0.023	0.017	0.029	0.031
Cyclopentane / 2,3-Dimethylbutane	0.033	0.030	0.031	0.035
2-Methylpentane	0.061	0.059	0.059	0.062
3-Methylpentane	0.027	0.025	0.028	0.029
n-Hexane	0.297	0.027	0.029	0.433
Methylcyclopentane	0.000	0.000	0.000	0.000
2,4-Dimethylpentane	0.018	0.017	0.018	0.020
Cyclohexane	0.046	0.015	0.021	0.064
2-Methylhexane	0.015	0.012	0.016	0.019
2,3-Dimethylpentane	0.013	0.007	0.009	0.017
3-Methylhexane	0.024	0.018	0.026	0.031
1,3-Dimethylcyclopentane (cis)	0.003	0.000	0.000	0.005
2,2,4-Trimethylpentane	0.012	0.011	0.012	0.013
Heptane	0.028	0.019	0.030	0.038
Methylcyclohexane	0.016	0.012	0.013	0.019
2,3,4-Trimethylpentane	0.010	0.009	0.010	0.011
2-Methylheptane	0.011	0.008	0.011	0.014
4-Methylheptane	0.008	0.003	0.004	0.010
3-Methylheptane	0.007	0.005	0.008	0.010
n-Octane	0.010	0.009	0.011	0.012
n-Nonane	0.007	0.005	0.006	0.008
n-Decane	0.008	0.005	0.006	0.010
n-Undecane	0.035	0.008	0.015	0.052
n-Dodecane	0.031	0.003	0.006	0.047
n-Tridecane	0.013	0.000	0.000	0.020
Alkenes				
Ethene	0.397	0.309	0.498	0.536
Acetylene	0.011	0.010	0.011	0.013
Propene	0.396	0.268	0.383	0.517
Propyne	0.020	0.017	0.021	0.023
1-Butene / i-Butene	0.297	0.172	0.236	0.391
1.3-Butadiene	0.150	0.087	0.101	0.189

Species	Mean	25% Quartile	Median	75% Quartile
trans-2-Butene	0.112	0.082	0.098	0.135
cis-2-Butene	0.109	0.094	0.101	0.121
1,2-Butadiene	0.011	0.000	0.000	0.017
3-Methyl-1-butene	0.024	0.017	0.035	0.035
1-Pentene	0.046	0.044	0.047	0.048
2-Methyl-1-butene	0.283	0.100	0.143	0.396
Isoprene	0.927	0.444	0.578	1.235
trans-2-Pentene	0.171	0.142	0.163	0.197
cis-2-Pentene	0.117	0.103	0.120	0.132
2-Methyl-2-butene	0.145	0.115	0.134	0.170
1,3-Pentadiene	0.030	0.000	0.000	0.045
Cyclopentadiene	0.000	0.000	0.000	0.000
Cyclopentene	0.030	0.000	0.000	0.045
1-Hexene	0.031	0.000	0.000	0.047
2-Methyl-1-Pentene	0.034	0.022	0.044	0.051
trans-2-Hexene	0.114	0.043	0.061	0.158
cis-2-Hexene	0.025	0.013	0.026	0.037
1,3-Hexadiene (trans)	0.000	0.000	0.000	0.000
Cyclohexene	0.012	0.000	0.000	0.018
1-Heptene	0.005	0.000	0.000	0.008
2,3-Dimethyl-2-pentene	0.024	0.000	0.000	0.036
Octene	0.000	0.000	0.000	0.000
1-Nonene	0.000	0.000	0.000	0.000
Aromatics				
Benzene	0.013	0.009	0.012	0.016
Toluene	0.147	0.140	0.146	0.154
Ethylbenzene	0.031	0.026	0.032	0.036
m/p-Xylenes	0.309	0.168	0.267	0.429
Styrene	0.088	0.054	0.074	0.115
o-Xylene	0.054	0.043	0.064	0.070
i-Propylbenzene	0.002	0.002	0.002	0.003
n-Propylbenzene	0.005	0.005	0.006	0.006
m-Ethyltoluene	0.065	0.047	0.064	0.083
p-Ethyltoluene	0.016	0.014	0.017	0.019
1,3,5-Trimethylbenzene	0.102	0.076	0.095	0.124
o-Ethyltoluene	0.012	0.010	0.016	0.016
1,2,4-Trimethylbenzene / t-Butylbenzene	0.073	0.060	0.083	0.090
1,2,3-Trimethylbenzene	0.047	0.036	0.048	0.058
1,3-Diethylbenzene	0.011	0.010	0.012	0.013
1,4-Diethylbenzene	0.008	0.005	0.007	0.010
Butylbenzene	0.005	0.004	0.006	0.006
Monoterpenes				
a-Pinene	0.061	0.036	0.054	0.082
Sabinene	0.002	0.001	0.002	0.003
	0.030	0.017	0.035	0.044

OH Reactivity [s ⁻¹], City co	enter			
Species	Mean	25% Quartile	Median	75% Quartile
Limonene	0.040	0.027	0.055	0.060
Indane	0.001	0.000	0.000	0.002
Oxigenated compounds				
Acetaldehyde	0.134	0.126	0.148	0.148
Methanol	0.059	0.053	0.062	0.066
Ethanol	0.162	0.026	0.042	0.239
Acetone	0.063	0.041	0.071	0.089
2-Propanol	0.641	0.013	0.020	0.959
Propanal	0.371	0.119	0.151	0.513
2-Butanol	0.000	0.000	0.000	0.000
Methyl ethyl ketone	0.000	0.000	0.000	0.000
1-Propanol	0.038	0.000	0.000	0.057
Methacrolein	0.058	0.039	0.045	0.071
Methyl vinyl ketone	0.051	0.033	0.040	0.063
Butanal	0.023	0.000	0.000	0.034
Isobutyl methyl ketone	0.000	0.000	0.000	0.000
1-Butanol	0.717	0.077	0.096	1.046
Pentanal	0.000	0.000	0.000	0.000
Hexanal	0.013	0.000	0.000	0.019
Heptanal	0.024	0.022	0.025	0.026
Octanal	0.000	0.000	0.000	0.000
Eucalyptol	0.001	0.000	0.000	0.002

 $\sum R_{voc} / s^{-1}$ 10.73 8.04 3.94 5.25

Table 8 c: Tiergarten tunnel, Berlin campaign, August 2017

Species	Mean	25% Quartile	Median	75% Quartile
Alkanes				
Ethane	0.011	0.009	0.011	0.013
Propane	0.035	0.027	0.032	0.040
2-Methylpropane	0.040	0.021	0.029	0.031
n-Butane	0.076	0.073	0.075	0.079
2-Methylbutane	0.378	0.271	0.378	0.464
n-Pentane	0.116	0.097	0.111	0.148
2,2-Dimethylbutane	0.058	0.046	0.057	0.070
Cyclopentane / 2,3-Dimethylbutane	1.153	0.057	0.085	0.117
2-Methylpentane	0.191	0.129	0.193	0.254
3-Methylpentane	0.082	0.055	0.069	0.102
n-Hexane	0.070	0.051	0.062	0.083
Methylcyclopentane	0.009	0.000	0.000	0.000
2,4-Dimethylpentane	0.045	0.028	0.041	0.065
Cyclohexane	0.037	0.028	0.030	0.042
2-Methylhexane	0.046	0.025	0.034	0.060
2,3-Dimethylpentane	0.018	0.011	0.017	0.020
3-Methylhexane	0.042	0.037	0.039	0.040
1,3-Dimethylcyclopentane (cis)	0.015	0.010	0.013	0.021
2,2,4-Trimethylpentane	0.017	0.013	0.014	0.021
Heptane	0.027	0.017	0.020	0.030
Methylcyclohexane	0.031	0.021	0.027	0.031
2,3,4-Trimethylpentane	0.019	0.014	0.018	0.021
2-Methylheptane	0.021	0.012	0.018	0.026
4-Methylheptane	0.014	0.014	0.016	0.016
3-Methylheptane	0.015	0.009	0.012	0.015
n-Octane	0.014	0.010	0.014	0.021
n-Nonane	0.022	0.017	0.022	0.026
n-Decane	0.026	0.022	0.023	0.024
n-Undecane	0.004	0.004	0.004	0.004
n-Dodecane	0.002	0.001	0.002	0.003
n-Tridecane	0.000	0.000	0.000	0.000
Alkenes				
Ethene	1.067	0.845	1.063	1.132
Acetylene	0.042	0.026	0.035	0.047
Propene	1.111	0.763	1.019	1.464
Propyne	0.049	0.028	0.040	0.056
1-Butene / i-Butene	0.429	0.312	0.398	0.527
1,3-Butadiene	0.413	0.359	0.428	0.585
trans-2-Butene	0.177	0.137	0.161	0.208
cis-2-Butene	0.159	0.124	0.148	0.181

Species	ten tunn	25% Quartile	Median	75% Quartile
1,2-Butadiene	0.004	0.000	0.000	0.000
3-Methyl-1-butene	0.004	0.000	0.000	0.000
1-Pentene	0.072	0.074	0.079	0.092
2-Methyl-1-butene	0.056	0.000	0.002	0.071
*	0.116	0.000	0.000	0.174
Isoprene trans-2-Pentene	0.323	0.073	0.379	0.476
cis-2-Pentene	0.354	0.221	0.328	0.348
2-Methyl-2-butene	0.283	0.243	0.000	0.061
1,3-Pentadiene	0.040	0.000	0.000	0.000
Cyclopentadiene	0.000	0.000	0.000	0.000
Cyclopentene	0.012	0.000	0.000	0.000
1-Hexene	0.000	0.000		0.000
2-Methyl-1-Pentene	0.028	0.000	0.000	0.000
trans-2-Hexene	0.109	0.047	0.088	0.100
cis-2-Hexene	0.000	0.070	0.067	0.100
1,3-Hexadiene (trans)	0.100	0.000	0.007	0.000
	0.004	0.000	0.000	0.000
Cyclohexene 1 Hentene	0.000		0.000	0.000
1-Heptene 2,3-Dimethyl-2-pentene	0.037	0.007	0.040	0.000
Octene	0.021	0.000	0.000	0.000
1-Nonene	0.002	0.000	0.000	0.000
1-Noticile	0.000	0.000	0.000	0.000
Aromatics				
Benzene	0.042	0.041	0.043	0.044
Toluene	0.369	0.248	0.297	0.461
Ethylbenzene	0.089	0.061	0.079	0.122
m/p-Xylenes	0.437	0.299	0.438	0.608
Styrene	0.151	0.137	0.145	0.164
o-Xylene	0.138	0.103	0.117	0.165
i-Propylbenzene	0.008	0.006	0.007	0.010
n-Propylbenzene	0.013	0.008	0.011	0.017
m-Ethyltoluene	0.115	0.080	0.102	0.158
p-Ethyltoluene	0.050	0.032	0.042	0.068
1,3,5-Trimethylbenzene	0.279	0.136	0.176	0.413
o-Ethyltoluene	0.042	0.026	0.037	0.057
1,2,4-Trimethylbenzene / t-Butylbenzene	0.205	0.164	0.183	0.244
1,2,3-Trimethylbenzene	0.090	0.079	0.088	0.109
1,3-Diethylbenzene	0.019	0.014	0.016	0.020
1,4-Diethylbenzene	0.017	0.012	0.015	0.023
Butylbenzene	0.012	0.009	0.012	0.014
Monoterpenes				
a-Pinene	0.000	0.000	0.000	0.000
Sabinene	0.000	0.000	0.000	0.000
Sabilierie				

OH reactivity [s ⁻¹], Tierga	rten tunn	el		
Species	Mean	25% Quartile	Median	75% Quartile
Limonene	0.000	0.000	0.000	0.000
Indane	0.004	0.000	0.000	0.003
Oxigenated compounds				
Acetaldehyde	0.223	0.182	0.225	0.257
Methanol	0.164	0.150	0.170	0.183
Ethanol	0.462	0.241	0.473	0.656
Acetone	0.036	0.017	0.026	0.036
2-Propanol	0.047	0.026	0.028	0.036
Propanal	0.155	0.137	0.169	0.264
2-Butanol	0.000	0.000	0.000	0.000
Methyl ethyl ketone	0.000	0.000	0.000	0.000
1-Propanol	0.064	0.043	0.054	0.062
Methacrolein	0.000	0.000	0.000	0.000
Methyl vinyl ketone	0.000	0.000	0.000	0.000
Butanal	0.144	0.118	0.146	0.191
Isobutyl methyl ketone	0.000	0.000	0.000	0.000
1-Butanol	0.419	0.162	0.190	0.223
Pentanal	0.006	0.000	0.000	0.000
Hexanal	0.030	0.000	0.000	0.032
Heptanal	0.000	0.000	0.000	0.000
Octanal	0.000	0.000	0.000	0.000
Eucalyptol	0.001	0.000	0.000	0.000

 $\sum R_{voc} / s^{-1}$ 11.62 7.10 9.49 12.77

Table 8 d: "In front of the city", regional background for easterly flows, Berlin campaign, August 2017.

Species	Mean	25% Quartile	Median	75% Quartile
Alkanes				
Ethane	0.013	0.012	0.013	0.014
Propane	0.024	0.019	0.020	0.028
2-Methylpropane	0.012	0.009	0.009	0.015
n-Butane	0.039	0.023	0.027	0.041
2-Methylbutane	0.021	0.016	0.020	0.023
n-Pentane	0.015	0.011	0.015	0.017
2,2-Dimethylbutane	0.004	0.002	0.002	0.003
Cyclopentane / 2,3-Dimethylbutane	0.008	0.006	0.006	0.007
2-Methylpentane	0.007	0.004	0.007	0.008
3-Methylpentane	0.006	0.004	0.006	0.009
n-Hexane	0.010	0.008	0.010	0.011
Methylcyclopentane	0.001	0.000	0.000	0.000
2,4-Dimethylpentane	0.004	0.004	0.004	0.005
Cyclohexane	0.004	0.003	0.004	0.006
2-Methylhexane	0.003	0.002	0.003	0.004
2,3-Dimethylpentane	0.001	0.001	0.001	0.001
3-Methylhexane	0.022	0.011	0.013	0.019
1,3-Dimethylcyclopentane (cis)	0.001	0.000	0.000	0.001
2,2,4-Trimethylpentane	0.001	0.000	0.001	0.002
Heptane	0.005	0.004	0.004	0.006
Methylcyclohexane	0.005	0.002	0.005	0.009
2,3,4-Trimethylpentane	0.003	0.002	0.002	0.003
2-Methylheptane	0.002	0.002	0.002	0.003
4-Methylheptane	0.001	0.001	0.002	0.002
3-Methylheptane	0.000	0.000	0.000	0.000
n-Octane	0.006	0.004	0.004	0.007
n-Nonane	0.004	0.003	0.003	0.005
n-Decane	0.003	0.002	0.003	0.004
n-Undecane	0.002	0.002	0.002	0.003
n-Dodecane	0.001	0.000	0.000	0.001
n-Tridecane	0.000	0.000	0.000	0.000
Alkenes				
Ethene	0.057	0.041	0.049	0.061
Acetylene	0.005	0.004	0.004	0.005
Propene	0.158	0.137	0.139	0.185
Propyne	0.009	0.008	0.008	0.010
1-Butene / i-Butene	0.400	0.126	0.393	0.487

Species	Mean	25% Quartile	Median	75% Quartile
1,3-Butadiene	0.050	0.026	0.047	0.065
trans-2-Butene	0.062	0.050	0.066	0.073
cis-2-Butene	0.047	0.034	0.044	0.055
1,2-Butadiene	0.000	0.000	0.000	0.000
3-Methyl-1-butene	0.000	0.000	0.000	0.000
1-Pentene	0.025	0.022	0.022	0.023
2-Methyl-1-butene	0.000	0.000	0.000	0.000
Isoprene	0.433	0.300	0.339	0.451
trans-2-Pentene	0.024	0.000	0.039	0.043
cis-2-Pentene	0.000	0.000	0.000	0.000
2-Methyl-2-butene	0.006	0.000	0.000	0.000
1,3-Pentadiene	0.000	0.000	0.000	0.000
Cyclopentadiene	0.083	0.059	0.076	0.093
Cyclopentene	0.018	0.000	0.000	0.020
1-Hexene	0.049	0.023	0.036	0.041
2-Methyl-1-Pentene	0.003	0.000	0.000	0.000
trans-2-Hexene	0.052	0.008	0.025	0.061
cis-2-Hexene	0.000	0.000	0.000	0.000
1,3-Hexadiene (trans)	0.000	0.000	0.000	0.000
Cyclohexene	0.000	0.000	0.000	0.000
1-Heptene	0.018	0.009	0.014	0.017
2,3-Dimethyl-2-pentene	0.000	0.000	0.000	0.000
Octene	0.000	0.000	0.000	0.000
1-Nonene	0.004	0.000	0.000	0.000
Aromatics				
Benzene	0.005	0.005	0.005	0.006
Toluene	0.036	0.023	0.033	0.038
Ethylbenzene	0.005	0.004	0.005	0.005
m/p-Xylenes	0.019	0.014	0.016	0.022
Styrene	0.037	0.035	0.039	0.050
o-Xylene	0.010	0.006	0.007	0.010
i-Propylbenzene	0.002	0.000	0.001	0.002
n-Propylbenzene	0.001	0.001	0.001	0.001
m-Ethyltoluene	0.005	0.003	0.005	0.006
p-Ethyltoluene	0.002	0.002	0.002	0.003
1,3,5-Trimethylbenzene	0.015	0.008	0.011	0.014
o-Ethyltoluene	0.005	0.002	0.004	0.007
1,2,4-Trimethylbenzene / t-Butylbenzene	0.007	0.004	0.007	0.010
1,2,3-Trimethylbenzene	0.009	0.005	0.006	0.013
1,3-Diethylbenzene	0.001	0.000	0.000	0.001
1,4-Diethylbenzene	0.000	0.000	0.000	0.000
Butylbenzene	0.000	0.000	0.000	0.000
Monoterpenes				
a-Pinene	0.024	0.012	0.030	0.036

OH reactivity [s ⁻¹], In front of the city					
Species	Mean	25% Quartile	Median	75% Quartile	
beta-Pinene	0.021	0.009	0.015	0.027	
Limonene	0.013	0.000	0.000	0.000	
Indane	0.000	0.000	0.000	0.000	
Oxigenated compounds					
Acetaldehyde	0.126	0.112	0.118	0.141	
Methanol	0.064	0.044	0.054	0.068	
Ethanol	0.017	0.013	0.016	0.019	
Acetone	0.012	0.009	0.009	0.010	
2-Propanol	0.005	0.005	0.006	0.006	
Propanal	0.047	0.009	0.014	0.021	
2-Butanol	0.000	0.000	0.000	0.000	
Methyl ethyl ketone	0.000	0.000	0.000	0.000	
1-Propanol	0.006	0.000	0.000	0.000	
Methacrolein	0.044	0.036	0.038	0.046	
Methyl vinyl ketone	0.037	0.029	0.034	0.037	
Butanal	0.098	0.068	0.093	0.124	
Isobutyl methyl ketone	0.000	0.000	0.000	0.000	
1-Butanol	0.057	0.043	0.058	0.069	
Pentanal	0.000	0.000	0.000	0.000	
Hexanal	0.186	0.049	0.062	0.085	
Heptanal	0.020	0.000	0.017	0.023	
Octanal	0.001	0.000	0.000	0.000	
Eucalyptol	0.002	0.001	0.002	0.002	

2.85

 $\sum R_{voc} / s^{-1}$ 2.76 1.56 2.20

Table 8 e: Mean OH reactivities "In front of the city" (regional background for westerly flows, Berlin campaign ALASKA, August 2016 and results from BMBF-projekt "Stadtklima im Wandel", summer campaign (IOP-2) Berlin July - August 2017. Comparison of the results for different years for summertime clear sky conditions. VOC samples were taken in 2016: 02.08.2016 11.00 - 11:05 UTC Sacrow; 02.08. 2016 12:15 - 12:20 UTC Pfaueninsel. VOC samples were taken in 2017: 29.07.2017 Pfaueninsel 12:50 - 12:55 UTC: 29.07. 2017 Sacrow 13:55 - 14:03 UTC.

Mean OH reactivity [s ⁻¹]		
in front of the city		
(westerly flows)	2016	2017
Species	Mean	Mean
Alkanes		
Ethane	0.005	0.007
Propane	0.011	0.007
2-Methylpropane	0.004	0.004
n-Butane	0.023	0.021
2-Methylbutane	0.030	0.021
n-Pentane	0.015	0.010
2,2-Dimethylbutane	0.007	0.007
Cyclopentane / 2,3-Dimethylbutane	0.027	0.004
2-Methylpentane	0.022	0.037
3-Methylpentane	0.011	0.001
n-Hexane	0.009	0.002
Methylcyclopentane	0.002	0.000
2,4-Dimethylpentane	0.008	0.002
Cyclohexane	0.006	0.000
2-Methylhexane	0.005	0.046
2,3-Dimethylpentane	0.004	0.000
3-Methylhexane	0.014	0.070
1,3-Dimethylcyclopentane (cis)	0.003	0.000
2,2,4-Trimethylpentane	0.002	0.001
Heptane	0.005	0.005
Methylcyclohexane	0.002	0.000
2,3,4-Trimethylpentane	0.003	0.006
2-Methylheptane	0.002	0.009
4-Methylheptane	0.000	0.014
3-Methylheptane	0.010	0.000
n-Octane	0.006	0.005
n-Nonane	0.004	0.005
n-Decane	0.018	0.004
n-Undecane	0.001	0.004
n-Dodecane	0.001	0.000
n-Tridecane	0.002	0.000

Mean OH reactivity [s ⁻¹]		
in front of the city		
(westerly flows)	2016	2017
Species	Mean	Mean
Alkenes		
Ethene	0.063	0.132
Acetylene	0.004	0.006
Propene	0.156	0.200
Propyne	0.000	0.000
1-Butene / i-Butene	0.082	0.118
1,3-Butadiene	0.000	0.013
trans-2-Butene	0.055	0.000
cis-2-Butene	0.072	0.000
1,2-Butadiene	0.000	0.000
3-Methyl-1-butene	0.000	0.000
1-Pentene	0.010	0.024
2-Methyl-1-butene	0.000	0.002
Isoprene	2.697	3.303
trans-2-Pentene	0.012	0.004
cis-2-Pentene	0.021	0.000
2-Methyl-2-butene	0.000	0.000
1,3-Pentadiene	0.000	0.000
Cyclopentadiene	0.000	0.000
Cyclopentene	0.000	0.000
1-Hexene	0.076	0.000
2-Methyl-1-Pentene	0.000	0.018
trans-2-Hexene	0.021	0.013
cis-2-Hexene	0.009	0.032
1,3-Hexadiene (trans)	0.047	0.126
Cyclohexene	0.000	0.003
1-Heptene	0.006	0.015
2,3-Dimethyl-2-pentene	0.000	0.000
Octene	0.000	0.000
1-Nonene	0.000	0.000
Aromatics		
Benzene	0.006	0.003
Toluene	0.035	0.024
Ethylbenzene	0.013	0.012
m/p-Xylenes	0.068	0.033
Styrene	0.025	0.068
o-Xylene	0.020	0.036
i-Propylbenzene	0.001	0.000
n-Propylbenzene	0.011	0.000
m-Ethyltoluene	0.014	0.006

Mean OH reactivity [s ⁻¹]		
in front of the city		
(westerly flows)	2016	2017
Species	Mean	Mean
p-Ethyltoluene	0.003	0.000
1,3,5-Trimethylbenzene	0.060	0.000
o-Ethyltoluene	0.004	0.021
1,2,4-Trimethylbenzene / t-Butylbenzene	0.050	0.017
1,2,3-Trimethylbenzene	0.225	0.000
1,3-Diethylbenzene	0.003	0.000
1,4-Diethylbenzene	0.000	0.000
Butylbenzene	0.002	0.000
Monoterpenes		
a-Pinene	0.072	0.128
Sabinene	0.000	0.000
beta-Pinene	0.034	0.014
Limonene	0.000	0.000
Indane	0.006	0.003
Oxigenated compounds		
Acetaldehyde	0.018	0.000
Methanol	0.018	0.000
Ethanol	0.079	0.132
Acetone	0.107	0.132
2-Propanol	0.107	0.027
Propanal	0.003	0.000
2-Butanol	0.000	0.000
Methyl ethy ketone	0.000	0.000
1-Propanol	0.006	0.000
Methacrolein	0.006	0.000
Methyl vinyl ketone	0.103	0.090
Butanal	0.133	0.130
Isobutyl methyl ketone	0.000	0.297
1-Butanol	0.000	0.000
Pentanal	0.000	0.070
Hexanal	0.000	0.000
Heptanal	0.218	0.919
Octanal	0.000	0.000
	0.000	
Eucalyptol	0.011	0.000

 $\sum R_{voc} / s^{-1}$

5.273

6.514

9 Literature

[Antolini, 2004] Antolini, E., Review in Applied Electrochemistry. Number 54, "Recent developments in polymer Electrolyte fuel cell electrodes", J. Appl. Electrochem., (2004), 34, 563.

[Benning and Wahner, 1998] "Measurements of Atmospheric Formaldehyde (HCHO) and Acetaldehyde (CH₃CHO) during POPCORN 1994 Using 2.4-DNPH Coated Silica Cartridges". In: Rudolph J., Koppmann R. (eds) Atmospheric Measurements during POPCORN — Characterisation of the Photochemistry over a Rural Area. Springer, Dordrecht, DOI, https://doi.org/10.1007/978-94-017-0813-5 5, ISBN 978-90-481-5158-5.

[Bonn et al., 2016] Bonn, B., von Schneidemesser E., Gerwig H., A. Lüdecke, A., Kura, J., Pietsch, A., Ehlers, C., Klemp, D, Kofahl, C., Junkermann, W., Grote, R., Pohl T., Weber K., Andrich, D., Lode, B., Schönberger, P., Quedenau, J., Churkina, G., Butler, T., Lawrence, M. G., "BAERLIN2014 – the influence of land surface types on and the horizontal heterogeneity of air pollutant levels in Berlin", Atmos Chem. Phys. (2016), 7785.

[BlmSchV, 2010] Neunundreißigste Verordnung zur Durchführung des Bundesimmissionschutzgesetzes, gültig ab 06. 08. 2010.

[Buers et al., 2011] Buers, H.-J., Klemp, D., Müller, K.-P., Rohrer, F., "Verfahren zur Feinstaubanalyse", in: Patentblatt 2011 / 20 18. 05. 2011 Germany WO 200 045534A17.

[Bukowiecki et al., 2002] Bukowiecki, N., Dommen, J., Prevot, A. S. H., Richter, R., Weingartner, E., Baltensberger., U., "A mobile pollutant measurement laboratory-measuring gas phase and aerosol ambient concentrations with high special and temporal resolution", Atmos. Environ., (2002), 36, 5569.

[Calpini et al., 1999] Calpini, B., Jeanneret, F., Bourqui, M., Clappier, A., Vaytai, R., and van den Bergh, H., "Direct measurement of the total reaction rate of OH in the atmosphere", Analusis, (1999), 27, 4.

[Chen et al., 2011] Chen, M., Du, C., Zhang, J., Zhu, I., "Effect, mechanism and recovery of nitrogen oxides poisoning on oxigen reduction reaction at Pt/C catalysts", Journal of Power Sources (2011), 19, 620.

[Daimler AG, 2017] Abschlußbericht Teilprojekt 03ET6036B: "Schädigungspotential Schadgase und Entwicklung von Regenerationsstrategien", Stuttgart (2017).

[Dornseiffer, 2018] Dornseiffer, J., FZ Jülich, IEK-1, 2018, private Mitteilung.

[Dunmore et al., 2015] Dunmore, R. E., Hopkins, J. R., Lidster, R. T., Lee, J. D., Evans, M. J., Rickard, A. R., Lewis, A., C., und Hamilton, J. F., "Diesel-related hydrocarbons can dominate gas phase reactive carbon in megacities", Atmos. Chem. Phys., (2015), 15, 9983-9996.

[Edwards et al., 2013] Edwards, P. M., Evans, M. J., Furneaux, K. L., Hopkins, J., Ingham, T., Jones, C., Lee, J. D., Lewis, A. C., Moller, S. J., Stone, D., Whalley, L. K., Heard, D. E., "OH reactivity in a South East Asian tropical rainforest during the Oxidant and Particle Photochemical Processes (OP3) project", Atmos. Chem. Phys., (2013), 13, 9497–9514.

[Ehlers et al., 2016] Ehlers, C., Klemp, D., Rohrer, F., Mihelcic, D., Wegener, R., Kiendler-Scharr, A., Wahner, A.: "Twenty years of ambient observations of nitrogen oxides and specified hydrocarbons in air masses dominated by traffic emissions in Germany", Faraday Discuss., (2016), 189, 407.

[Ehlers et al., 2017] Ehlers, C., Klemp, D., Kofahl, C., Fröhlich, H., Möllmann-Coers, M., und Wahner, A.: "Untersuchungen zur Luftqualität in Bad Homburg", Reihe Energie und Umwelt, Verlag des Forschungszentrums Jülich, (2017), ISBN 978-3-95806-199-6, pp. 96.

[Ehlers, 2013] Ehlers, C. "Mobile Messungen – Messung und Bewertung von Verkehrsemissionen", Dissertation, Universität zu Köln, (2013), pp. 139.

[Ehlers et al., 2014] Ehlers, C., Elbern, H., Klemp, D., Rohrer, F., Wahner, A., "Comparison of measured data and model results during PEGASOS 2012", Poster presented at EGU conference, 27. 05. - 2. 06. 2014 Vienna (2014).

[El-Deab et al., 2013] El-Deab, M. S., Kitamurea, F., Ohsaka, T., "Poisoning effect on selected hydrocarbon impurities on the catalyst performance of Pt/C catalysts towards the oxygen reduction reaction", Journal of the Electrochemical Society, (2013) 160, 651.

IEPA 1997 EPA. Procedure for the detailled hydrocarbon analysis of gasolines by single column high effficency (capillary) column gas chromatography Standard Operating Procedures. El Monte, U.S.A.: California Environmental Protection Agency Air Resources Board, (1997).

[Fuchs et al., 2017] Fuchs, H., Novelli, A., Rolletter, M., Hofzumahaus, A., Pfannerstill, E., Stephan Kessel, St., Edtbauer, A., Williams, J., Michoud, V. Dusanter, S., Locoge, N., Zannoni, N., Gros, V., Truong, F., Sarda-Esteve, R., Cryer, D. R., Brumby, C. A., Whalley, L. K., Stone, D., Seakins, P. W., Heard, D. E., Schoemaecker, C., Blocquet, M., Coudert, S., Batut, S., Fittschen, C., Thames, A. B., Brune, W. H., Ernest, C., Harder, H., Muller, J. B. A., Elste, T., Kubistin, D., Andres, S., Bohn, B., Hohaus, T., Holland, F., Li, X., Rohrer, F., Kiendler-Scharr, A., Tillmann, R., Wegener, R., Yu, Z., Zou, Q., and Wahner, A., "Comparison of OH reactivity measurements in the atmospheric simulation chamber SAPHIR", Atmos. Meas. Tech., (2017), 10, 4023-4053.

[Halseid, et al., 2006] Halseid, R., Vic, P. J., Tunold, R., "Effect of ammonia on the performance of polymer electrolyte membrane fuel cells", Journal of Power Sources, (2006), 154, 343.

[Imamura et al., 2009] Imamura, D., Yamaguchi, E., "Effect of air contaminants on the electrolyte degradation in polymer electrolyte membrane fuel cells". ECS Transactions. (2009), 25, 813,

[Ingham et al., 2009] Ingham, T., Goddard, A., Whalley, L. K., Furneaux, K. L., Edwards, P. M., Seal, C. P., Self, D. E., Johnson, G. P., Read, K. A., Lee, J. D., and Heard, D. E., "A flow-tube based laser-induced fluorescence instrument to measure OH reactivity in the troposphere", Atmos. Meas. Techn., (2009), 2, 465-477, doi:10.5194/amt-2-465-2009.

[Jenkin et al., 1997] Jenkin, M. E., S., Saunders, S., and Pilling, M. J., "The tropospheric degradation of volatile organic compounds: a protocol for mechanism development", Atmospheric Environment (1997), 31(1), 81.

[Keller et al., 2017] Keller, M., Hausberger, St., Matzer, C., Wüthrich, P., Notter, B., HBEFA version 3.3, background information, Berne, 25. 04.2017.

[Kern et al., 1998] Kern, T., Metz, N., und Kley, D., "Untersuchungen von Verkehrsabgasemissionen insbesondere im Hinblick auf die Ozonbildung", (1998), Abschlußbericht des Gemeinschaftsprojektes zwischen BMW AG und der Forschungszentrum Jülich GmbH, München und Jülich.

[Kessler and Platt, 1984] Kessler C., Platt U. (1984) "Nitrous Acid in Polluted Air Masses — Sources and Formation Pathways." In: Commission of the European Communities, Versino B., Angeletti G. (eds) Physico-Chemical Behaviour of Atmospheric Pollutants. Springer, Dordrecht.

[Kittelsen et al., 2004] Kittelsen, D. B., Watts, W. F., Johnson, J. P., "Nanoparticle emissions on Minnesota highways", Atmos. Environ., (2004), 38, 9.

[Klemp et al., 2012] Klemp, D., Mihelcic, D., Mittermaier, B., "Messung und Bewertung von Verkehrsemissionen", Reihe Energie und Umwelt, Band 21, ISBN 978-3-89336-546-3, Jülich, (2012), pp. 319.

[Klemp et al., 2002] Klemp, D., Mannschreck, K., Paetz, H.-W., Habram, M., Matuska, P., Slemr, F. "Determination of anthropogenic emission ratios in the Augsburg area from concentration ratios: results from long-term measurements", Atmos. Environ. 36, Supplement 1, (2002), 61.

[Klemp et al., 2020] Klemp, D., Wegener, R., Dubus, U., Javed, U., "Acquisition of temporally and spatially highly resolved data sets of relevant trace substances for model development and model evaluation purposes using a mobile measuring laboratory", Energy and Environment, volume 497, ISBN 978-3-95806-465-2, Jülich (2020), pp. 110.

[Konrad und Volz-Thomas, 2000] Konrad, S., and Volz-Thomas, A., "Characterization of a commercial gas chromatography-flame ionization detection system for the in situ determination of C₅-C₁₀ hydrocarbons in ambient air" Journal of Chromatography A 878(2), 215-234.

[Kovacs et al., 2003] Kovacs, T. A., Brune, W. H., Harder, H., Martinez, M., Simpas, J. B., Frost, G. J., Williams, E., Jobson, T., Stroud, C., Young, V., Fried, A., and Wert, B., "Direct measurement of urban OH reactivity during Nashville SOS in summer 1999", J. Environ. Monitor., (2003) 5, 68–74.

[Landesamt für Umwelt BW, 2016] Landesamt für Umwelt: Stickstoffoxide. http://www.lubw.baden-wuerttemberg.de/servlet/is/18622/, 02.10. 2016.

[Lenschow et al., 2001] Lenschow, P., Abraham, H.-J., Kutzner, K., Lutz, M., Preuss, J.-D., Reichenbacher, W., "Some ideas about the sources of PM10", Atmos Envir. (2001), 35, 23.

[Leyrer, AMS, 2010] Leyrer, G.: "Benzinverbrauch. Wie wir testen", Auto, Motor und Sport, (2010) 14, S. 46-47.

[Lopes et al., 2014] Lopes, T., Sansinea, J.-M., Mukundan, R., Hussey, D. S., Jakobson, D., Garzon, F. H., "Diagnosing the effects of ammonia exposure on PEFC cathodes". Journal of the Electrochemical Society. (2014), 161, 703.

[Lou et al., 2010] Lou, S., F. Holland, F. Rohrer, K. Lu, B. Bohn, T. Brauers, C.C. Chang, H. Fuchs, R. Häseler, K. Kita, Y. Kondo, X. Li, M. Shao, L. Zeng, A. Wahner, Y. Zhang, W. Wang, A. Hofzumahaus, "Atmospheric OH reactivities in the Pearl River Delta-China in summer 2006: Measurement and model results", Atmos. Chem. Phys. Discuss. (2009), 9, 17035-17072.

[Mann und Hummel, 2017] Abschlußbericht 03ET6036C: "Ermittlung der Filterkapazität", Himmelcron (2017).

[Madronich and Calvert, 1990] Madronich, S., Calvert, J. G., "Permutation reactions of organic peroxy radicals in the troposphere", Journal of Geophysical Research-Atmospheres, (1990) 95(D5), 5697.

[Mannschreck et al., 2002] Mannschreck, K., Klemp, D., Kley, D., Friedrich, R., Kühlwein, J., Wickert, B., Matuska, P., Habram, M., Slemr, F., "Evaluation of an emission inventory by comparisons of modelled and measured emission ratios of individual HCs, CO and NO_x", Atmos. Environ. 36, Supplement 1, (2002), S81.

[Michoud et al., 2015] Michoud, V., Hansen, R. F., Locoge, N., Stevens, P. S., and Dusanter, S., "Detailed characterizations of the new Mines Doual comparative reactivity method instrument via laboratory experiments and modeling", Atmos. Meas. Tech., (2015) 8, 3537–3553, https://doi.org/10.5194/amt-8-3537-2015.

[Misz, 2015] Misz, U., Zentrum für Brennstoffzellentechnologie, Duisburg, 2015, private Mitteilung.

[Mittermaier und Klemp, 2004] Mittermaier, B., Klemp, D., "Messung wichtiger Abgaskomponenten am fahrenden Pkw im realen innerstädtischen Straßenverkehr", Gefahrstoffe- Reinhaltung der Luft, (2004),11/12, 64, 487.

[Mittermaier et al., 2004] Mittermaier, B., Schmitz, T. Hassel, D., Klemp, D., Weber, F. J., "VOC-split of gasoline and diesel passenger cars" in: R. Friedrich and St. Reis (editors): "Emissions of Air Pollutants" (2004), ISBN 978-3-662-07015-4, Springer Verlag Berlin Heidelberg.

[Moore et al., 2000] Moore, J. M., Adcock, P. L., Lakeman, J. B., Mepsted, G. O., "The effect of battlefield contaminants on PEMFC performance", Journal of Power Sources, (2000), 85, 254.

[Mothadi et al., 2004] Mothadi, R., Lee, W.-K., van Zee, J.: "Assessing durability of cathodes exposed to common air impurities", Journal of Power Sources, (2004) 138, 216.

[openstreetmap, 2018] https://wiki.openstreetmap.org/wiki/ Attributierung von Straßen in Deutschland

[Pijola et al., 2004] Pijola, J., Parviainen, H., Hussein, T., Valli, A., Hämeri, K., Aaalto, P., Virtanen, A., Keskinen, J., Pakkanen, T., Mäkela, T., Hillamo, R. E., "Sniffer- a novel tool for chasing vehicles and measuring traffic pollutants", Atmos. Environ., (2004), 38, 3625.

[Sadanaga et al., 2004] Sadanaga, Y., Yoshino, A., Watanabe, K., Yoshioka, A., Wakazano, Y., Kanaya, Y., and Kajii, Y., "Development of a measurement system of OH reactivity in the atmosphere by using a laserinduced pump and probe technique", Rev. Sci. Instrum., (2004) 75, 2648–2655.

[Sadanaga et al., 2005] Sadanaga, Y., Yoshino, A., Kato, S., Kayii, Y., "Measurements of OH reactivity and photochemical ozone roduction in the urban atmosphere", Environ. Sci. Technol. (2005), 39, 8847-8852.

[Schmitz et al., 1997] Schmitz, T., D. Klemp, D., und Kley, D., "Messungen der Immissionskonzentrationen verschiedener Ozonvorläufersubstanzen in Ballungsgebieten und an Autobahnen: Charakterisierung der Emissionsverhältnisse des Straßenverkehrs unter verschiedenen Verkehrssituationen durch Messungen in Quellnähe". Berichte des Forschungszentrums Jülich: Forschungszentrum Jülich, Zentralbibliothek.

[Schmitz et al., 2000] Schmitz, T., Hassel, D., und Weber, F.-J., "Determination of VOC components in the exhaust of gasoline and diesel passenger cars", Atmospheric Environment, (2000), 34(27), 4639-4647.

[Talke, A., 2017] Talke, A. "Der Einfluss von ausgewählten Luftschafstoffen auf die Brennstoffzelle unter fahrzeugnahen Betriebsbedingungen", Dissertation, Duisburg, 2017.

[Talke et al., 2015] Talke, A., Misz, U., Konrad, G., Heinzel., A., "Impact of air contaminants on subscale single fuel cells and in an automotive short stack", Journal of Electrical Engineering (2015), 3, 70.

[Talke et al., 2018] Talke, A., Misz, U., Konrad, G., Heinzel, A., Klemp., D., Wegener, R., "Influence of urban air on PEMFC vehicles - long term effects of air contaminants in an authentic driving cycle", Journal of Power Sources, 400 (2018), 556 – 565.

[UBA, 2017] Umweltbundesamt, Nationale Trendtabellen für die deutsche Berichterstattung atmosphärischer Emissionen seit 1990 (Stand 2 2017), Dessau,

[UBA, 26. 04. 2017] in:

https://www.umweltbundesamt.de/presse/pressemitteilungen/stickoxid-belastungdurch-diesel-pkw-noch-hoeher, Umweltbundesamt, Mitteilung Nr. 16, 2017, Dessau den 26. 04. 2017

[Urban, 2010] Urban, S., "Charakterisierung der Quellverteilung von Feinstaub und Stickoxiden in ländlichem und städtischem Gebiet", Dissertation, Universität Wuppertal, (2010), pp. 210.

[Wegener et al., 2017] Wegener, R., Klemp, D., Rohrer, F., Ehlers. C., Wahner, A., "Mobile measurements reveal high ammonia concentrations in German inner cities", GAIA conference (09/13/2017). Hamburg.

[Weijers et al., 2004] Weijers, E. P., Khlystov, A. Y., Kos, G. P. A., Erishmen, J. M, "Variabitity of particulate matter concentrations along roads and motorways determined by a moving measurement unit", Atmos. Environ., (2004), 38, 2993.

[Wenk, 2016] Wenk, A.-K., "Optimierung und Anwendung eines schnellen GC-MS-Systems für mobile Messungen flüchtiger organischer Substanzen", Dissertation, Universität zu Köln, (2016), pp. 188.

[Westerdahl et al., 2005] Westerdahl, D., Fruin, S., Sax, T. Fine, P. M., Sioutas, C., "Mobile platform measurements of ultrafine particle an associated pollutant concentrations on freeways and residential streets in Los Angeles", Atmos. Environ., (2005), 39, 3597.

[J. Williams et al., 2016] Williams, J., Keßel, S. U., Nölscher, A. C., Yang, Y., Lee, Y., Wolf, S., J., Kesselmeier, J., Klüpfel, Th., Lelieveld J., ShaoMin, "Opposite OH reactivity and ozone cycles in the Amazon rainforest and megacity Beijing: Subversion of biospheric oxidant control by anthropogenic emissions", Atmospheric Environment, (2016), 125 Part A, 112-118.

[Wichmann-Fiebig, 2017] Wichmann-Fiebig, M., "Gefahr durch Stickoxide – Verursacher, Grenzwerte und Folgen", Umweltbundesamt, Dessau 2017, https://www.stephankuehn.com/fileadmin/user_upload/20170213_01_Wichmann-Fiebig.pdf.

[Yang et al., 2006] Yang, D., Ma, J., Xu, L., Wu, M., Wang, H.: "The effect of nitrogen oxides in air on the performance of proton exchange membrane fuel cells", Electrochimica Acta, (2006), 51, 4039 - 4044.

[Yang et al., 2017] Yang, Y., Shao, M., Keßel, S., Li, Y., Lu, K., Lu, S., Williams, J., Zhang, Y., Zeng, L., Nölscher, A. C., Wu, Y., Wang, X., and Zheng, J., "How the OH reactivity affects the ozone production efficiency: case studies in Beijing and Heshan, China", Atmos. Chem. Phys., (2017) 17, 7127-7142, https://doi.org/10.5194/acp-17-7127-2017.

[Zamel und Li, 2011] Zamel, N., Li, X., "Effect on contaminants on polymer electrolyte membrane fuel cells", Progress in Energy and Combustion Science, 03. 06. 2011, Vol. 37, Issue 3, 292.

[ZBT, IUTA, 2009] "Entwicklung eines Filtersystems für partikuläre und gasförmige Schadstoffe zur Erhöhung der Standzeit", Duisburg, 29. 05. 2009:

[ZBT, IUTA, 2012] "Evaluierung der kathodenseitigen Schädigungsmechanismen durch partikuläre und gasförmige Luftschadstoffe mit Hilfe von elektrochemischen Messmethoden zur Standzeiterhöhung von PEM Brennstoffzellen, 14. 08. 2012.

[ZBT, 2017] Abschußbericht ZBT: Teilprojekt 03ET6036A: "Ermittlung des Schädigungspotenzials relevanter Luftschadgase im Realbetrieb (Einzelzellen]", Duisburg (2017).

[Zellner, 2012] Zellner, A., "Grundlegende experimentelle Untersuchungen zur Oxidation von Wasserstoff, Stickstoffmonoxid und deren Mischungen an einem Platinkatalysator", Diplomarbeit am Institut für Technische Chemie und Polymerchemie des KIT, Karlsruhe, 2012.

[Zhai et al., 2010] Zhai, Y., Bethune, K., Dorn, S., Bender, G., Rocheleau, R., ECS Transactions (2010) 28, 313.

10 List of Figures

Fig. 1: Mean daily cycles of the monthly average for nitrogen oxides in an inner-city environment (city park
distance approx. 100 m from the next road used, so-called "urban background") for the months of
February and September. In addition, the 1-sigma fluctuation ranges of the concentrations of NO, NO
and NO _x (colored grey) are given. To record the nitrogen oxide data, high-resolution chemiluminescence
analysis (Eco-Physics) with an upstream photolysis converter for the conversion of NO ₂ to NO was used
The time of day is given in UTC, i.e. time offset to CET (winter): 1 hour or to CEST (summer): 2 hours. From
[Ehlers et al., 2017]
Fig. 2: Averaged NO/NO ₂ ratios [ppb/ppb] for March 2014 as a function of time of day (MEZ), measured in Bar
Homburg city center (red). The measurements were performed at a distance of approx. 100 m from
through road in a park. On the right axis the intensity of the averaged photolysis frequency jNO ₂ (blue) is
also plotted as a function of the time of day. It can be seen that the available solar radiation significantly
influences the NO/NO2 ratio (from: [Ehlers et al., 2017]): It decreases from morning conditions of almost
1.5 over the day and reaches a minimum of NO/NO_2 of 0.25, only to rise again after sunset (for details o
the responsible air-chemical processes, see e. g. Klemp et al., 2012])1
Fig. 3: Mobile measurement laboratory (MobiLab-I) at Forschungszentrum Jülich. Expansion stage: Summer 201
[Ehlers, 2013], measurement platform: Mercedes VITO, energy supply: Generator + battery buffering
position GPS, meteorology: wind direction, wind speed, humidity
temperature.
Fig. 4: Investigation of NO _x concentrations in the inner city of a metropolis (Berlin, summer 2016, urban are
Neukölln) using MobiLab-I. Determination of the local background for NO _x (background) by applying a 2
minute 5% filter and calculating the associated 5% percentiles from the recorded NO _x measurement dat
set (measurement period, August 2016): The associated one-hour NO _x average, on the other hand
provides a value of about 120 ppb1
Fig 5: Schematic representation of the formation of a trace substance in the inner city: "Regional Background
entered from the outside. In the urban area, the "local background" and the emission "peaks" of the
nearby sources (e.g. exhaust emissions from vehicles) are added to the regional background. After a shor
time, mixing and dilution ensure that the emission "peaks" will be dissolved down to the local background
value. (According to: Lenschow et al., 2001.)18
Fig. 6: MobiLab-II with schematic representation of the built-in trace analytics: Aerosol inlet: isokinetic suctio
of the particle phase to avoid errors in the measured aerosol distributions due to high speed difference
between the own movement of the MobiLab and the speed at the entry point into the "aerosol inlet'
Gas phase analysis: CO, CO ₂ and CH ₄ , SO ₂ , NH ₃ , H ₂ O, NO _x , NO and NO ₂ , O ₃ (UV absorption), O ₃ (rapid O ₃
detection by chemiluminescence), VOC canister samples, aerosol analysis: ELPI, CPC, filter samples
gravimetric analysis, EC/OC distribution [Ehlers et al., 2017]1

Fig. 7. Mobileab-II III winter measurements to record a climatology of relevant trace gases in stuttgart. The suc	LIOII
point for the aerosol and gas phase is located on the driver's side at a height of approx. 2 m above	the
road. The gas phase inlet is additionally protected against the additional suction of water by a conic	ally
expanding funnel. The meteorological measuring apparatus (WXT 520, Vaisala) is attached to the up	per
edge of the wind deflector. The heat exchanger of the air conditioning system can be seen on the roo	f of
the box body	_20
Fig. 8: Results of the NO ₂ measurements (cf. color scale) when crossing the city of Berlin in east-west direct	tion
and investigations in the windward and leeward area of Berlin under winter conditions and north-v	vest
wind direction (see wind arrow). The measurements with MobiLab presented here took place of	n a
weekday in January 2017 between 9:00 and 12:30 UTC	_25
Fig. 9: Measurement drive with MobiLab-II in August 2017 in Berlin. Concentration distribution of NO_2 in	the
inner city area of the city of Berlin (surroundings of Ernst-Reuter-Platz). High NO₂ mixing ratios were fo	und
on main roads and at intersections. Low NO2 values close to local background values were observe	d in
secondary roads and/or residential areas, cf. concentration color scale. For the typical mixing ratios	and
variation range of inner-city NO _x values (Berlin Neukölln, summer 2017) see also	Fig.
4	26
Fig. 10: Test drive with MobiLab in August 2017 in Berlin. Result of NO _x measurements during mult	iple
circumnavigations of Tegel Airport with the mobile measurement laboratory). The measured	NOx
concentration was clearly influenced by the prevailing traffic density and traffic light phases. A c	ear
influence of the NO_x emissions emitted by air traffic on the measured NO_x concentration levels could	not
be determined in the leeward area of the airport.	_27
Fig. 11: Measurement run with MobiLab-II in August 2017 in Berlin and in the windward Berlin hinterla	nd.
$\label{eq:maximum NO} \textbf{Maximum NO}_{x} \text{values were found in the inner-city area and on the inner-city motorways.} \textbf{In the windways} In the win$	ard
Berlin hinterland the NO _x background value was only about 3 ppb	_28
Fig. 12: NO ₂ mixing ratio [ppb] for February 2017 (2017-02-20), measured in the Stuttgart basin and in	the
surrounding marginal areas (Kaltental and Botnang). Highest NO ₂ mixing ratios were observed in	the
urban area of Stuttgart along the B-14, while the travel sections in the peripheral areas of Stutt	gart
(Kaltental and Botnang) with about 21 ppb NO ₂ are more than a factor 5 lower than those of the ini	าer-
city area around the Neckartor.	29
Fig. 13: NO ₂ mixing ratio [ppb] for February 2016, measured in the Stuttgart basin in the Neckartor area and	l on
the adjacent Kernerviertel at Uhlandshöhe (wind speed 2 - 3 m/s). Highest NO ₂ mixing ratios w	ere
observed along the B14. Already at a distance of 50 - 100 m the NO ₂ -mixture ratios decrease significan	ıtly.
In the area of the Kernerplatz, the NO ₂ mixing ratios of about 27 ppb were only a few ppb above	the
regional background values determined on the same day (c. f. Fig. 13)	_30

Fig. 14: Overview of the various measuring sections of the Rhine-Ruhr measuring area which we travelled with
MobiLab several times in the course of 2015. In addition to the motorway sections in the Ruhr area, the
routes include urban areas and rural backgrounds in the Eifel. The different areas are color coded:
Autobahn (blue), trunk roads (Bundesstraßen, red), primary roads (Hauptstraßen, yellow), secondary
roads (Landstraßen, green), tertiary roads (Nebenstraßen white), road tunnels (Tunnel, light grey) and
small sections not classified in the previous areas (black)
Fig. 15: Concentration overview of NO, NO ₂ and total nitrogen oxides (NO _x), for the different road types (cf.
classification, as indicated in Fig. 14). The black crossline indicates the respective mean value of the
concentration, the blue dot indicates the median value. The grey box marks the 25 to 75 $\%$ percentile and
the vertical black lines indicate minimum and maximum values
Fig. 16: Characterization of the MobiLab driving speed distribution during the measurements for the different
road types (cf. classification in Fig. 15). The number values arranged above the road types indicate the
respective ensemble size for the nitrogen oxides minute averages (minute averages; consisting of 20
individual measurements each + 2 background determinations). While on multi-lane road types
$(Autobahn, trunk\ roads\ (Bundesstraßen))\ the\ MobiLab\ driving\ speed\ can\ be\ lower\ than\ that\ of\ the\ average$
car fleet due to its truck speed limitation, for single-lane road courses the given profile is a good measure
for the speed profile of the entire car fleet. The black transverse line indicates the respective mean value
of the speed, the blue dot indicates the median value. The grey box marks the 25 to 75 $\%$ percentile and
the vertical black lines indicate minimum and maximum values35
Fig. 17: Temperature dependence of the total nitrogen oxide (NO_x) concentration for measurements on primary
roads (Hauptstraßen). The maximum concentrations (black), the median concentrations (blue), the mean
concentrations (red) and the minimum concentrations (grey) are plotted as diamonds. The solid line show
the linear trend. For the mean concentrations (black line) there is a linear correlation with a slope of -12
ppb/ $^{\circ}$ C and an axial section of 460 ppb. The correlation coefficient is R^2 =
0.62 36
Fig 18: Concentration patterns of CO ₂ , NO ₂ , CO and NO during the passage of the Stuttgart Heslacher Tunnel in
November 2016 with MobiLab-II (tunnel passage 8:16 - 8:19 UTC). It can be seen that the NO mixing ratios
[NO (CL)] measured in the tunnel are four times higher than the NO_2 mixing ratios [NO $_2$ (CAPS)] measured
simultaneously
Fig. 19: Trace gas measurements of CO ₂ , NO ₂ , NH ₃ and SO ₂ during the passage of the Heslach Tunnel in Stuttgart
on 10. 11. 2016. The trace gases rise synchronously with the measured CO_2 . For the NO/NO_2 ratio see also
Fig. 7 from another Heslach tunnel passage on 16.11.2016
Fig. 20: Examples for correlation plots of the second data of NO ₂ /CO ₂ and SO ₂ /CO ₂ during the passage of the
Heslacher Tunnel on 10.11.2016 10:55 - 11:10 UTC (see Fig. 19). These measurements were carried out
outside the rush hour times, so that constant speed conditions (45 +- 5) km/h prevailed during these
measurements. It can be seen that the CO_2 second data have an offset of 400 ppm caused by the
atmospheric background of the CO ₂ 41

Fig. 2	21: NO $_x$ /CO $_2$ ratios measured in the Berlin Tiergarten Tunnel and in the Stuttgart Heslach Tunnel as a function
	of the outside temperature (mean value before/after the tunnel)43
Fig. 2	22: NO ₂ /CO ₂ ratios measured in the Berlin Tiergarten Tunnel and in the Stuttgart Heslach Tunnel as a function
	of the outside temperature (mean value before/after the tunnel)44
Fig.	23: SO ₂ /CO ₂ ratios measured in the Tiergarten Tunnel (Berlin) and in the Heslacher Tunnel (Stuttgart) as a
	function of the outside temperature (mean value before/after the tunnel)46
Fig.	24: "Auto, Motor und Sport"-measuring round, [Leyrer, AMS, 2010]47
Fig.	25a: Observed concentrations of CH4, NH3_LosGatos, SO2 and Ozone on the "Auto, Motor und Sport"
	measuring drive. The AMS test drive was passed three times by MobiLab on 9. 11. 2016. The recorded
	data set contains second data of gaseous compounds as well as second data of 12 size classes of particle
	numbers in the range of 5 nm to 10 μm . These trace gas data are supplemented by GPS information
	accurate to the second and meteorological parameters. The dotted line marks the passages through the
	Fellbach Tunnel48
Fig. 2	25b: Observed concentrations of CO ₂ , CO, NO ₂ _CAPS and NO_CL on the "Auto, Motor und Sport" measuring
	drive. The AMS test drive was passed three times by MobiLab on 9. 11. 2016. The recorded data set
	contains second data of gaseous compounds as well as second data of 12 size classes of particle numbers
	in the range of 5 nm to 10 μm . These trace gas data are supplemented by GPS information accurate to
	the second and meteorological parameters. The dotted line marks the passages through the Fellbach
	Tunnel 49
Fig.	26 a: Averaged NO ₂ (CAPS) concentrations for the various road types of the AMS test round, determined
	from the measured second data. All data in ppb51
Fig. 2	26 b: Averaged methane concentrations for the various road types of the AMS test round, determined from
	the measured second data. All data in ppm51
Fig. 2	26 c: Averaged NH₃ concentrations (Los Gatos Inc., OA-ICOS, Off-Axis Integrated Cavity Output Spectroscopy)
	for the various road types of the AMS test round, determined from the measured second data. All data
	in ppb52
Fig. 2	26 d: Averaged CO concentrations for the various road types of the AMS test round, determined from the
	measured second data. All data in ppb53
Fig. 2	26 e: Averaged NH₃ concentrations (Picarro Inc, cavity ringdown detection system) for the various road types
	of the AMS test round, determined from the measured second data. All data in ppb53
Fig. 2	26 f : Averaged CO₂ concentrations (Picarro Inc, cavity ringdown detection system) for the various road types
	of the AMS test round, determined from the measured second data. All data in ppm54
Fig. 2	26 g: Averaged H_2O concentrations (Picarro Inc, cavity ringdown detection system) for the various road types
	of the AMS test round, determined from the measured second data. All data in ppm * 1000054
Fig. 2	26 h: Averaged NO concentrations (EcoPhysics) for the various road types of the AMS test round, determined
	from the measured second data. All data in ppb55
Fig. 2	$26i$: Averaged NO $_{x}$ concentrations (EcoPhysics) for the various road types of the AMS test round, determined
	from the measured second, data. All data in ppb.

Fig. 2	6 j: Averaged O ₃ concentrations (Environnement S. A.) for the various road types of the AMS test round
	determined from the measured second data. All data in ppb56
Fig. 2	${f 6}$ k: Averaged SO $_2$ concentrations (ThermoFisher Inc.) for the various road types of the AMS test round
	determined from the measured second data. All data in ppb56
Fig. 2	7: Flow diagram of the GC-MS system " $GC/MS \ 1 \ (C2 - C12)$ " used. Sample preparation system: A set of 10
	Silco-steel cylinders previously filled with sample air can be connected to the system for analysis
	Cryogenic preconcentration: Used to increase the concentration of air samples by about a factor of 1000
	Gas chromatograph: Equipped with FID and MSD, column 120 m DB1, 0.32 mm ID63
Fig. 2	8: Overview of the separation performance achievable with the system. Chromatogram from a cold petro
	car. The peaks are labeled as follows: 01 – Ethene; 02 – Ethane; 03 – Propene; 04 – Propane; 05 – Propyne
	06 – Methylpropane; 07 – Methanol; 08 – 1-Butene / i-Butene; 09 – n-Butane; 10 - trans-2-Butene; 11
	cis-2-Butene; 12 – Ethanol; 13 – 2-Methylbutane; 14 – Acetone; 15 – 1-Pentene; 16 – 2-Propanol; 17 – n
	Pentane; 18 – Isoprene; 19 – cis-2-Pentene; 20 – 2,2-Dimethylbutane; 21 – Cyclopentane / 2,3
	Dimethylbutane; 22 – 2-Methylpentane; 23 – 3-Methylpentane; 24 – n-Hexane; 25 – trans-1,3-Hexadiene
	26 – Methycyclopentane / 2,4-Diimethylpentane; 27 – Methylcyclopentene; 28 – Benzene; 29 – 1-Butanol
	30 – Cylohexane; 31 – 2-Methylhexane; 32 – 2,3-Dimethylpentane; 33- 3-Methylhexane; 34 – Pentanal
	35 – 1-Heptene; 36 – 2,2,4-Trimethypentane; 37 – Heptane; 38 – 2,3-Dymethyl-2-pentene; 39 – 2,3,4
	Trimethylpentane; 40 – Toluene; 41 – 2-Methylheptane; 42 – 4-Methylheptane; 43 3-Methylheptane; 44
	– Hexanal; 45 – n-Octane; 46 – Ethylbenzene; 47 – m/p-Xylene; 48 – Styrene; 49 – o-Xylene; 50 – n
	Nonane; 51 – i-Propylbenzene; 52 – n-Propylbenzene; 53 – m-Ethyltoluene; 54 – p-Ethyltoluene; 55 –
	1,3,5-Trimethylbenzene; 56 – o-Ethyltoluene; 57 – Octanal; 58 – 1,2,4-Trimethylbenzene / t
	Butylbenzene; $59 - Decane$; $60 - 1,2,3-Trimethylbenzene$; $61 - Indane$; $62 - 1,3-Diethylbenzene$; $63 - 1,4-Diethylbenzene$
	Diethylbenzene / Butylbenzene; 64 – Undecane64
Fig. 2	9: Comparison of two calibration gas samples after 8 days storage time, in which one of the samples was
	additionally moistened during filling66
Fig. 3	Oa: MS chromatogram (left) and FID chromatogram of a diesel exhaust sample measured with "GC/MS 2
	(C ₉ – C ₁₆)"67
Fig. 3	0b: Retention times of various n-alkanes in the FID chromatogram of a diesel exhaust sample measured
	with "GC/MS 2 (C ₉ – C ₁₆)"
Fig. 3	1: Simplified scheme of the reaction paths of OH radicals in the degradarion of nitrogen oxides and VOCs
	Only on the reaction path R_{VOC} additional ozone is formed in the atmosphere; the reaction path R_{NO}
	converts the nitrogen oxides present in the form of NO ₂ to HNO ₃ , which is removed from the atmosphere
	by leaching processes. The ratio of reactivities. R_{VOC}/R_{NO2} controls the relative importance of the two
	processes in the degradation of trace substances
Fig. 3	2: Variational calculation of P(O ₃) with MCM-3.3 (Details: cf. [Klemp et al. 2012] for different start ration
	and start reactivities of VOC and NO ₂ . The results are presented as an isoplethe plot of local ozone
	avaduation rate. Bandary conditions: Latitude: F2.F° north latitude radiation conditions: 24.00

12:00. A fast transformation between NO and NO_2 occurs at noon via the photostationary equilibrium	n on
the time scale of 1 - 2 minutes	_71
Fig. 33: Comparison of the VOC concentration distributions ("patterns" of the mixing ratios) of a tur	nnel
measurement on the Berlin motorway ring road under congestion conditions with that of a tur	nnel
measurement under constant speed conditions (approx. 60 km/h). The scaling for the tunnel pattern	was
chosen so that the aromatic toluene has equal proportions in both patterns. The relative increase	ases
occurring in the congestion pattern for the light hydrocarbons (C_2 - and C_3 -alkenes and C_5 - and C_6 -alkana occurring in the congestion pattern for the light hydrocarbons (C_2 - and C_3 -alkenes and C_5 - and C_6 -alkana occurring in the congestion pattern for the light hydrocarbons (C_2 - and C_3 -alkenes and C_5 - and C_6 -alkana occurring in the congestion pattern for the light hydrocarbons (C_2 - and C_3 -alkenes and C_5 - and C_6 -alkana occurring in the congestion pattern for the light hydrocarbons (C_2 - and C_3 -alkenes and C_5 - and C_6 -alkana occurring in the congestion pattern for the light hydrocarbons (C_2 - and C_3 -alkenes and C_5 - and C_6 -alkana occurring in the congestion pattern for the light hydrocarbons (C_3 - and C_3 -alkenes and C_5 - and C_6 -alkana occurring in the congestion pattern for the light hydrocarbons (C_3 - and C_3 -alkenes and C_5 - and C_6 -alkana occurring in the congestion pattern for the congestion occurring the congestion occu	nes)
can be inferred from increased evaporation fractions (C_5 - and C_6 -alkanes) or different conversion rate	es of
the vehicle catalysts	_74
Fig. 34: Comparison of the VOC concentration distributions ("pattern" of the mixing ratios) of a VOC cani-	ster
sample from the inner city area (Hermannplatz, Berlin Neukölln) with a windward drawn sample from	the
eastern Berlin foreland (Alt Landsberg).	_76
Fig. 35: Reactivity-weighted VOC profiles (so-called "Rorschach" plots) from a measurement campaign v	with
MobiLab-I in summer 2014 [Bonn et al., 2016] and from measurements in the inner city area of Mur	nich
in 1997 (February 1997) [Kern et al., 1998]. Both VOC profiles are normalized to the most abund	dant
species. The reactivity contributions of the alcohols (methanol, ethanol, propanol) (red), those of	the
isoprene (green) and those of some aromatics (toluene, trimethylbenzenes) (mint green) are highlight	nted
in colour	_77
Fig. 36: Reactivity-weighted VOC profiles (so-called "Rorschach" plots) of a gasoline engine in a cold-start fi	rom
2015 and from the inner city area of Munich from 1997 (February 1997) [Kern et al., 1998]. The reacti	ivity
fractions of the alcohols (methanol, ethanol, propanol) (red), those of isoprene (green) and those of so	ome
aromatics (toluene, trimethylbenzenes) (mint green) are highlighted in colour. It has to be noted, that	the
VOC emissions from traffic have decreased by at least one order of magnitude [Ehlers et al., 2016] du	ring
the last 20 years mainly due to the shortening of the cold-start phases. Nevertheless, as in 1997 the c	old-
start emissions from gasoline cars are dominating the average VOC emissions pattern for	rom
traffic	_78
Fig. 37: Relative contributions of the various drive concepts in the VOC emissions of road traffic.	The
standardized VOC reactivity distributions calculated from the measured emission patterns for pe	trol
engines with catalytic converters and diesel vehicles with oxidation catalytic converters are shown	_79
Fig. 38 a – e: (a): Cumulative mixing ratios for five different VOC subgroups; shown are the medians for the	four
different pollution scenarios, (b) - (e): Percentages of the mixing ratios for the sum of alkanes, alker	nes,
aromatics, oxigenated and biogenously emitted species (i.e. isoprene and terpenes) for different emiss	sion
szenarios (city background, city center, tiergarten tunnel, windward of the city (rural environment v	with
agricultural use (Alt Landsberg))	_82
Fig. 39 a – e: (a): Cumulative reactivities for five different VOC subgroups; shown are the medians for the	four
different emission scenarios, (b) - (e): Reactivity contribution for the sum of alkanes, alkenes, aroma	tics,
oxigenated and biogenously emitted species (i.e. isoprene and terpenes) for different emission scena	rios

(city background, city center, tiergarten tunnel, windward of the city (rural environment with agricultural use (Alt Landsberg)). Fig. 40a: Combined chromatogram of canister measurement (GC/FID 1: range C2 - C12) and tube collection (Carbotrap® collection tubes, GC/FID 2: range C9 - C16) from simultaneous sample collections in the Bonn tunnel in autumn 2015. Fig. 40b: Calculated reactivities of the C₂ - C₁₁-VOCs, measured in the exhaust gas of the MobiLab diesel vehicle (EURO-6 with SCR catalytic converter and particulate filter, year of construction 2016).

1: ethene; 2: ethyne; 3: ethane; 4: propene; 5: propane, 6: cyclopropene; 7: propyne; 8: methyl nitrite; 9: isobutane; 10: acetaldehyde; 11: 1,3-butadiene; 12: butane; 13: 1-butene-3-yne; 14: trans-butene, 15: 1-butyne; 16: methylethyl-ether; 17: cisbutene; 18: 1,2-butadiene; 19: 3-methyl-1-butene; 20: ethanol; 21: acrolein; 22: isopentane; 23: acetone; 24: 1,4-pentadiene; 25: 1-pentene; 26: furan; 27: 2-methyl-1-butene; 28: pentane; 29: trans-pentene; 30: cis-pentene; 31: methyl nitrate; 32: 2-methyl-2butene; 33: methyl acetate; 34: trans-1,3-pentadiene; 35: nitromethane; 36: methyl-propanal; 37: metacrolein; 38: cyclopentene; 39: 4-methyl-1-pentene: 40: 3-methyl-1-pentene: 41: 2.3-dimethylbutane: 42: methyl vinyl ketone: 43: butanal: 44: methyl ethyl ketone; 45: 3-methyl-pentane; 46: 2-methyl-1-pentene; 47: hexane; 48: trans-2-hexene; 49: 2-methylfuran; 50: 3methylcyclopentene; 51: cis-2-hexene; 52: ethyl tertbutyl ether; 53: trans-1-3-hexadiene; 54: methylcyclopentane; 55: 2-butenal; 56: butanol; 57: cis-2-methyl-3-hexene; 58: benzene; 59: 2-methyltetrahydrofuran; 60: cyclohexane; 61: 2-methylhexane; 62: pentanal; 63: 3-methylhexane; 64: cyclohexene; 65: cis-1,3-dimethylcyclopentane; 66: 1-heptene; 67: trans-1,3dimethylcyclopentane; 68: 2,2,4-trimethylpentane; 69: methyl 3-butenoate; 70: 2-methyl-2-hexen; 71: 3,5-dimethylcyclohexene; 72: trans-2-heptene; 73: cis-2-heptene; 74: 2,3-dimethyl-2-pentene; 75: 3-ethylcyclopentene; 76: 1-ethylcyclopentene; 77: cyclopentanone; 78: cis-1,2-dimethylcyclopentane; 79: methylcyclohexane; 80: 2,5-dimethylhexane; 81: 2,4-dimethylhexane; 82: ethylcyclopentane; 83: 4-methylcyclohexene; 84: cis-2-octene; 85: cis-3-octene; 86: 2,3,4-trimethylpentane; 87: toluene; 88: 2methylheptane; 89: 4-methylheptane; 90: 2-ethyl-1-hexene; 91: 1-methylcyclohexene; 92: 3-methylheptane; 93: trans 1,4dimethylcyclohexane: 94: 1-octene; 95: 1,1-dimethylcyclohexane; 96: butyl-acetate; 97: trans-4-octene; 98: cis-1-ethyl-3methylcyclopentane; 99: trans-1-ethyl-3-methylcyclopentane; 100: trans-3-octene; 101: octane; 102: trans-2-octene; 103: cis-1,4dimethylcyclohexane; 104: cis-1,3-dimethylcyclohexane; 105: isopropylcyclopentane; 106: 1-propylcyclopentene; 107: 1,2dimethylcyclohexene; 108: (E)-2-Hexen-1-al; 109: trans 3,5-dimethylcyclohexene; 110: 2-methylcyctane; 111: cis-3,5dimethylcyclohexene; 112: ethylcyclohexane; 113: 1,1,3-trimethylcyclohexane; 114: ethylbenzene; 115: 4-methylcyclohexane; 116: meta and para xylene; 117: 3-methyloctane; 118: styrene; 119: o-xylene; 120: nonane; 121: 1-ethyl-2-methylcyclohexane; 122: 1-ethyl-4methylcyclohexabe; 123: isopropylbenzene; 124: 2,6-dimethyloctane; 125: butylcyclopentane; 126: 1-propenylbenzene; 127: benzaldehydene; 43: butanal; 44: methyl ethyl ketone; 45: 3-methyl-pentane; 46: 2-methyl-1-pentene; 47: hexane; 48: trans-2hexene; 49: 2-methylfuran; 50: 3-methylcyclopentene; 51: cis-2-hexene; 52: ethyl tertbutyl ether; 53: trans-1-3-hexadiene; 54: methylcyclopentane; 55: 2-butenal; 56: butanol; 57: cis-2-methyl-3-hexene; 58: benzene; 59: 2-methyltetrahydrofuran; 60: cyclohexane; 61: 2-methylhexane; 62: pentanal; 63: 3-methylhexane; 64: cyclohexene; 65: cis-1,3-dimethylcyclopentane; 66: 1heptene; 67: trans-1,3-dimethylcyclopentane; 68: 2,2,4-trimethylpentane; 69: methyl 3-butenoate; 70: 2-methyl-2-hexen; 71: 3,5dimethylcyclohexene; 72: trans-2-heptene; 73: cis-2-heptene; 74: 2,3-dimethyl-2-pentene; 75: 3-ethylcyclopentene; 76: 1ethylcyclopentene; 77: cyclopentanone; 78: cis-1,2-dimethylcyclopentane; 79: methylcyclohexane; 80: 2,5-dimethylhexane; 81: 2,4dimethylhexane; 82: ethylcyclopentane; 83: 4-methylcyclohexene; 84: cis-2-octene; 85: cis-3-octene; 86: 2,3,4-trimethylpentane; 87: toluene; 88: 2-methylheptane; 89: 4-methylheptane; 90: 2-ethyl-1-hexene; 91: 1-methylcyclohexene; 92: 3-methylheptane; 93: trans 1,4-dimethylcyclohexane: 94: 1-octene; 95: 1,1-dimethylcyclohexane; 96: butyl-acetate; 97: trans-4-octene; 98: cis-1-ethyl-3-methylcyclopentane; 99: trans-1-ethyl-3-methylcyclopentane; 100: trans-3-octene; 101: octane; 102: trans-2-octene; 103: cis-1,4dimethylcyclohexane; 104: cis-1,3-dimethylcyclohexane; 105: isopropylcyclopentane; 106: 1-propylcyclopentene; 107: 1,2dimethylcyclohexene; 108: (E)-2-Hexen-1-al; 109: trans 3,5-dimethylcyclohexene; 110: 2-methyloctane; 111: cis-3,5dimethylcyclohexene; 112: ethylcyclohexane; 113: 1,1,3-trimethylcyclohexane; 114: ethylbenzene; 115: 4-methylcyclohexane; 116: meta and para xylene; 117: 3-methyloctane; 118: styrene; 119: o-xylene; 120: nonane; 121: 1-ethyl-2-methylcyclohexane; 122: 1-ethyl-4methylcyclohexabe; 123: isopropylbenzene; 124: 2,6-dimethyloctane; 125: butylcyclopentane; 126: 1-propenylbenzene; 127: benzaldehyde; 128: cyclooctatetraene; 129: propylbenzene; 130: 3,6-dimethyloctane; 131: 3-ethyltoluen;132: 4-ethyltoluene; 133: trans-pinane; 134: mesitylene; 135: 1-propenylbenzene; 136: 1,1,2,3-tetramethylcyclohexane; 137: 2-ethyltoluene; 138: 1-decene; 139: tert-butylbenzene; 140: 1,2,4-trimethylbenzene; 141: decane; 142: 1,3-methyl-isopropylbenzene; 143: 1,2-methylisopropylbenzene; 144: 1,2,3-trimethylbenzene; 145: indane; 146: 1,3-diethylbenzene; 147: 1,3-methyl-propylbenzene; 148: 1-4diethylbenzene; 149: butylbenzene; 150: 1,2-methyl-propylbenzene; 151: 1,2-diethylbenzene; 152: 1,3-dimethyl-4-ethylbenzene; 153: 1,2-dimethyl-4-ethylbenzene; 154: 1,3-dimethyl-2-ethylbenzene; 155: 1,3-dimethyl-2-ethylbenzene; 156: 1-ethenyl-3ethylbenzene; 157: undecane; 158: (1-methylbutyl)-benzene; 159: 1,2,4,5-tetramethylbenzene; 160: 1,2,3,4-tetramethylbenzene; 161: 1,2,3,5-tetramethylbenzene; 162: dodecane; 163: naphthalene.

Fig. 40 c: VOC concentration and reactivity fractions in the exhaust gas of the MobiLab vehicle under cold-start conditions (MobiLab: year of construction 2016, EURO 6 diesel, 6 cylinders, 212 hp, manufacturer: Daimler AG). The C1 - C12 range was measured with the GC/FID-1 system. The C1 components listed were supplemented by the methane mixing ratio (9 ppm or 1.5 s⁻¹) and by the respective formaldehyde mixing ratio (7.7 ppm or 1550 s⁻¹), both measured with cavity-ringdown systems (Picarro Inc.). The range C₁₃ - C₁₈

was covered by the GC/FID-System-2 (see also Fig.30b). The necessary harmonization of both GC systems
was performed on the basis of the adjustment of the range of the C_8 - C_9 components accessible for both
systems
Fig. 41: Results (yellow circles) of the Berlin summer measurement campaigns (August 2016 and July/August
2017) in the isopleth plot. Isopleth plot with 1994 trend and 2014 trend: [Ehlers et al., 2016, Fig. 25). The
mean values of the reactivities from the 5 pollution scenarios are shown (see Table 4). The red line from:
[Ehlers et al., 2016] describes the basic behaviour of an air mass from 2014 during transport and
photochemical processing from the city to biogenically dominated areas. For all 5 scenarios the respective
averages group quite well around the dilution and processing course assumed for 2014 [Ehlers et al.,
2016]. The trend indicated in Ehlers et al. is also supported by the measurements for the range of low
NO ₂ values

11 List of Tables

Table 1: Gas phase analysis of MobiLab-I at the beginning of the ALASKA project. In a later phase of the project					
the existing NH ₃ analysis (IR-Cavity ringdown, Picarro) was supplemented by a fast tunable diode lase					
system with long path absorption cell. (Manufacturer: LosGatos). A fast SO ₂ measuring system (TI 43					
system with long path absorption cell. (Manufacturer: LosGatos). A fast SO ₂ measuring system (11 4 manufacturer Thermo Fisher, detection limit 1 - 2 ppb, second resolution) was procured from the o					
funds of Forschungszentrum Jülich and integrated into the MobiLab-I successor system. 15					
Table 2: Measurement equipment of MOBILAB-II, available from 2016, power requirement of analytics: approx					
7 kW, supply by a 380 V three-phase generator driven by the vehicle engine (6 kW power); (MobiE) and					
an underfloor generator (3 kW power); (Dometic TEC40 D).					
Table 3: Percentage of total measuring time for the different road types (cf. explanation of Fig. 15) of the					
Rhine-Ruhr measuring area					
Table 4 a: Diesel exhaust composition – cold-start conditions (MobiLab, year of construction 2016, EURO 6 diesel					
6 cylinders, 212 hp, manufacturer: Daimler AG). Listed are relevant OH-reactive species that were					
measured with different techniques, their corresponding rate coefficients ($k_{(x+OH)}$) for 298 K, thei					
concentrations (in ppb) and calculated OH reactivity values in s ⁻¹ . The comparison of the sum of the trace					
gas measurements with the total OH-reactivity investigation yields a discrepancy of 23 %, with the total					
OH-reactivity investigation value exceeding that of the sum of the individual trace gas measurements					
94					
Table 4 b: Diesel exhaust composition – warm operating conditions (MobiLab, year of construction 2016, EURC					
6 diesel, 6 cylinders, 212 hp, manufacturer: Daimler AG, same load conditions than for cold-star					
conditions). Listed are relevant OH-reactive species that were measured with different techniques, their					
corresponding rate coefficients ($k_{(x+OH)}$) for 298 K, their concentrations (in ppb) and calculated OH					
reactivity values in s ⁻¹ . The comparison of the sum of the trace gas measurements with the result of the					
total OH-reactivity investigation yields a discrepancy of 21 %, with the total OH-reactivity investigation					
value exceeding that of the sum of the individual trace gas measurements95					
Table 5: Mean values of the NOx, VOC, CO and CH4 measurements for the associated VOC reactivities of the					
various exposure scenarios (Berlin summer measurement campaigns)					
Appendix					
A: AMS test round: Concentration tables for different trace gases					
Table 6 a: Statistical parameters for the measured methane concentrations for the various road types of the AMS					
test round, determined from the measured second data. All data in ppm106					
Table 6 b: Statistical parameters for the measured CO concentrations for the various road types of the AMS test					
round, determined from the measured second data. All data in ppb107					
Table 6 c: Statistical parameters for the measured NH ₃ concentrations (LosGatos Inc.) for the various road types					
of the AMS test round, determined from the measured second data. All data in ppb107					

$\textbf{Table 6 d:} Statistical\ parameters\ for\ the\ measured\ NH_3\ concentrations\ (Picarro\ Inc.)\ for\ the\ various\ roughly also also also also also also also also$	ad types of
the AMS test round, determined from the measured second data. All data in ppb	108
Table 6 e: Statistical parameters for the measured CO ₂ concentrations (Picarro Inc.) for the various ro	ad types of
the AMS test round, determined from the measured second data. All data in ppm	108
Table 6 f: Statistical parameters for the measured H ₂ O concentrations (Picarro Inc.) for the various ro	ad types of
the AMS test round, determined from the measured second data. All data in %-mixing rati	o [10000 *
ppm]	109
Table 6 g: Statistical parameters for the measured NO concentrations (EcoPhysics) for the various ro	ad types of
the AMS test round, determined from the measured second data. All data in ppb	109
Table 6 h: Statistical parameters for the measured NO ₂ concentrations (Aerodyne Inc.) for the various	road types
of the AMS test round, determined from the measured second data. All data in ppb	110
$\textbf{Table 6 i:} Statistical \ parameters \ for \ the \ measured \ NO_x \ concentrations \ (EcoPhysics) \ for \ the \ various \ roughly \ and \ roughly \ arrows \ and \ roughly \ arrows \ arrow$	ad types of
the AMS test round, determined from the measured second data. All data in ppb	110
$\textbf{Table 6 j:} \ Statistical \ parameters \ for \ the \ measured \ NO_x \ concentrations \ (EcoPhysics) \ for \ the \ various \ roughly \ for \ roughly \ for$	ad types of
the AMS test round, determined from the measured second data. All data in ppb	111
Table 6 k: Statistical parameters for the measured SO ₂ concentrations (ThermoFisher) for the various	road types
of the AMS test round, determined from the measured second data. All data in ppb	111
B. <u>Determination of VOC concentrations for different load scenarios</u>	
Table 7 a: City background, Berlin-campaign, August 2017	112
Table 7 b: City center, Berlin-campaign, August 2017	115
Table 7 c: Tiergarten tunnel (weekday traffic, Mean velocity: 40 – 60 km/h, Berlin campaign,	
August 2017	118
Table 7 d: "In front of the city" (regional background for easterly flows, Berlin campaign,	
August 2017	121
C: OH-reactivity determinations for the considered pollution scenarios	
Table 8 a: City background, Berlin campaign, August 2017	124
Table 8 b: City center, Berlin campaign, August 2017	127
Table 8 c: Tiergarten tunnel, Berlin campaign, August 2017	130
Table 8 d: "In front of the city", regional background for easterly flows, Berlin campaign,	
August 2017	133
Table 8 e: Mean VOC reactivities "In front of the city" (regional background for westerly flows, Berlin	n campaign
ALASKA, August 2016 and results from BMBF-projekt "Stadtklima im Wandel", summer campa	ign (IOP-2)
Berlin July – August 2017. Comparison of the results for different years for summertime	e clear sky
conditions. VOC samples were taken in 2016: 02.08.2016 11.00 - 11:05 UTC Sacrow; 02.08. 20	16 12:15 –
12:20 UTC Pfaueninsel. VOC samples were taken in 2017: 29.07.2017 Pfaueninsel 12:50 –	12:55 UTC:
29.07. 2017 Sacrow 13:55 – 14:03 UTC.	136

12 List of Abbreviations

AMS test round: Test Round developped by "Auto, Motor und Sport" journal
BMBF: Bundesministerium für Bildung und Forschung
BMWi: Bundesministerium für Wirtschaft und Energie
CAPS: Cavity Attenuated Phase-shift Spectroscopy
SCR: Selective Catalytic Reduction
CLD: NO Detector based on the radiative deactivation (Chemiluminescence) of NO2 * after NO + O3 reaction
CMB: Chemical Mass Balance
CPC: Condensation Particle Counter
ELPI: Electrical Low Pressure Impactor
FID: Flame Ionization Detector
FZJ: Forschungszentrum Jülich GmbH
GC/MS: Gas Chromatography / Mass Spectrometry
GPS: Global Positioning System
HBEFA: Handbook Emission Factors for Road Transport
IEK: Institut für Energie- und Klimasorschung des Forschungszentrums Jülich GmbH
IOP: Intensive Observation Period
MCM: Master Chemical Mechanism
MSD: Mass Selective Detector
PEGASOS: Pan-European Gas-AeroSOIs-climate interaction Study
PEM fuel cell: Polymer Electrolyte Membrane fuel cell
VOC: Volatile Organic Compounds
ZBT: Zentrum für Brennstoffzellentechnik GmbH

Band / Volume 525

ETV Online Tagung 2020

Industrielle Groß- und Hochtemperaturwärmepumpen im Energiesystem

D. Stolten, G. Markowz (Hrsg.) (2020), ca. 71 pp

ISBN: 978-3-95806-519-2

Band / Volume 526

Atmospheric Trace Gas Measurements Using Chemical Ionisation Time-of-Flight Mass Spectrometry

Y. Li (2020), xi, 110 pp ISBN: 978-3-95806-520-8

Band / Volume 527

Uranium accumulation in agricultural soils as derived from long-term phosphorus fertilizer applications

Y. Sun (2020), XII, 136 pp ISBN: 978-3-95806-521-5

Band / Volume 528

Entwicklung von Schutzschichten für nicht-oxidische Faserverbundwerkstoffe

M. Wolf (2021), VI, 150, 2 pp ISBN: 978-3-95806-524-6

Band / Volume 529

Mechanical reliability and oxygen permeation of $Ce_{0.8}Gd_{0.2}O_{2-\delta}$ -FeCo₂O₄ dual phase membranes

F. Zeng (2021), IV, VI, 222 pp ISBN: 978-3-95806-527-7

Band / Volume 530

Capacitance-Based Methods to Study Charge Transport and Recombination in Organic Solar Cells

I. Zonno (2021), vi, 153 pp ISBN: 978-3-95806-528-4

Band / Volume 531

Einflüsse von Klimavariabilität und -wandel auf Ausbau und Erzeugung im Europäischen Stromsystem

F. P. Gotzens (2021), XXIII, 231 pp

ISBN: 978-3-95806-530-7

Band / Volume 532

Weltweite Infrastruktur zur Wasserstoffbereitstellung auf Basis erneuerbarer Energien

P.-M. Heuser (2021), VII, 231 pp

ISBN: 978-3-95806-531-4

Band / Volume 533

Mechanische Eigenschaften von katalysatorbeschichteten Membranen für die Polymer-Elektrolyt-Membran Elektrolyse

E. Borgardt (2021), viii, 181 pp ISBN: 978-3-95806-533-8

Band / Volume 534

Techno-economic Assessment of Hybrid Post-combustion Carbon Capture Systems in Coal-fired Power Plants and Steel Plants

Y. Wang (2021), IV, xx, 230 pp ISBN: 978-3-95806-545-1

Band / Volume 535

Wissenschaftliche Begleitstudie der Wasserstoff Roadmap Nordrhein-Westfalen

S. Cerniauskas, P. Markewitz, J. Linßen, F. Kullmann, T. Groß, P. Lopion, P-M. Heuser, T. Grube, M. Robinius und D. Stolten (2021), IV, 89 pp ISBN: 978-3-95806-547-5

Band / Volume 536

High-Resolution Photocurrent Mapping of Thin-Film Silicon Solar Cells Using Scanning Near-Field Optical Microscopy

Z. Cao (2021), xiii, 148 pp ISBN: 978-3-95806-548-2

Band / Volume 537

Kompressionseigenschaften der Gasdiffusionslage einer Hochtemperatur-Polymerelektrolyt-Brennstoffzelle

E. Hoppe (2021), viii, 153 pp ISBN: 978-3-95806-549-9

Band / Volume 538

Transparent Passivating Contact for Crystalline Silicon Solar Cells

M. Köhler (2021), 186 pp ISBN: 978-3-95806-550-5

Band / Volume 539

Distribution of trace gases with adverse effects on fuel cells

D. Klemp, R. Wegener, R. Dubus, L. Karadurmus, N. Kille, Z. Tan (2021), 160 pp

ISBN: 978-3-95806-551-2

Weitere Schriften des Verlags im Forschungszentrum Jülich unter

http://wwwzb1.fz-juelich.de/verlagextern1/index.asp

Energie & Umwelt / Energy & Environment Band / Volume 539 ISBN 978-3-95806-551-2

